2013

Glass fiber reinforced biorenewable polymer composites and the fabrication with pultrusion process

Hongyu Cui
Iowa State University

Glass fiber reinforced biorenewable polymer composites and the fabrication with pultrusion process

by

Hongyu Cui

A dissertation submitted to the graduate faculty

in partial fulfillment of the requirements for the degree of

DOCTOR OF PHILOSOPHY

Major: Materials Science and Engineering

Program of Study Committee:
Michael R. Kessler, Major Professor
Mufit Akinc
Xiaoli Tan
Kaitlin Bratlie
David Grewell

Iowa State University
Ames, Iowa
2013

TABLE OF CONTENTS

LIST OF FIGURES

Page

LIST OF TABLES

Page

ACKNOWLEDGEMENTS

First and foremost, I would like to sincerely thank my advisor, Dr. Michael R. Kessler, for his guidance, technical support, and encouragement throughout the research process. I would also like to thank Dr. Mufit Akinc, Dr. Xiaoli Tan, Dr. David Grewell, and Dr. Kaitlin Bratlie for serving on my advisory committee and providing additional technical guidance. A special thank you is to be given to James Anderegg and Roger Jones in Ames lab for their help in characterizations and inspired discussions. I also want to thank Bill Halterman and Bruce Erickson in chemistry machine for their help and suggestions in building the table-top pultrusion machine.

Funding support of this work from the Consortium for Plant Biotechnology Research (CPBR) through USEPA grant EM-83438801 is gratefully acknowledged. I would additionally like to thank current and former members of the polymer composites research group—Dr. Xia Sheng, Dr. Tim Mauldin, Dr. Ying Xia, Dr. Mahendra Thunga, Dr. James Bergman, Dr. Peter Hondred, Dr. Eliseo De Leon, Danny Vennerberg, Chaoqun Zhang, and Rui Ding—for their valuable technical expertise and helpful discussions.

Finally, I need to thank my parents for all the love and support they have provided me over the years. Last, but not least, I would to thank my husband, Shan, for his unwavering love, support, and encouragement throughout this whole process.

ABSTRACT

A novel bio-renewable thermoset which is synthesized from modified linseed oil (Dilullin) and dicyclopentadiene (DCPD) through ring opening metathesis polymerization (ROMP) method has been characterized and further developed. The fracture toughness of the Dilulin/DCPD copolymer system has been evaluated by essential work of fracture (EWF). Dynamic mechanical analysis (DMA) and scanning electron microcopy (SEM) examinations both demonstrated a reaction-induced phase separation in the copolymers. The correlation between fracture toughness and microphase morphology has been analyzed.

Interfacial adhesion of glass fiber reinforced Dil30DCPD70 (containing 30% Dilulin in weight) composites has been improved with two types of silane coupling agents, monochlorosilane (MCS) and trichlorosilane (TCS). The interfacial shear strength which is evaluated by microbond technique shows significant increases with both silanes. All characterizations of composites made with silane-treated fibers indicate the interfacial adhesion was improved significantly and MCS worked better than TCS due to the simple and reproducible grafting mechanism.

The Dil30DCPD70 copolymer has been applied in pultrusion process for manufacturing glass fiber reinforced composites. A table-top pultrusion machine was built for running those experiments. The resin formulation with the optimum percentage of lubricant and clay and pultrusion processing parameters were investigated based on processing performance. MCS silane was used to modify glass fiber with a simple dipping method. The influences of silane concentration were examined. The optimized

silane concentration is 3% and the resulting composites show best results in all characterizations.

The short-term stability of Dil30DCPD70 under UV radiation has been studied with accelerated aging. Time-dependent degradation and surface confined effect have been confirmed by Photoacoustic FTIR and SEM measurements. The presence of unreacted carbon-carbon double bonds after cure is responsible for the relatively fast degradation effect.

CHAPTER 1: GENERAL INTRODUCTION

1.1 Introduction

Nowadays, plastics play an important role in almost every aspect of our life, such as packaging, construction, electronic engineering, transportation, etc. The manufacturing of plastic still relies on raw materials from petroleum industry. As we know, processing of crude oil causes many environmental impacts, such as releasing of greenhouse gases and oil spills. In addition, the price of petroleum raw material is likely to increase in the future due to the finite amount of fossil fuel on the earth [1, 2]. Therefore, there is a growing urgency to develop polymeric materials from renewable resource to reduce the widespread dependence on petro-chemical based polymers and resins.

A wide range of biopolymers have been developed from various bio-renewable sources in the past decades. Biodegradable PLA is a promising bio-based thermoplastic derived from corn starch. As a cost-effective alternative to petroleum-based plastics, it has been used in the fields of packaging and medical implant [1]. Novel thermosets synthesized from natural oils show properties ranging from soft and flexible to rigid and hard which may have applications in different fields [2, 3]. However, most biopolymers are not as strong as commercially petroleum plastics, limiting them from applications as structural materials. To overcome this problem, reinforcements, such as fibers and

nanoparticles, are introduced to biopolymer to make biocomposites with better mechanical properties.

Glass fiber is one of the cheapest reinforcements with high tensile strength, good chemical resistance and excellent insulating properties. Now, glass fiber reinforced polymer composites are widely used in many fields, especially in the construction area due to their relatively low price and good mechanical properties [4]. Among various manufacturing methods, pultrusion is found to be the most cost-effective one for producing glass fiber reinforced composites [4, 5]. Therefore, the combination of biopolymer with pultrusion would provide possibilities to produce structural composite materials at low cost. In this work, a novel ROMP-based bio-renewable polymer was applied in pultrusion process for producing glass fiber reinforced composites. The best resin formulation and processing parameters were optimized based on processing performance. The interfacial adhesion of the composite was improved by surface modification of glass fiber with silane coupling agents. The facture toughness and short-term stability under UV radiation of the bio-renewable polymer were also studied.

1.2 Dissertation Organization

This work is organized into main chapters, which are each manuscripts that have either been published in or prepared for submission to scholarly journals.

Chapter 1 gives a general introduction that outlines the background and motivation for developing novel bio-renewable polymers from vegetable oils and their applications in fiber reinforced polymer composites. This chapter also includes a review of biopolymers that have been developed in Iowa state university, introductions of glass

fiber reinforced polymer composites industry, and pultrusion process for manufacturing of FRP composites.

Chapter 2 involves the study of morphology and toughness of the ROMP-based biopolymer system. The facture toughness was evaluated by essential work of fracture (EWF) method. Both DMA and SEM were utilized to characterize the reaction-induced phase separation. The structure-property relationship was analyzed. This study is helpful to explore any potential applications for the biopolymer materials.

Chapter 3 presents the work to improve the interfacial adhesion of glass fiber reinforced ROMP-based Dilulin/DCPD copolymer composites with silane coupling agents. Two types of silanes were characterized and compared in terms of the improved interfacial strength that measured through microbond, DMA, and short beam shear test. The better one was chose as the primary surface modification agent that suitable for this polymer matrix.

Chapter 4 covers the research on pultrusion process with the Dilulin/DCPD resin. The resin formulation and processing parameters were optimized based on processing performances. This chapter mainly focuses on tuning silane concentration to give the best interfacial adhesion with a simply dipping method.

Chapter 5 discusses the aging effect of the bio-renewable Dilulin/DCPD polymer by UV radiation. A series of techniques were used to characterize the crack formation and chemical evolution during the aging process. It has been shown that the presence of unreacted carbon-carbon double bonds is responsible for the relatively fast degradation effect.

Chapter 6 gives a general discussion of conclusions drawn through this project, as well as recommendations for future research.

1.3 Background and Literature Review

1.3.1 Bio-renewable Polymers from Vegetable Oils

In recent years, natural oils have attracted increasing attention as raw materials for the preparation of polymeric materials due to their capability of being chemically modified and the sustainability. Vegetable oils are general triglycerides with varying composition of fatty acids depending on the plants [6]. The general structure of triglycerides is shown in Figure 1-1. The existence of double bonds and ester groups in the structure make oils capable to be modified and then polymerized or polymerized directly. A wide range of bio-based polymers have been synthesized and prepared from vegetable oils through various polymerization methods in our group and Larock's group at Iowa State University [2, 3]. Those materials show properties from soft and flexible to rigid and hard.

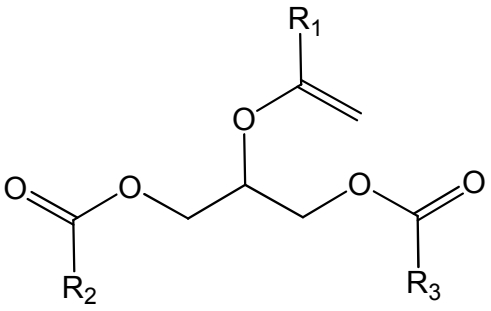

Figure 1-1 Structure of the vegetable oils (R_1, R_2, and R_3 represent fatty acid chains).

Vegetable oils contain carbon-carbon double bonds capable of being polymerized through a free radical mechanism. Copolymerization of conjugated low saturation

soybean oil (CLS) and conjugated linseed oil (CLIN) with acrylonitrile (AN) and either dicyclopentadiene (DCPD) or divinylbenzene (DVB) using AIBN as the initiator have been prepared through free-racial mechanism [7, 8]. The resulting polymers are transparent yellow with properties ranging from hard to slightly rubbery. When 40% oil is incorporated, all copolymers show T_g higher than 100ºC and the storage modulus at room temperature is over 1.6 GPa. Those thermosets are thermally stable up to 350 ºC. As the oil content increased, T_g and modulus of copolymers decreased significantly.

Some bio-based polymers were prepared through cationic polymerization due to the slightly nucleophilic nature of vegetable oils. A series of thermosets have been prepared by cationic polymerization of various vegetable oils with DVB or a combination of DVB and styrene which were initiated by an NFO-modified BF_3•OEt_2 (BFE) catalyst [9]. The OIL-DVB copolymers have Young's modulus ranging from 20 to 100 MPa and ultimate strength ranging from 1.2 to 5.6 MPa. All of them show two glass transition temperatures due to the extensive phase separation, one is around 50 ºC and the other is lower than room temperature. The incorporation of styrene had improved the miscibility and only one T_g can be seen. Mechanical properties were not affected greatly by the adding of styrene. The cationic copolymerization of soybean oil and conjugated soybean oil with DCPD has also been studied [10]. The resulting copolymers show good damping properties as indicated in DMA tests. All materials have high bio-mass contents, ranging from 53% to 86%. Ying have developed a series of copolymer from modified linseed oil and DCPD through cationic polymerization [11]. With 57% modified linseed oils in the composition, copolymer show a T_g at around 80

ºC and a storage modulus of 1500 MPa, which is promising among all bio-based polymers we have developed.

Ring opening metathesis polymerization (ROMP) method polymerizes monomers containing strained rings, such as norbornene units. The modified linseed oils (Dilulin) containing norbornenyl groups have been copolymerized with dicyclopentadiene (DCPD) or other crosslinkers through ROMP [12-14]. The ROMP of pure Dilulin itself gives a soft and flexible rubber with T_g of -29°C. As the DCPD content increased, the resulting thermosets gradually became hard and stiff. The thermoset with 70 wt% DCPD has a Young's modulus of 525 MPa and a tensile strength of 29 MPa, which are comparable to polyethylene. Composites reinforced with 40% glass fiber exhibit a Young's modulus of 1.5 GPa and a tensile strength of 145 MPa [14]. These mechanical properties suggest potential applications of the composite as structural materials. Norbornenyl-functionalized fatty alcohols derived from vegetable oils have been successfully synthesized by Ying [15]. Totally bio-based thermosets were obtained by homopolymerization of those monomers using Grubbs 2nd generation catalyst. The resulting polymers show Young's modulus ranging from 155 to 310 MPa and ultimate strength ranging from 10 to 15 MPa. Although mechanical properties are not promising, it provides a new way to modify vegetable oils for preparing bioplastics.

1.3.2 Fiber Rreinforced Polymers (FRP) Composites

Fiber reinforced polymer composites consist of fibers of high strength and high modulus embedded in a polymer matrix. In the composites, fiber and polymer both maintain their original physical and chemical characteristics. The composite they

produced has combined mechanical properties which are lower than either component acting alone. In the composite, fiber is the load-carrying component and the main source of strength while the matrix “glues” all fibers together in position, acts as a load transfer medium between them, and protects fibers from environmental damages [16]. The most common fibers used in advanced composites for structural applications are glass, aramid, and carbon fibers. Other fibers, such as boron, silicon carbide, and aluminum oxide, are used in limited quantities. Properties of selected commercial reinforcing fibers are listed in Table 1-1 [4]. Glass fibers are the most widely used reinforcing fibers due to their low cost, high tensile strength, high chemical resistance, and excellent insulating properties. Carbon fibers are famous for their exceptionally high specific tensile strength and modulus, very low thermal expansion, high thermal conductivity as well as good resistance to high temperature. Those advantages make carbon fibers very popular in aerospace, civil engineering, military, and automotive where weight saving is considered more critical than cost. However, the high cost of carbon fibers has excluded them from widespread commercial applications. Aramid fiber has the highest specific tensile strength among current reinforcing fibers, which is why they are commonly used in armor and ballistic protection applications. Boron fibers are featured by their extremely high tensile modulus but application is restricted by the high cost. Ceramic fibers, such as SiC and Al_2O_3, are notable for their high-temperature in metal and ceramic matrix composites. Natural fibers have attracted more attentions as reinforcement in recent years, such as flax, hemp, sisal, and jute fibers, because they are environmental friendly and available in large quantity at low cost.

Table 1-1 Properties of selected commercial reinforcing fibers [4]

Fiber	Density g/cm^3	Modulus GPa	Tensile Strength GPa	Strain-to-Failure (%)	CTE (10^{-6}/°C)
E-glass	2.54	72.4	3.45	4.8	5
T-300 (Pan carbon)	1.76	231	3.65	1.4	-0.6(long), 7-12 (radial)
P-55 (Pitch carbon)	2.0	380	1.90	0.5	-1.3
P-100 (Pitch carbon)	2.15	758	2.41	0.32	-1.45
Kevlar49 (Aramid)	1.45	131	3.62	2.8	-2 (long), 59 (radial)
Boron	2.7	393	3.1	0.79	5
Monofilament, SiC	3.08	400	3.44	0.86	1.5
Nextel 610 (Al_2O_3)	3.9	380	3.1		8

Thermosets are widely used as polymer matrix in FRP composites, such as epoxy, polyester, vinyl ester, cyanate ester and polyimides [17]. They usually have low viscosity at room temperature which is good for processing and the cured polymer has cross-linked structure with good mechanical properties for high temperature uses. Epoxy resins have widespread applications from construction to aerospace due to the availability of epoxy with different backbone structures and molecular weight. Unsaturated polyesters (UP) are the most widely used thermosets in polymeric composites because of their versatility and low cost. Glass fiber reinforced polyester composites are used extensively in construction, transportation and electric industries. Polyimides and cyanate ester are advance materials in the area of military and aeronautic applications. Polyimides show superior resistance to thermal oxidation. Cyanate ester resin has a high glass transition temperature (T_g = 265°C), lower moisture absorption, good chemical resistance and good dimensional stability.

As we know that mechanical properties of a composite cannot be as good as either component acting alone due to the presence of interface [18]. The adhesion between fiber and matrix affects the ultimate mechanical properties of a composite greatly. Interface is the weakest region in a composite where cracks are usually initiated from due to the mismatch physical and chemical properties. Tailoring of well-bonded, durable interface between fibers and matrix is very important to increase the stability and mechanical properties of a composite [19]. Here, I will focus on interface in glass fiber reinforced polymer composites.

Glass fibers are hydrophilic and water is likely accumulated on unprotected surface over times causing losses of adhesion and fiber strength. The most common treated method for glass fiber is modifying fiber surface with silane coupling agents. As a difunctional chemical, silane can form covalent bonding with both glass fiber and polymer matrix, thereby improving the interfacial interaction in the composite. A schematic diagram showing how silane works is presented in Figure 1-2. A wide variety of silane coupling agents has been developed since 1951[20]. The silane chemistry and its interaction with both glass fiber and polymer matrix have been studied extensively [21, 22]. A number of factors affect the microstructure of the coupling agent interphase which, in turn, controls the mechanical and physical properties of the composites. It has been found that silane concentration, reaction temperature and the length of treatment time have significant effects on structure of silane absorbed [23-25]. Careful optimization is necessary to find the best combination for treatment. The *pH* of the silane solution is also important, since the acidic or basic conditions affect the relative rates of

silane hydrolysis and condensation [20, 26]. Mechanical properties of the composites made from catalyzed silanes are greatly improved [27, 28]. Mild acidic or basic conditions are also found to increase the amount of silane adsorption [29-31]. The drying conditions used for the silane-treated substrate also affect the microstructure of silane interphase [32, 33]. Improved abrasion resistance was obtained after drying the silane-treated substrate at higher temperature [32].

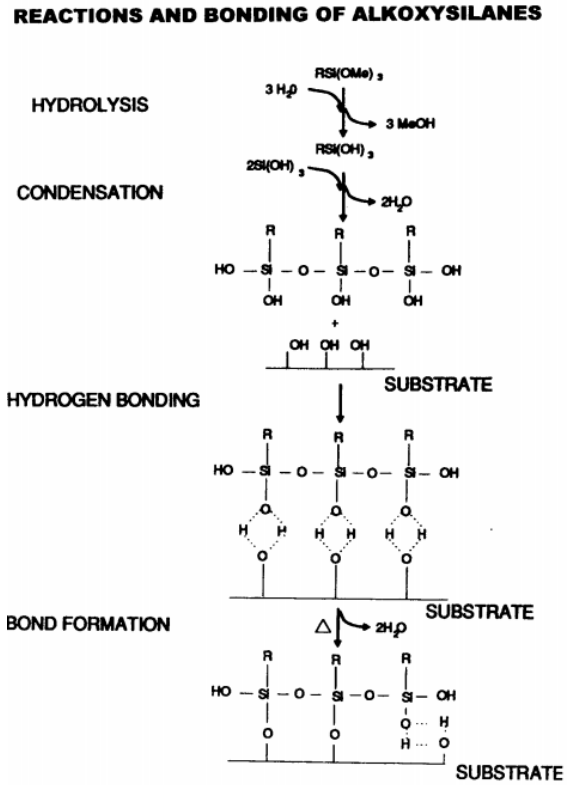

Figure 1-2 Reaction and bonding of alkoxysilanes [20]

Besides mechanical properties, water resistance of the FRP composites is another important characteristic that we want to improve through silane coupling agent. The effect of water degradation on untreated glass fiber-polymer matrix interface is found to be much pronounced. Ishida and Koenig have found that chemically bonded interphase

cannot be extracted by hot water and the hydrothermal stability of the composite is improved [33].

The most common cutting-edge techniques for characterization of interface in composites such as microbond, single-fiber fragmentation, micro-indentationhas, have been reviewed thoroughly by Herrera-Franco and Drzal [34]. The experimental apparatus and test procedures are all described, as well as the advantages and limitations of each technique.

Fiber reinforced polymer composites can be manufactured by various methods, such as bag molding, compression molding, pultrusion, filament winding and resin transfer molding (RTM) [4, 35, 36]. With bag molding method, a lot of labors are required to layup ply which usually results in non-consistent qualities of the composites. Compression molding is suitable for the high-volume production of composites parts, such as structural automotive parts. Pultrusion is a continuous manufacturing method with high productivity and low cost. Detailed discussion will gave in the next section. Filament winding is good for producing cylindrical hallow core structures with high volume fraction of fiber. RTM has a very low tooling cost and simple mold clamping requirements. And RTM allows the encapsulation of metal inserts, stiffeners, washers, as well as foam core of a hollow part.

1.3.3 Pultrusion Process

Pultrusion is a continuous manufacturing process for producing long, straight fiber reinforced composites with constant cross-sectional area. A schematic diagram for this process is shown in Figure 1-3. Fibers are draw from a creel stand and then

gradually brought together and pulled into a resin bath in which fibers are impregnated. Then after removing excess resin by pre-former, impregnated fibers go through the hot die where resins are cured and solidified. After coming out from the die, the formed composites enter the pulling system. The pulling machine provides the continuous force to moving everything forward. Then the production was cut into desired length.

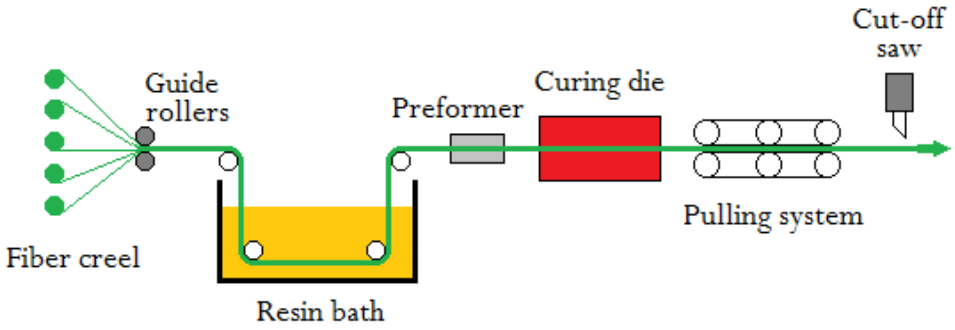

Figure 1-3 Schematic diagram of pultrusion process

Pultrusion system was first developed by W. Brandt Goldsworthy in 1950s. With the appearance of high capacity pulling machine in the 1990s, it is able to make pultruded composites with complex profile shapes and large sizes. In addition, the cost is greatly reduced by applying highly automatic process in manufacturing. Although cost effective is one of the most important advantages for pultrusion, it is not limited to that. Pultruded composites exhibit increased strength due to the well-aligned fibers and high fiber content involved. Pultrusion can produce composites with consistent quality since it is highly automated and manual interface is eliminated [5]. Now pultrusion occupies a stable position in composite market and grows steadily.

In traditional pultrusion, continuous glass fiber is the most widely used reinforcement which dominates the market with over 90% share. Although carbon fiber

and aramid fiber show high performance in many aspects, the application of these fibers is limited in aerospace and aeronautical field where price is not the primary concern. As for resin matrix, thermosets is widely used due to their low viscosity under room temperature and controllable cure kinetics. Due to the continuous manufacturing nature, resin used in pultrusion must meet some specific requirements. Fast cure kinetics of resin is required to polymerize in short time inside the die. Moreover, cure time is an essential factor to determine the line speed in pultrusion. Resin should have proper viscosity to wet out fiber reinforcement effectively and long shelf life [5]. A series of resins were developed for the application in pultrusion, for example unsaturated polyester, vinyl ester, epoxies, acrylic and phenolic-based thermosets. Among them, polyester, vinyl ester and epoxy resin dominate almost the whole resin market for pultrusion process and the polyester takes much larger percentage than the other two.

Table 1-2 Characteristics of thermoset matrixes commonly used in pultrusion [5]

System	Polyester	Vinylester	Epoxy
Rein type	Orthophthalic, isophthalic, low profile, halogenated	Epoxy Novolak, methacrylate esters of bisphenol epoxy resins	Epichlorohydrin/bisphenol-A
Initiator type	Organic peroxide	Organic peroxide	Amines, acid anhydrides
Polymerization	Gelation occurs prior to exotherm	Gelation occurs prior to exotherm	Exotherm occurs prior to gelation
Volume shrinkage	7-9%	7-9%	1-4%
Interfacial adhesion	Low	Medium	High
Relative line speed	Normal	Slower	Very slow
Pultrusion difficulty	Normal	More difficult	Very difficult
Die temperature	100-150°C	125-160°C	200°C
Posttreatment	None	None	Post cure

The characteristics of the three most common thermosets used in pultrusion are listed in Table 1-2. Polyester shows the best processability in pultrusion with a low viscosity and fast cure procedure. If the cost is considered, the superiority of polyester is more promising than other resins. Vinyl ester has some similar advantages as polyester with improved toughness and better chemical and environmental resistance, but the price is higher. The Epoxy resin has the worst processability but the shrinkage is the lowest among the three resins. Epoxy is selected when very high toughness, fatigue and creep performance are required together with chemical and environmental resistance.

In recent year, applying bio-based resins or natural fibers or both together in pultrusion is of great interests since it provides possible ways to make composites at very low cost. Natural fiber reinforced composites have shown a growth of interest due to the economic and environmental advantages and the attractive specific properties [37, 38]. Although natural fibers normally present lower strength than traditional fibers used in current composites, the natural fibers are strong enough as reinforcements for making composites used in packaging, construction, and electrical engineering where high performance is not required. The most common natural fibers that may suitable for using in pultrusion are flax, hemp, and jute, because they are all long fibers with light weight and acceptable properties. In Table 1-3, mechanical characteristics of sisal, hemp and flax are compared with glass fiber. As we know, all natural fibers are non-continuous fibers. To apply them in pultrusion, they need to be wound into strand or rope.

Table 1-3 Properties of natural fibers and glass fiber [39]

Properties	Sisal	Flax	Hemp	E-glass
Tensile trength (MPa)	610	900	690	2300
Elastic modulus (GPa)	28	50	64	73
Elongation at break (%)	2.2	1.8	1.8	3.2
Density (g/cm^3)	1.3	1.5	1.45	2.6
Specific strength (MPa/r)	470	600	476	880
Specific stiffness (GPa/r)	22	33	44	28
Cost price (US$/kg)		1.2-1.75		1.5-5

Flax fiber reinforced polypropylene (PP) composites has been developed with pultrusion process and their mechanical properties were evaluated [39]. The resulting composites show a similar property to the composites made by compression molding. It has been found that flax fibers are high moisture sensitive and pre-drying is necessary before processing. The impregnation of flax fiber with PP should be optimized to obtain the best strength properties of the pultruded composites. Zamri and coworkers have studied the effect of water absorption on pultruded jute/glass fiber reinforced UP composites [40]. They found that water absorptions of pultruded composites follow non-Fickian behavior and the flexural and compression properties were found to decrease with increasing water uptake. Pultruded composites from hemp/wool hybrid fiber and three types of resins, polyester, vinyl estera and polyurethane, were studied by Peng [41]. He concluded that polyester composites have the great potential for commercial manufacture. However, the poor interface is found and assumed responsible for the high water absorbability. Pultruded kenaf fiber [42], jute fiber [43] and hybrid jute/glass and kenaf/glass fiber [44] reinforced polyester composites were investigated. Dynamic

mechanical properties, compression properties and flexural behaviors of composites were evaluated.

In professor Kapila's group at University of Missouri-rolla, a novel soy-based resin system for pultrusion has been synthesized [45]. The effect of pultrusion process variables on the cure of composites was studied with the combination of experimental and numerical methods [46]. The results indicate that the soy-based epoxy resin is suitable for application in pultrusion process. Co-resin systems contain EPON epoxy and one of the three types of soyate resins up to 30% were successfully applied in pultrusion process. Mechanical properties of the resulting composites were evaluated. Tests results indicate that epoxy resin could contain up to 30% soyate resin with similar or improved mechanical properties [47]. Partially replacing epoxy with soyate resin will not only lower the cost but also reduce the pulling force significantly.

1.4 **Research Objectives**

The objectives of this project are to further characterize the ROMP-based biopolymer system to explore potential applications based on properties, further improve properties of the glass fiber reinforced ROMP-polymer composites through enhancing interface quality, develop appropriate resin formulations with the ROMP-based biopolymers and to apply those resins in the pultrusion process to make glass fiber reinforced composites, finally evaluate short and long-term performances and durability of the biopolymer and composites. The specific objectives for each sub-project are listed below.

Tensile testing of ROMP-based Dilulin/DCPD copolymers showed that these materials exhibit good toughness properties with optimized composition. Therefore, the fracture toughness properties of this copolymer system will be investigated with the relatively new essential work of fracture (EWF) method. Dynamic mechanical analysis (DMA) and scanning electron microscopy (SEM) will be used to examine the phase separation and morphologies in the copolymers. The correlation between toughness and microstructure will be discussed thoroughly.

Previous study of glass fiber reinforced Dilulin/DCPD copolymer composites have shown that poor interface existed in these materials. Two types of silane coupling agents are selected to do the surface modification of glass fiber. Interfacial shear strength will be evaluated with microbond technique. Mechanical and thermo-mechanical properties will be examined with short beam shear test and DMA. The observation of morphologies of the fracture surfaces will be done with SEM. The best silane selected after this study will be used in the pultrusion process in the future.

A table-top pultrusion machine will be built for running experiments in lab-scale. Resin formulation with right percentages of lubricant and clay filler will be developed based on Dil30DCPD70 (containing 30 % Dilulin in weight) copolymer, because this composition possesses properties that may have the best combination of processing abilities and mechanical properties for pultrusion manufacturing. Processing parameters, such as die temperature, line speed, and fiber content, will be optimized based on processing performances. Finally, the best silane for Dilulin/DCPD system will be

applied with a simple method. The influences of silane concentration will be examined with DMA, flexure test and SEM.

The short-term strength and durability of the Dilulin30DCPD70 copolymer will be evaluated through accelerated aging and environmental exposure. Mechanical properties after aging will be examined with tensile test. Soxhlet extraction combined with ^{1}H NMR will be used to study the aging effects on cross-link density. The exposed surfaces and cross-sectional surfaces of aged samples will be observed with SEM. Chemical evolution during aging process will be analyzed with Fourier transform infrared photo-acoustic spectroscopy (PAS-FTIR).

1.5 References

[1] K Van de Velde, P Kiekens (2002) Polym Test 21: 433.

[2] Y Xia, RC Larock (2010) Green Chem 12: 1893.

[3] YS Lu, RC Larock (2009) Chemsuschem 2: 136.

[4] PK Mallick (2008) Fiber-reinforced composites : materials, manufacturing, and design. CRC Press, Boca Raton, FL

[5] TF Starr (2000) Pultrusion for engineers. CRC Press, Boca Raton, FL

[6] MAR Meier, JO Metzger, US Schubert (2007) Chem Soc Rev 36: 1788. Doi:Doi 10.1039/B703294c

[7] M Valverde, D Andjelkovic, PP Kundu, RC Larock (2008) J Appl Polym Sci 107: 423.

[8] PH Henna, DD Andjelkovic, PP Kundu, RC Larock (2007) J Appl Polym Sci 104: 979.

[9] DD Andjelkovic, M Valverde, P Henna, FK Li, RC Larock (2005) Polymer 46: 9674.

[10] DD Andjelkovic, YS Lu, MR Kessler, RC Larock (2009) Macromol Mater Eng 294: 472. Doi:DOI 10.1002/mame.200900053

[11] Y Xia, PH Henna, RC Larock (2009) Macromol Mater Eng 294: 590.

[12] P Henna, RC Larock (2009) J Appl Polym Sci 112: 1788.

[13] TC Mauldin, K Haman, X Sheng, P Henna, RC Larock, MR Kessler (2008) J Polym Sci Pol Chem 46: 6851. Doi:Doi 10.1002/Pola.22995

[14] PH Henna, MR Kessler, RC Larock (2008) Macromol Mater Eng 293: 979.

[15] Y Xia, YS Lu, RC Larock (2010) Polymer 51: 53.

[16] AR Bunsell, J Renard (2005) Fundamentals of fibre reinforced composite materials. Institute of Physics Publishing, Bristol

[17] K Friedrich, S Fakirov, Z Zhang (2005) Polymer composites : from nano-to-macro-scale. Springer, New York

[18] J-K Kim, YW Mai (1998) Engineered interfaces in fiber reinforced composites. Elsevier Sciences, Amsterdam ; New York

[19] AT DiBenedetto (2001) Mat Sci Eng a-Struct 302: 74. Doi:Doi 10.1016/S0921-5093(00)01357-5

[20] EP Plueddemann (1991) Silane coupling agents. Plenum Press, New York

[21] EP Plueddemann (1974) Interfaces in polymer matrix composites. Academic Press, New York,

[22] JL Koenig, H Emadipour (1985) Polym Composite 6: 142. Doi:Doi 10.1002/Pc.750060303

[23] S Debnath, SL Wunder, JI McCool, GR Baran (2003) Dent Mater 19: 441. Doi:Doi 10.1016/S0109-5641(02)00089-1

[24] CM Halliwell, AEG Cass (2001) Anal Chem 73: 2476. Doi:Doi 10.1021/Ac0010633

[25] SJ Park, JS Jin (2001) J Colloid Interf Sci 242: 174. Doi:DOI 10.1006/jcis.2001.7788

[26] U Schubert, N Hüsing (2000) Synthesis of inorganic materials. Wiley-VCH, Weinheim

[27] CM Bertelsen, FJ Boerio (2001) Prog Org Coat 41: 239. Doi:Doi 10.1016/S0300-9440(01)00135-7

[28] CM Vaz, RL Reis, AM Cunha (2002) Biomaterials 23: 629. Doi:Doi 10.1016/S0142-9612(01)00150-8

[29] S Naviroj, SR Culler, JL Koenig, H Ishida (1984) J Colloid Interf Sci 97: 308. Doi:Doi 10.1016/0021-9797(84)90301-1

[30] D Suryanarayana, KL Mittal (1984) J Appl Polym Sci 29: 2039. Doi:DOI 10.1002/app.1984.070290612

[31] H Watson, A Norstrom, A Torrkulla, J Rosenholm (2001) J Colloid Interf Sci 238: 136. Doi:DOI 10.1006/jcis.2001.7506

[32] MW Daniels, LF Francis (1998) J Colloid Interf Sci 205: 191. Doi:DOI 10.1006/jcis.1998.5671

[33] H Ishida, JL Koenig (1980) J Polym Sci Pol Phys 18: 233. Doi:DOI 10.1002/pol.1980.180180206

[34] PJ Herrerafranco, LT Drzal (1992) Composites 23: 2.

[35] BT Åström (1997) Manufacturing of polymer composites. Chapman & Hall, London

[36] FC Campbell (2004) Manufacturing processes for advanced composites. Elsevier, Oxford, UK ; New York

[37] O Faruk, AK Bledzki, HP Fink, M Sain (2012) Prog Polym Sci 37: 1552. Doi:DOI 10.1016/j.progpolymsci.2012.04.003

[38] DN Saheb, JP Jog (1999) Adv Polym Tech 18: 351. Doi:Doi 10.1002/(Sici)1098-2329(199924)18:4<351::Aid-Adv6>3.3.Co;2-O

[39] I Angelov, S Wiedmer, M Evstatiev, K Friedrich, G Mennig (2007) Compos Part a-Appl S 38: 1431. Doi:DOI 10.1016/j.compositesa.2006.01.024

[40] MH Zamri, HM Akil, A Abu Bakar, ZAM Ishak, LW Cheng (2012) J Compos Mater 46: 51. Doi:Doi 10.1177/0021998311410488

[41] X Peng, MZ Fan, J Hartley, M Al-Zubaidy (2012) J Compos Mater 46: 237. Doi:Doi 10.1177/0021998311410474

[42] N Nosbi, HM Akil, ZAM Ishak, A Abu Bakar (2010) Mater Design 31: 4960. Doi:DOI 10.1016/j.matdes.2010.04.037

[43] MF Omar, HM Akil, ZA Ahmad, AAM Mazuki, T Yokoyama (2010) Mater Design 31: 4209. Doi:DOI 10.1016/j.matdes.2010.04.036

[44] HM Akil, IM De Rosa, C Santulli, F Sarasini (2010) Mat Sci Eng a-Struct 527: 2942. Doi:DOI 10.1016/j.msea.2010.01.028

[45] J Zhu, K Chandrashekhara, V Flanigan, S Kapila (2004) J Appl Polym Sci 91: 3513. Doi:Doi 10.1002/App.13571

[46] G Liang, A Garg, K Chandrashekhara, V Flanigan, S Kapila (2005) J Reinf Plast Comp 24: 1509. Doi:Doi 10.1177/0731684405050387

[47] J Zhu, K Chandrashekhara, V Flanigan, S Kapila (2004) Compos Part a-Appl S 35: 95. Doi:DOI 10.1016/j.compositesa.2003.08.007

CHAPTER 2: MORPHOLOGY AND FRACTURE TOUGHNESS OF BIO-BASED DILULIN/DCPD COPOLYMERS

A paper to be submitted to *J of materials Science*

Hongyu Cui[1], Michael R. Kessler[2,3]

2.1 Abstract

The fracture toughness of a series of bio-based Dilulin/DCPD copolymers was evaluated by utilizing the essential work of fracture method and the structure-fracture property relationship was thoroughly analyzed. Both DMA and SEM demonstrated a reaction-induced phase separation in the copolymers. The copolymers' composition-dependent morphologies showed a significant effect on their fracture behavior. The maximum value for the essential work of fracture was found with Dil30DCPD70 composites, which may be explained by their less heterogeneous structure and high cross-link density. The highest non-essential work of fracture was observed with samples made from Dil40DCPD60, which is possibly a consequence of the formation of a rigid DCPD-phase.

Keywords: copolymer, essential work of fracture, morphology

2.2 Introduction

In recent years, the development of polymeric materials from bio-renewable resources has attracted increasing attention as a promising, alternative route to the use of

[1] Dept. of Materials Science and Engineering, Iowa State University, Ames, IA

[2] School of Mechanical and Materials Engineering, Washington State University, Pullman, WA

[3] Author for correspondence.

petroleum-based polymers. Both the finite petroleum resources and the environmental impact of plastics made from petroleum raw materials have driven these efforts [1, 2]. Vegetable oils are renewable feedstocks available in very large quantities at affordable cost and tung oil and linseed oil for example have been used in paints and coatings for centuries. Vegetable oils are generally triglyceride esters of fatty acids with varying numbers of carbons and unsaturated bonds in the fatty acid chain depending on the specific oil. The existence of unsaturated bonds in the structure make oils can be chemically modified and then polymerized or be polymerized directly. A wide range of bio-based polymers have been synthesized from vegetable oils or their derivatives using free radical, cationic, or ring opening metathesis polymerization (ROMP) methods [3-6].

Henna [3] developed novel thermoset copolymers from modified linseed oil (Dilulin) and dicyclopentadiene (DCPD) using ROMP. Varying the compositions led to a series of materials that ranged from hard and rigid to soft and ductile. Tensile testing revealed that copolymers with 30% Dilulin were tough, exhibiting up to 100% breaking strain and good tensile strength of more than 30 MPa. The cured samples were opaque, indicating the presence of phase separation. It was shown that the morphology of materials strongly affects their toughness [7]. It is of interest to measure the fracture toughness and understand the structure/fracture property relationships in these copolymeric systems.

In general, the fracture toughness of highly ductile polymer materials under large-scale plastic deformation is characterized by the well-established *J*-integral method. However, the strict size requirements and multiple specimen test procedure

greatly limit the application of this method. Recently, a new test method, based on the concept of the essential work of fracture (EWF) [8], was proposed to characterize the fracture toughness of ductile materials. The essential work of fracture (EWF) concept was first proposed by Broberg [9, 10] and then further developed by Cottrell and Reddel [8]. The EWF method becomes more popular for studying the fracture behavior of polymeric materials [11-17] due to the simple experimental procedures and loose dimensions requirements of specimens.

The aim of this study was to characterize the toughness of Dilulin/DCPD blend copolymers with different compositions by applying the essential work of fracture method (EWF) on deeply double-edge notched (DDENT) specimens. The validity of using EWF with the bio-based copolymers was analyzed. In addition, the correlation between phase morphology and fracture properties was thoroughly investigated.

2.3 Essential Work of Fracture

When utilizing the EWF method, the fracture area of a ductile material is divided into two different regions, as shown in Figure 2-1a: the inner process zone where the actual fracture takes place and the outer plastic deformation zone where various types of plastic deformation, such as shear yielding and microvoiding, may occur. Accordingly, the total work of fracture (W_f) can be separated into two parts: the essential work of fracture (W_e) and the non-essential work of fracture (W_p). W_e is the energy dissipated in the process zone to create new fracture surfaces, and W_p is the energy consumed by plastic deformation around the crack. Therefore, the total work of fracture can be written as

$$W_f = W_e + W_p \tag{1}$$

Physically, W_e is a surface energy that is proportional to the ligament length, l, for a given specimen thickness. W_p is a volume energy that is proportional to l^2 for a given specimen thickness t. Thus the total work of fracture can be rewritten as

$$W_f = w_e \cdot tl + \beta w_p \cdot tl^2 \tag{2}$$

Where t is the specimen thickness and β is a shape factor associated with the dimension of the plastic zone. The specific work of fracture w_f is obtained after dividing W_f by the ligament area tl:

$$w_f = \frac{W_f}{tl} = w_e + \beta w_p \cdot l \tag{3}$$

Where the w_e and w_p are the specific essential work of fracture and the specific non-essential work of fracture, respectively. If it is assumed that both w_e and w_p are material constants and β is independent of l, a linear relationship between w_f and l should be expected when w_f is plotted against l according to Eq. (3), see Figure 2-1b. Then w_e can be determined by extrapolating the fitting line to zero ligament length and the slope of the line gives βw_p.

For a valid EWF test, the following requirements must be satisfied: (1) the ligament of the specimen is fully yielded prior to crack propagation; (2) the ligament length must be large enough to ensure that fracture is under pure plane-stress conditions. When the ligament length is reduced below a critical value, the stress state will be in a mixed mode of both plane-stress and plane-strain characteristics. In the mixed mode region, the variation of w_f with ligament length often tends to be non-

linear, as shown in Figure 2-1b. Therefore, the minimum ligament length should be set to a value greater than three to five times the specimen thickness; (3) the load-displacement curves of different ligaments should be similar in shape. The validity of the EWF approach for our materials will be discussed in a later section.

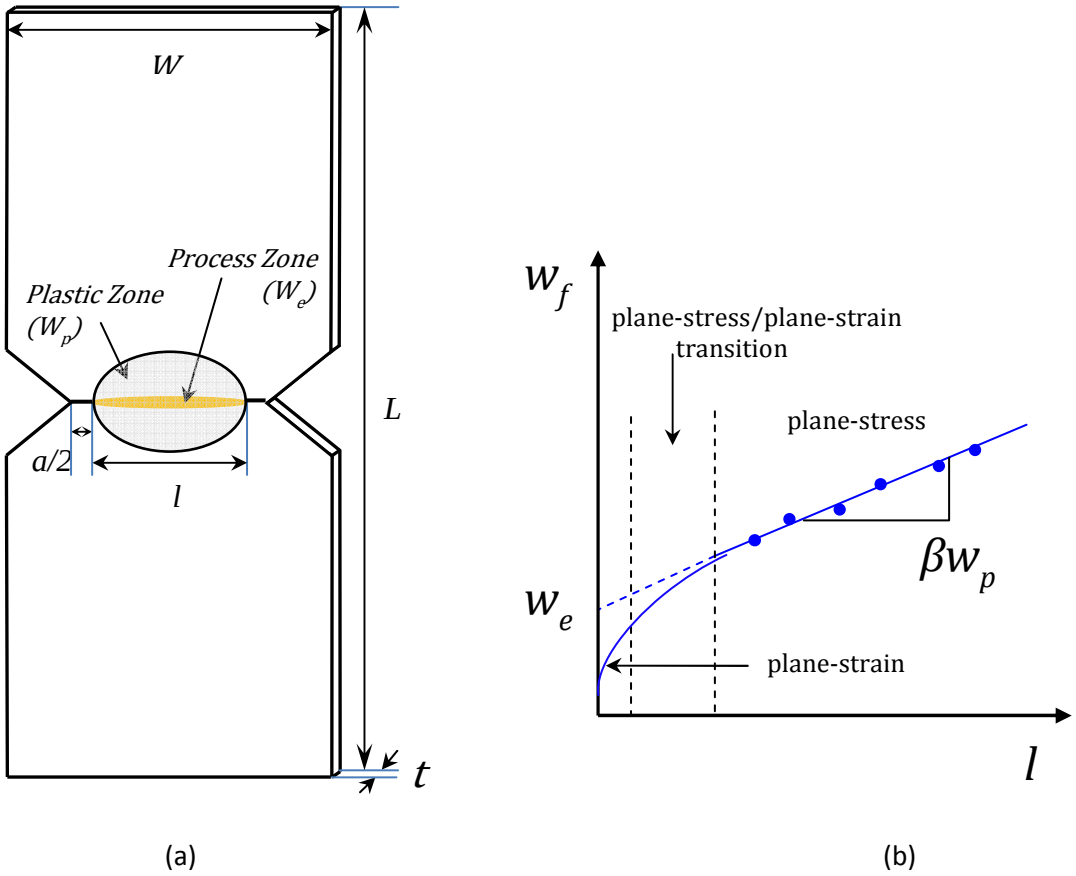

Figure 2-1 Schematic diagram of the essential work of fracture (EWF) approach: (a) the deeply double edge notched tensile (DDENT) specimen with two energy dissipation zones; (b) a curve of specific total work of fracture vs. ligament length.

2.4 Experimental

2.4.1 Sample Preparation

Dicyclopentadiene (DCPD) and 2nd generation Grubbs' catalyst were purchased from Sigma-Aldrich (Milwaukee, WI). Dilulin is commercially available from Cargill

(MN). It is synthesized from linseed oil and dicyclopentadiene through a high temperature, high pressure Diels-Alder reaction. The chemical structure of Dilulin has been studied thoroughly by NMR and FTIR, revealing an average of one norbornene ring pendant group per triglyceride [3, 18]. Grubbs' catalyst was recrystallized by freeze-drying from benzene [19] to allow better dissolution in the resin. A series of bio-renewable polymers with Dilulin content ranging from 20 wt.% to 50 wt.% was prepared with a modified injection molding method. The mold consisted of a rubber gasket sandwiched between two glass plates. Resin was injected slowly from the top of the mold with a syringe and then cured in a convection oven with a cure schedule of 1 h at 65 °C and subsequent 3 h at 150 °C.

2.4.2 Test Procedure

The EWF fracture tests were performed with deeply double edge notched-tension (DDENT) specimens on an Instron 5569 universal testing machine (50 kN load cell and Bluehill software) at a crosshead speed of 2 mm/min. The DDENT specimen had an overall height of 100 mm, a width of 30 mm, and a constant thickness of 1.0 mm. Specimens were pre-notched with a V-shaped punch press machine, and subsequently the notch was sharpened using a fresh razor blade. Eight ligament lengths, varying from 2 mm to 16 mm with an interval of 2 mm, were prepared to determine the value of w_e. For specimens made from Dil50DCPD50, the ligament length was controlled within 10 mm with a smaller steps to avoid the edge effect. Three specimens were tested for each ligament length to calculate the average value of w_f. The load-displacement curve for

each test was recorded for further analysis. The ligament length was measured with a microscope after fracture.

Tests to determine the dynamic mechanical properties of the copolymers were carried out using a TA Q800 dynamic mechanical analyzer (DMA) in tension mode. Tests were operated with an oscillation amplitude of 10 μm, a preload force of 0.01 N, and a force track of 125%. Samples were cooled down to –20 °C and held isothermally for 2 min, followed by heating them to 250 °C at a rate of 3 °C/min. The glass transition temperature (T_g) was determined by the peak of the tan δ curve.

The fracture surfaces of the DDENT specimens were investigated using a field-emission scanning electron microscope (FE-SEM, FEI Quanta 250) operating at 8 kV in high vacuum to correlate the microstructure and the fracture behavior. The samples was sputtered with 5 nm Iridium film.

2.5 **Results and Discussion**

2.5.1 DMA Test

Figure 2-2a shows the temperature dependence of the storage modulus, E', and of tan δ for biopolymers with varied Dilulin content. As shown in Figure 2-2a, the storage modulus curves shift to lower temperatures with increasing amount of Dilulin. According to the theory of rubber elasticity, the crosslink density of a thermoset can be estimated with the following equation:

$$E' = 3\nu_e RT \tag{1}$$

where E' is the storage modulus in the rubbery plateau region, υ_e is the crosslink density, R is the gas constant, and T is the absolute temperature in K [20]. The storage

modulus in the rubbery state (~150 °C) decreased with increasing Dilulin content, indicating that higher levels of incorporated Dilulin will lower the crosslink density. From Figure 2-2a we can see that the storage modulus at room temperature (25 °C) also decreased significantly with the increasing amount of Dilulin incorporated in copolymers, apparently due to the reduction of crosslink density.

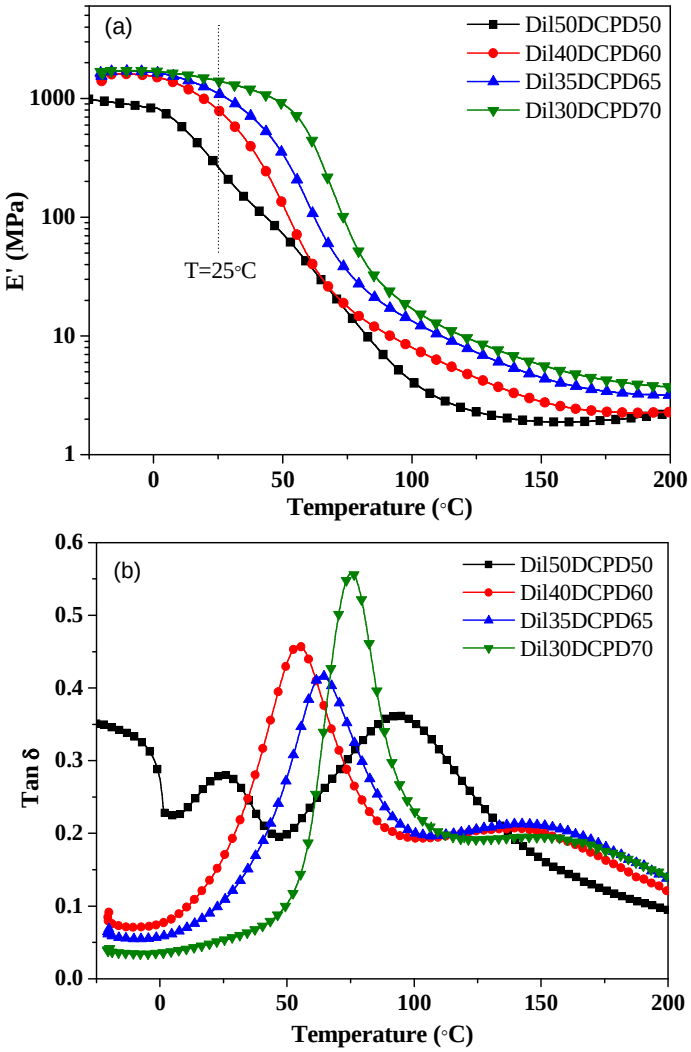

Figure 2-2 (a) Storage modulus of Dilulin/DCPD copolymers as a function of temperature; (b) tan δ of Dilulin/DCPD copolymers as a function of temperature

Dynamic mechanical analysis not only provides information about the viscoelastic properties, but also about the phase structure of a material. The tan δ curves for different Dilulin/DCPD copolymers are shown in Figure 2-2b. It can be seen that for copolymers with less than 50% Dilulin, the curves exhibited one sharp relaxation peak and one broad shoulder to the right. This shoulder at higher temperatures corresponded to the T_g of the DCPD-rich phase while the sharp peak corresponded to the T_g of the Dilulin-rich phase. For copolymers containing 50% Dilulin, the broad shoulder representing the DCPD-rich phase grew and became a new peak at around 100 °C, with both peaks significantly shifting to lower temperatures. As the Dilulin content increased, the T_g for both phases shifted to lower temperatures. The decrease in T_g was attributed to the reduction in cross-link density in each phase. Each triglyceride in Dilulin has only one norbornene group that can undergo ROMP to form a crosslink structure with DCPD. The addition of Dilulin reduced the cross-link density of the copolymers and increased the flexibility of the cross-linked structure. In all cases, the T_g of the DCPD-rich phase was slightly lower than the T_g of neat poly-DCPD, which is at 153.9 °C as reported in [21]. This shows that the DCPD-rich phase has some Dilulin molecules involved in the cross-linked structure.

2.5.2 SEM of Phase Separation

All uncured Dilulin/DCPD blends were initially homogeneous as clear mixture. However, the cured Dilulin/DCPD copolymers displayed decreased transparency and gradually became opaque with increasing Dilulin content, indicating reaction-induced phase separation, which is commonly seen in reactive copolymers. As we mentioned

earlier, Dilulin monomers have only one reactive norbornene group per triglyceride. In addition, long fatty acid chains in the Dilulin molecule greatly reduce its molecular mobility. Compared to DCPD, Dilulin exhibits relatively low reactivity during ring opening metathesis polymerization. We observed that pure DCPD turned solid in 30 s after the addition of Grubbs' catalyst at room temperature. Blends with 30% Dilulin gelled in 45 min after the addition of the catalyst at room temperature. The phase separation seen in the different blends was attributed to the differences in reactivity between DCPD and Dilulin monomers.

The morphologies of the cured Dilulin/DCPD copolymers were investigated by SEM, as shown in Figure 2-3. The specimens were fractured under cryogenic conditions (liquid nitrogen). All fracture surfaces in Figure 3 exhibited the characteristics of brittle fracture. The SEM micrograph of the copolymer containing 30% Dilulin (Figure 2-3a) showed that the Dilulin-rich phase was homogeneous and the second phase barely detectable. As the Dilulin content increased, the DCPD-rich phase was more easily detected. Figure 2-3b shows a micrograph of a copolymer containing 40% Dilulin, in which the DCPD-rich phase is randomly dispersed in the Dilulin-rich phase. There is no uniform shape or size for the second phase, which is detected in clusters of many agglomerated small particles. Detailed features of the DCPD-rich phase are shown in Figure 2-3d.

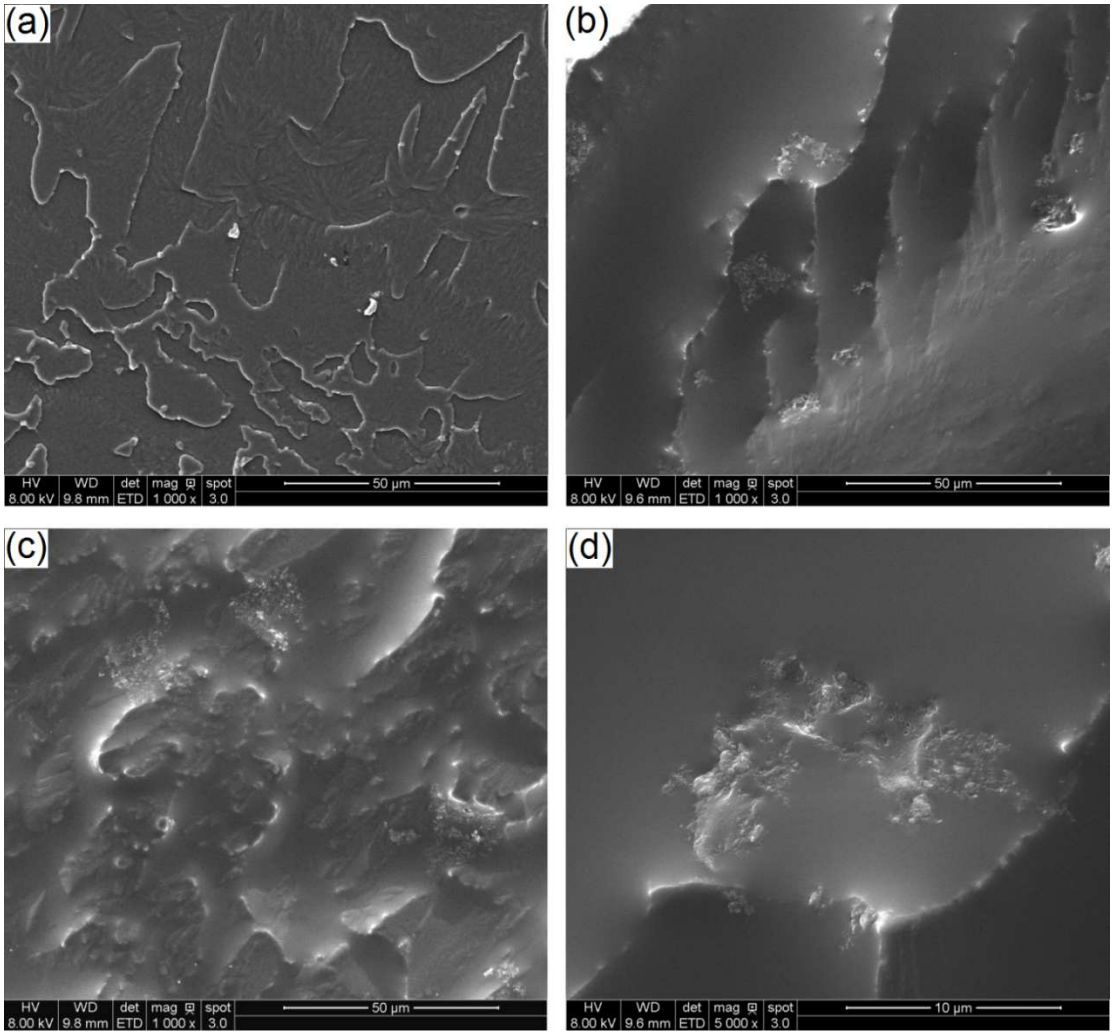

Figure 2-3 SEM micrographs of: (a) Dil30DCPD70, 500×; (b) Dil40DCPD60, 1000×; (c) Dil50DCPD50, 1000×; (d) Dil40DCPD60, 5000×

As the Dilulin content increased to 50%, a dual phase morphology was formed in which the two phases were present in almost equal parts (Figure 2-3c). DMA measurements showed that both phases in the Dil50DCPD50 copolymers showed lower glass transition temperatures compared to other compositions. As discussed earlier, the increase in Dilulin in the copolymer may have reduced the cross-link density in both phases. The changes in morphology and properties for each phase significantly influenced the fracture toughness of the copolymeric materials.

2.5.3 Fracture Test Analysis

Figure 2-4 shows typical load-displacement curves obtained with the DDENT specimens in EWF fracture tests for different Dilulin/DCPD copolymer compositions. Dil20DCPD80 showed typical brittle behavior while all other specimens exhibited ductile fracture behavior. The geometrical similarity between the curves for specimens with different ligament length observed for all compositions not only fulfilled an essential pre-requisite for EWF testing, but also indicated that the fracture mechanism was independent of ligament length. With the exception of Dil20DCPD80, all other specimens showed extensive crack tip yielding during fracture testing; however, the plastic deformation zone was not clearly visible. Thus, it could not be visually confirmed whether complete ligament yielding occurred at or prior to the maximum load.

Figure 2-4f illustrates the typical load-displacement curves for various Dilulin/DCPD copolymer compositions at a constant ligament length (≈ 10 mm). For a given ligament length, the maximum load decreased, while the displacement at break increased with increasing Dilulin content. The figure also shows a clear transition in the fracture mechanism from brittle to ductile caused by the increased Dilulin content in the copolymer. Dil20DCPD80 failed in brittle manner with unstable crack propagation. The deformation behavior of Dil30DCPD70 showed a prominent stress-drop after reaching the maximum, which corresponded to a full ligament yielding of the DDENT specimen, followed by crack propagation. The load-displacement curves for the 35/65, 40/60, and 50/50 Dilulin/DCPD copolymers indicate that the specimens failed by ductile tearing.

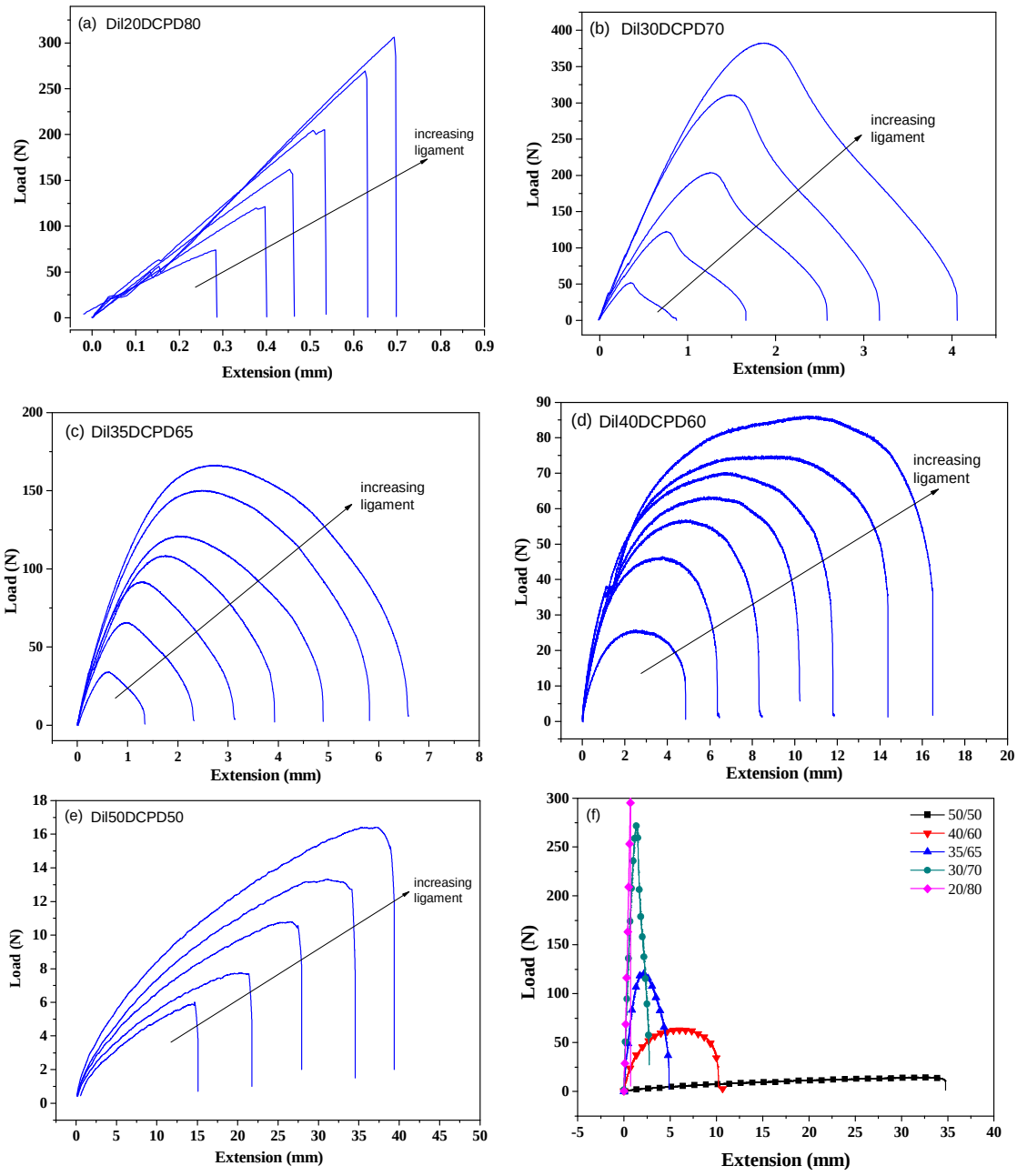

Figure 2-4 Load-displacement diagrams for Dilulin/DCPD copolymers with varied composition

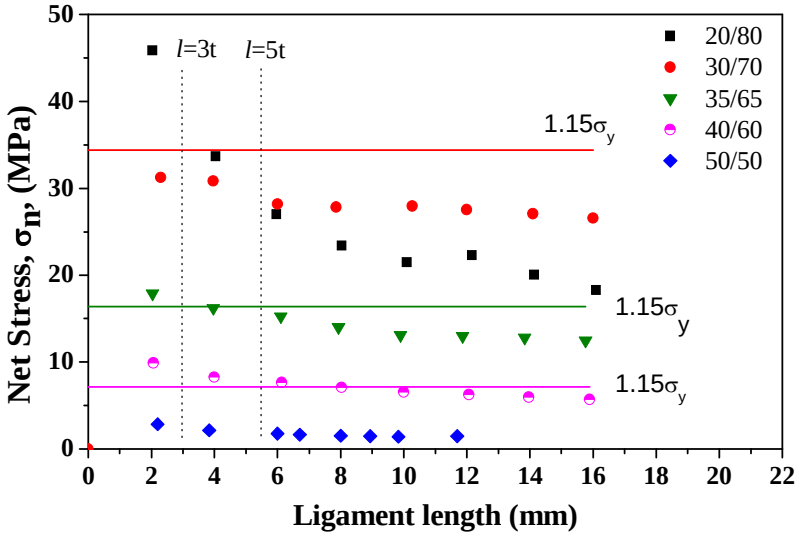

Figure 2-5 S_{max}/F_{max} as a measure of ductility for different Dilulin/DCPD copolymer compositions

The plane-stress condition was verified by measuring the net-section stress (maximum load divided by the ligament area) for different ligament lengths. According to Hill [22], the maximum value of the net-section stress, σ_n, is independent of or only weakly dependent on the ligament length. In the mixed fracture mode region, the net-section stress increased greatly with reduced ligament length. Following Hill's predictions, the theoretical values of the net-section stress for DDENT specimens are 1.15 σ_y (σ_y is the yield stress in tensile mode) for pure plane-stress conditions and 2.97 σ_y for pure plane-strain conditions, respectively [22].

Figure 2-5 shows change in net-section stress σ_n as a function of ligament length for Dilulin/DCPD copolymers with different compositions. The theoretical limits σ_y of the net-section stress for the 30/70, 35/65, and 40/60 Dilulin/DCPD compositions were also plotted in the same figure. The figure shows that the net-section stress increased

rapidly with reduced ligament length for Dil20DCPD80 copolymer specimens, indicating that a non-pure plane-stress condition existed during the fracture test. It is therefore not possible to measure the fracture toughness of Dil20DCPD80 using the EWF method. The net-section stress for all other compositions followed the same general trend of increasing slightly with decreasing ligament length. Only samples made from 40/60 composition show close to 1.15 σ_y. Other two compositions both have smaller values than the theoretical one. Ours is not the only case. Previous studies have shown that it is very common to see a greater or smaller net-section stress value than the theoretical value [14, 15, 23, 24]. As long as σ_n is not significantly affected by the ligament length, the EWF method should be applicable. The most widely accepted threshold for the minimum ligament length is 3 to 5 times of thickness; however, many researchers have demonstrated that there is no universal value for the transition point of the *l/t* ratio because it varies with the type of material [12, 14, 25, 26]. Figure 2-5 shows that the net section stresses didn't increased significantly when the ligament length fell into 2-4 mm. Therefore, all data points were used to calculate the essential work of fracture for our investigations.

The specific work of fracture was plotted versus the ligament length and the EWF specific fracture parameters were assessed by a linear regression according to the equation shown in Figure 2-6. As mentioned in the experimental section, w_e and βw_p were determined by taking the Y-intercept at zero ligament length and the slope of the linear regression line, respectively. It is worthwhile noting that the w_f-l diagrams provided very good linear regression coefficients. The essential work of fracture w_e and

the non-essential work of fracture βw_p are summarized in Figure 2-7. The calculation of the shape factor β was not considered because of the inaccuracy and complexity of its determination. As in other works in the literature, βw_p describes the plastic work evolution sufficiently for our purpose.

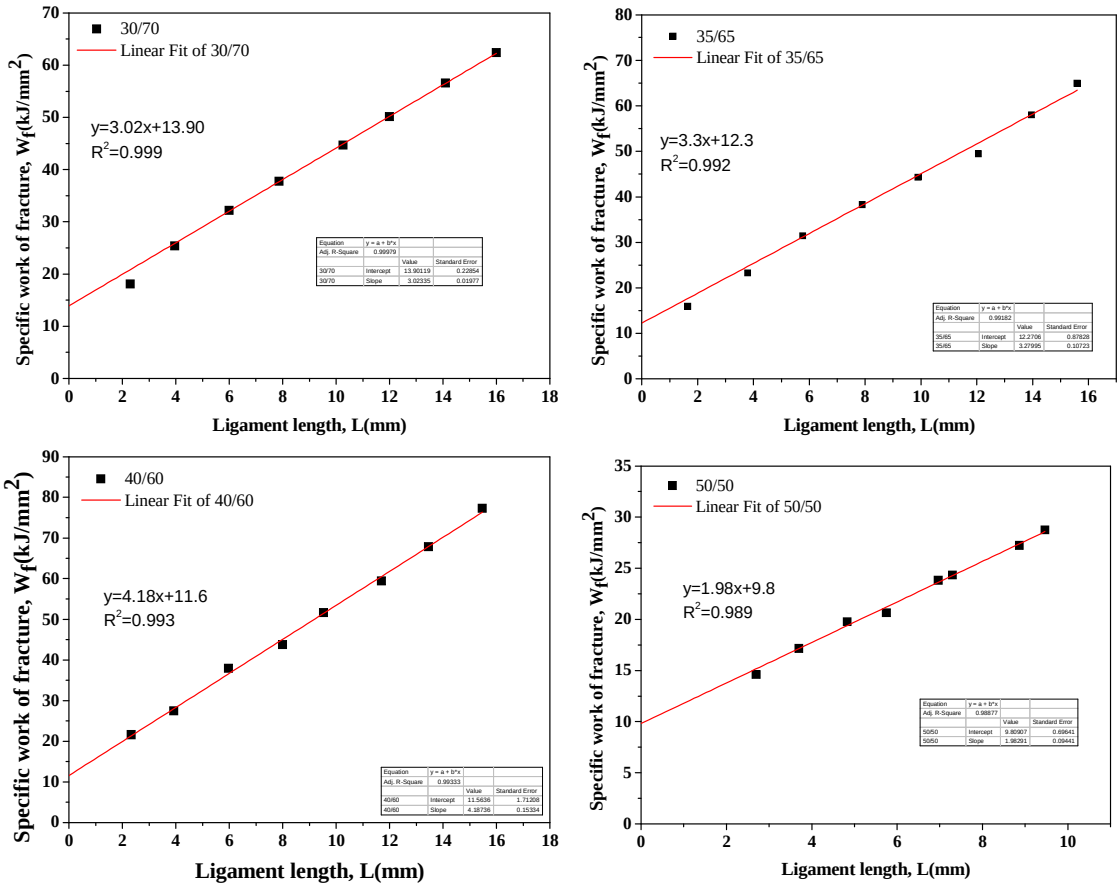

Figure 2-6 Specific work of fracture (w_e) versus ligament length (L) for Dilulin/DCPD copolymers of different compositions

Figure 2-7 shows that w_e decreased with increasing Dilulin content, and βw_p initially increased until it reached a critical Dilulin content and then dropped. Many studies have demonstrated that the specific essential work of fracture (w_e) is a measure of a material's resistance to crack initiation and the βw_p component is seen as a measure

of the resistance to crack propagation [14, 27]. The crack propagation resistance characterized by βw_p is a highly morphology-sensitive parameter while the crack initiation resistance, which is characterized by w_e, is matrix sensitive [28, 29]. Our investigation showed that as the Dilulin content increased in the copolymer, the major phase (Dilulin-rich phase) showed reduced thermo-mechanical properties because of the decrease in cross-link density. In addition, the strong heterogeneity seen in the micrographs increased the chance for crack initiation. Therefore, it was expected to see an increase in w_e with increasing Dilulin content. The nonessential work of fracture βw_p showed an increase when the Dilulin content increased from 30% to 40%, which was probably caused by the formation of a DCPD-rich phase. Compared to the Dilulin-rich phase, the DCPD phase has a higher T_g and acts as a hard reinforcement in a less stiff matrix, enhancing the copolymer's crack propagation resistance through a crack-pinning mechanism. When the rigid DCPD-phase interacts with a crack, it behaves like an impenetrable object, so that more energy is required for the crack to propagate. The morphology analysis of copolymers containing 30%-40% of Dilulin showed that with an increase in Dilulin content, more DCPD-rich phase was formed and those DCPD-rich phases act similar in different copolymers since similar shoulder peaks were observed in tan δ curves in DMA test. The increasing DCPD-rich phases resulted in an increase in resistance to crack propagation. It can be seen from the micrograph of the Dil50DCPD50 copolymer that, more DCPD-rich phases were formed. However, the T_g of the DCPD-rich phase shifted to lower temperatures significantly, indicating large property changes in these phases, which may be responsible for the sudden drop of βw_p.

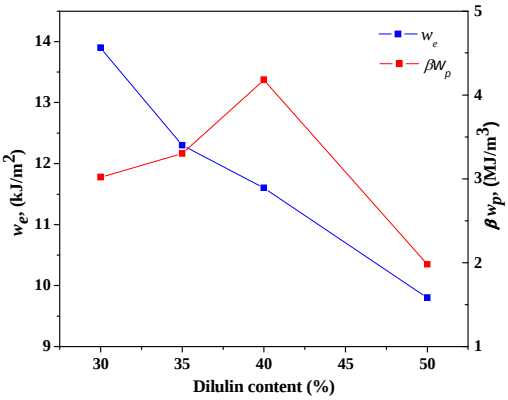

Figure 2-7 **w_e and βw_p for Dilulin/DCPD copolymers of different compositions**

2.5.4 Morphology of Fracture Surfaces

Figure 2-8 shows SEM micrographs of the fracture surfaces generated in the EWF tests. Morphological analyses revealed clear differences between the five blend compositions. Pre-crack fronts can be seen clearly in Figure 2-8a and c. Dil20DCPD80 (Figure 2-8a and b) exhibited relatively smooth fracture surfaces with the typical fractography features of brittle fracture behavior. Fan-shaped appearance was observed in Figure 2-8b, in which river lines point to an initiation site. Inclusions and second phase boundaries were typical initiation sites. The fracture surfaces of all other Dilulin/DCPD specimens showed large-scale shear yielding. The micrograph of Dil30DCPD70 clearly shows shear bands, which were formed by shear yielding during deformation. Close examination of the smooth area between shear bands shows river-like features aligned along the direction of crack propagation. In Figure 2-9, the fracture surface of Dil40DCPD60 shows more shear bands. It is worth noting that crack initiation started from multi-sites at the pre-crack front. These sub-cracks propagated simultaneously on slightly different crack planes normal to the tensile stress. And the

side boundaries of adjacent cracks is subjected to shear stress under tensile mode in EWF testing which leads to shear yielding and consumption of a large amount of strain energy in the deformation process. When the material at the crack boundaries failed under shear stress, adjacent cracks encountered with each other, a shear band was left behind as a result. The enlarged micrograph (Figure 2-9b) of the smooth area shows that a small piece of material was pulled out under shearing stress. Similar features were also seen on the fracture surface of Dil50DCPD50. As the amount of Dilulin increased in the copolymer, the fracture surface became rougher because of increased plastic flow on the fracture surface and the initial sites of sub-cracks that were formed as a result of increased heterogeneity.

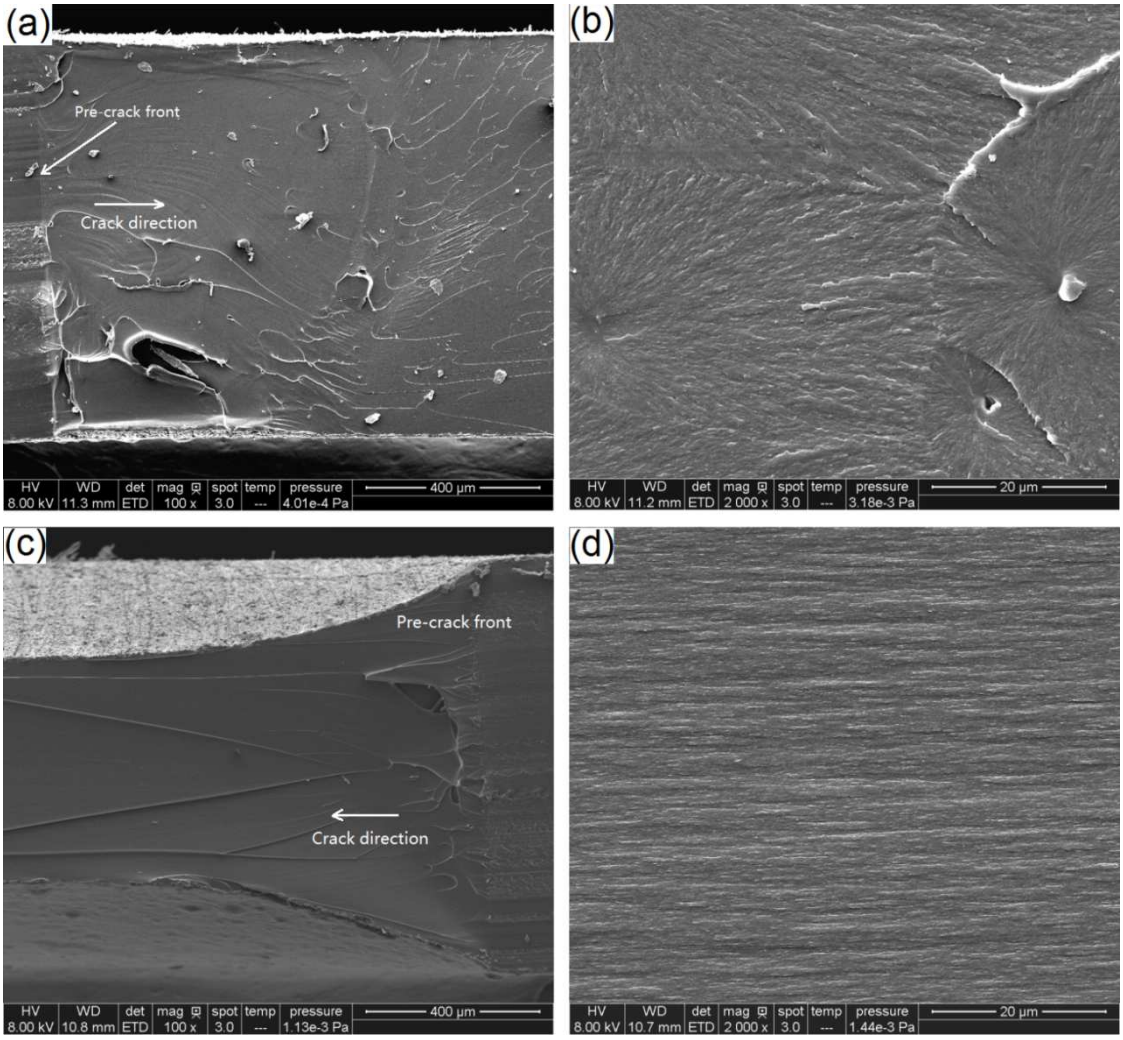

Figure 2-8 SEM micrographs of fracture surfaces: (a) Dil20DCPD80, 100×; (b) Dil20DCPD80, 2000×; (c) Dil30DCPD70, 100×; (d) Dil30DCPD70, 2000×.

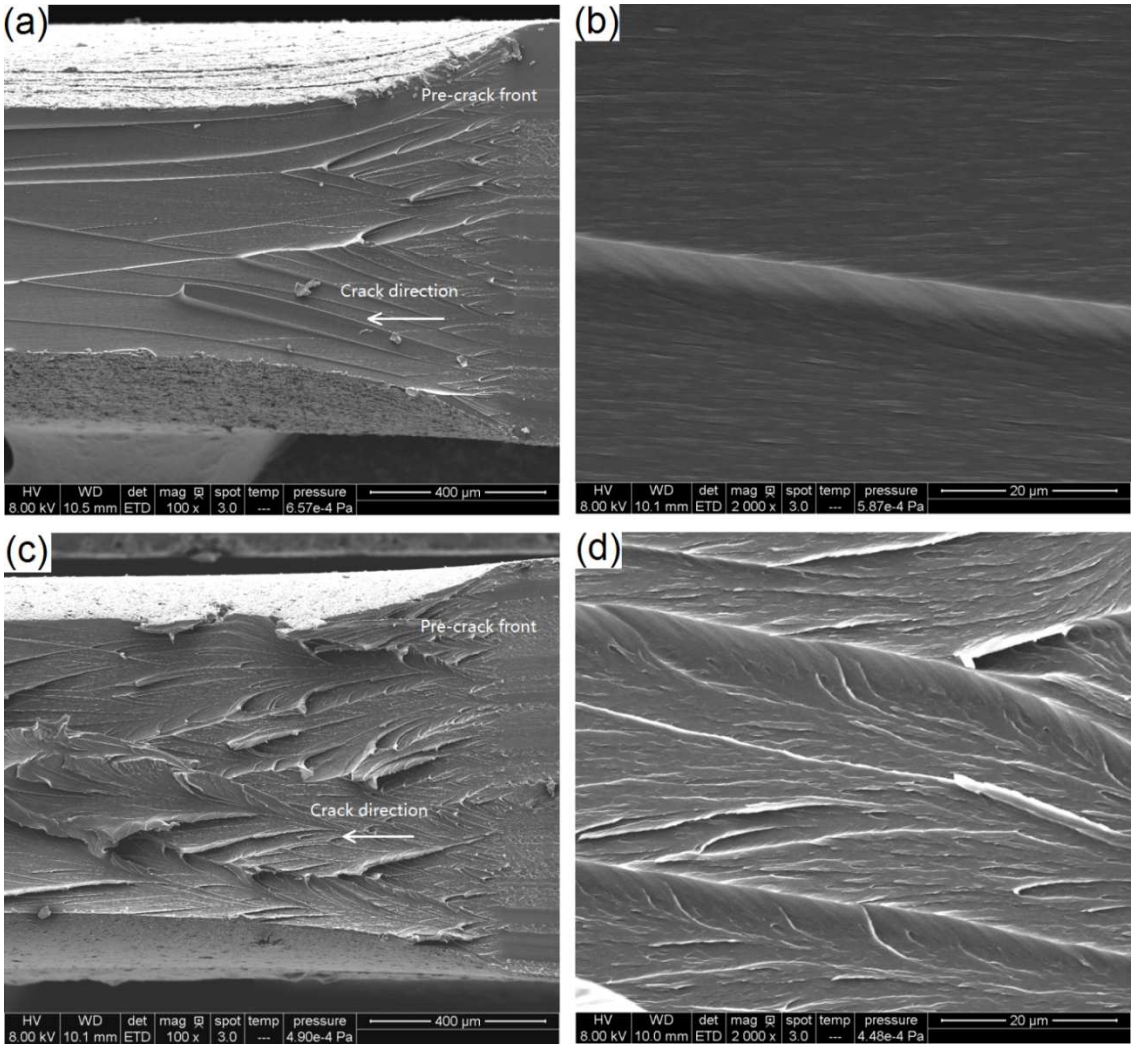

Figure 2-9 SEM micrographs of fracture surfaces: (a) Dil40DCPD60, 100×; (b) Dil40DCPD60, 2000×; (c) Dil50DCPD50, 100×; (d) Dil50DCPD50, 2000×.

2.6 **Conclusions**

DMA measurement revealed that the glass transition temperature of Dilulin/DCPD copolymers decreased with increasing Dilulin content because of a decrease in cross-link density. Two α-transition peaks on the tan δ curves indicated that reaction-induced phase separation occurred in the copolymer. SEM investigations confirmed that the morphologies of the Dilulin/DCPD copolymers were composition-

dependent. The Dilulin/DCPD copolymers showed significant variations in mechanical properties, ranging from very brittle to very ductile with only small changes in composition. The EWF concept is reasonable for evaluating the fracture toughness of copolymers with ductile properties. Our investigation indicated that the mechanical and fracture mechanical properties of Dilulin/DCPD copolymers are largely controlled by both composition and morphological structure. Fracture surface analysis by SEM revealed a clear transition in the fracture mechanism from brittle failure to ductile failure as the incorporation of Dilulin increased. The increased resistance to crack propagation of Dil40DCPD60, indicated by the maximum in the non-essential work of fracture, was attributed to the formation of a rigid DCPD-phase that toughened the copolymer through a crack pinning mechanism. The highest essential work of fracture (as measurement of resistance to crack initiation) was observed for Dil30DCPD70 and was probably the result of its less heterogeneous structure and high cross-link density.

2.7 References

[1] M Eissen, JO Metzger, E Schmidt, U Schneidewind (2002) Angew Chem Int Edit 41: 414. Doi:Doi 10.1002/1521-3773(20020201)41:3<414::Aid-Anie414>3.0.Co;2-N

[2] MAR Meier, JO Metzger, US Schubert (2007) Chem Soc Rev 36: 1788. Doi:Doi 10.1039/B703294c

[3] P Henna, RC Larock (2009) J Appl Polym Sci 112: 1788.

[4] YS Lu, RC Larock (2009) Chemsuschem 2: 136.

[5] Y Xia, RC Larock (2010) Green Chem 12: 1893.

[6] Y Xia, YS Lu, RC Larock (2010) Polymer 51: 53.

[7] SH Wu (1985) Polymer 26: 1855. Doi:Doi 10.1016/0032-3861(85)90015-1

[8] B Cotterell, JK Reddel (1977) Int J Fracture 13: 267.

[9] KB Borberg (1968) Int J Fract Mech 4: 11.

[10] KB Broberg (1975) J Mech Phys Solids 23: 215. Doi:Doi 10.1016/0022-5096(75)90017-4

[11] YW Mai, B Cotterell (1986) Int J Fracture 32: 105. Doi:Doi 10.1007/Bf00019787

[12] YW Mai, B Cotterell, R Horlyck, G Vigna (1987) Polym Eng Sci 27: 804. Doi:DOI 10.1002/pen.760271106

[13] J KargerKocsis (1996) Polym Bull 37: 119. Doi:Doi 10.1007/Bf00313827

[14] JS Wu, YW Mai (1996) Polym Eng Sci 36: 2275. Doi:Doi 10.1002/Pen.10626

[15] S Hashemi (1997) J Mater Sci 32: 1563. Doi:Doi 10.1023/A:1018582707419

[16] J KargerKocsis, T Czigany, EJ Moskala (1997) Polymer 38: 4587. Doi:Doi 10.1016/S0032-3861(96)01061-0

[17] DE Mouzakis, F Stricker, R Mulhaupt, J Karger-Kocsis (1998) J Mater Sci 33: 2551. Doi:Doi 10.1023/A:1004345017105

[18] TC Mauldin, K Haman, X Sheng, P Henna, RC Larock, MR Kessler (2008) J Polym Sci Pol Chem 46: 6851. Doi:Doi 10.1002/Pola.22995

[19] AS Jones, JD Rule, JS Moore, SR White, NR Sottos (2006) Chem Mater 18: 1312.

[20] PJ Flory (1953) Principles of polymer chemistry. Cornell University Press, Ithaca,

[21] W Jeong, MR Kessler (2008) Chem Mater 20: 7060. Doi:Doi 10.1021/Cm8020947

[22] R Hill (1952) J Mech Phys Solids 1: 19. Doi:Doi 10.1016/0022-5096(52)90003-3

[23] A Arkhireyeva, S Hashemi (2002) Polymer 43: 289. Doi:Doi 10.1016/S0032-3861(01)00623-1

[24] J Karger-Kocsis, T Czigany, EJ Moskala (1998) Polymer 39: 3939. Doi:Doi 10.1016/S0032-3861(98)00029-9

[25] A Arkhireyeva, S Hashemi, M O'Brien (1999) J Mater Sci 34: 5961. Doi:Doi 10.1023/A:1004776627389

[26] ECY Ching, RKY Li, YW Mai (2000) Polym Eng Sci 40: 310. Doi:Doi 10.1002/Pen.11164

[27] G Levita, L Parisi, A Marchetti, L Bartolommei (1996) Polym Eng Sci 36: 2534. Doi:Doi 10.1002/Pen.10652

[28] SH Wu (1990) Polym Eng Sci 30: 753. Doi:DOI 10.1002/pen.760301302

[29] BK Satapathy, R Lach, R Weidisch, K Schneider, A Janke, K Knoll (2006) Eng Fract Mech 73: 2399. Doi:DOI 10.1016/j.engfracmech.2006.04.016

CHAPTER 3: GLASS FIBER REINFORCED ROMP-BASED BIO-RENEWABLE POLYMERS: ENHANCEMENT OF THE INTERFACE WITH SILANE COUPLING AGENTS

A paper published in *Composites Science and Technology*

Hongyu Cui[1], Michael R. Kessler[2,3]

3.1 **Abstract**

In this study, the influence of silane coupling agents on interfacial adhesion in glass fiber reinforced polymers from the ring-opening metathesis polymerization (ROMP) of a linseed oil-based monomer and dicyclopentadiene is investigated experimentally. Two types of silane coupling agents, norbornenylethyldimethylchlorosilane (MCS) and norbornenylethyltrichlorosilane (TCS), are examined. Interfacial shear strength (IFSS) is evaluated by the microbond technique. The IFSS increases by about 150% for the MCS-treated fibers and by about 50% for the TCS-treated fibers compared to untreated fibers. Dynamic mechanical analysis of composite panels made with untreated and silane-treated fibers reveals that MCS-treated fiber composites have the highest storage modulus and glass transition temperature, indicating strong interfacial interactions at the glass/matrix interface. Short beam shear tests and scanning electron microscopy of fracture surfaces also confirm that MCS is more effective than TCS at improving interfacial adhesion.

[1] Dept. of Materials Science and Engineering, Iowa State University, Ames, IA

[2] School of Mechanical and Materials Engineering, Washington State University, Pullman, WA

[3] Author for correspondence

Keywords: Bio-renewable polymer; A. Glass fibers; A. Coupling agents; B. Surface treatments; B. Interfacial strength

3.2 **Introduction**

Polymers and composite materials are typically derived from petroleum; however, due to increasing energy and environmental concerns, there is an increasing interest in the development of plastics from readily available renewable resources, such as vegetable oil. [1-2] At Iowa State University, a wide range of promising bio-based thermosets were produced in the past decade from original or modified vegetable oils [1-4], by using cationic, thermal, free radical and ring-opening metathesis polymerization methods [5-8]. The resulting polymers possess similar or even better thermal and mechanical properties than commercially available plastics, allowing the replacement of petroleum-based polymers in some applications. In addition, fillers can be introduced to bio-based polymers to create bio-based composites with even better mechanical properties compared with pure resin. Reinforcing phases investigated with these resins include glass fiber, carbon fiber, nanoparticles, nanotubes, and some natural fibers [9-11].

In the recent past, the ring-opening metathesis polymerization (ROMP) has become popular after the development of the highly effective Grubbs' ruthenium catalyst in the 1990s [12]. The ring-opening metathesis copolymerization of Dilulin with dicyclopentadiene (DCPD) has been studied by Henna [13]. Dilulin is a commercially available norbornene-modified linseed oil offered by Cargill, which on average contains one bicyclic moiety per triglyceride. The ROMP of Dilulin and DCPD is shown inFigure 3-1. The resulting polymers range from flexible to hard as DCPD content increases.

Short glass fiber mat reinforced Dilulin/DCPD resin composites were also prepared and examined. After reinforcement with glass fiber, the mechanical properties improved significantly. However, mechanical properties were lower than model predictions. This underperformance was attributed to the poor interface between the glass fiber and the polymer matrix which was observed in SEM images of the fracture surface.

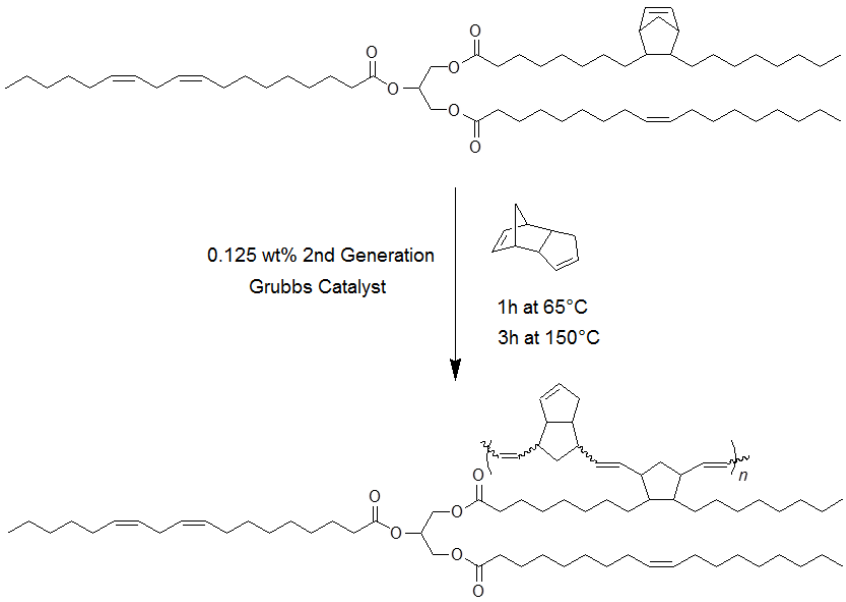

Figure 3-1 ROMP of Dilulin and DCPD

It is well known that the interphase quality between the matrix and reinforcement has significant effect on the ultimate properties of composite materials [14]. Good interfacial adhesion allows more effective stress transfer from the matrix to the reinforcement and increase the ultimate strength of the composite. Surface modification with silane coupling agents [15-17] is commonly used to improve interfacial adhesion in glass fiber reinforced polymer composites. Silane coupling agents are difunctional organosilicon compounds with the general structural formula R-Si-X_3, where X is a hydrolyzable group, such as alkoxy, chlorine, or acyloxy [18]. Following hydrolysis,

reactive silanol groups are formed, which can undergo condensation with hydroxyl groups on the glass fiber surface. The R group is a non-hydrolyzable group, which is able to react chemically with the polymer matrix. Silane coupling agents improve the interfacial adhesion by forming covalent bonds with both fiber and matrix.

In this paper, effects of different silanes on interfacial adhesion for glass fiber reinforced bio-renewable resins, are studied. Silane coupling agents with pendent norbornyl groups were selected to functionalize the glass fiber, because the norbornyl groups are compatible with the Dilulin/DCPD resin. Functionalized glass fibers are examined by X-ray photoelectron spectroscopy. The interfacial shear strength is evaluated using the microbond technique and short beam shear tests [14, 19-22]. In addition, effects of silane treatment on thermal and mechanical properties of composites are also studied.

3.3 **Experimental**

3.3.1 Materials and Glass Fiber Surface Modification

Dicyclopentadiene (DCPD) and 2nd generation Grubbs' catalyst were purchased from Sigma-Aldrich (Milwaukee, WI). Dilulin is a commercially available modified linseed oil from Cargill (MN), which is synthesized from linseed oil and cyclopentadiene. The resulting Dilulin monomer has approximately one norbornyl ring per triglyceride. Norbornenylethyldimethylchlorosilane (MCS) was obtained from Hybrid Plastics (Hattiesburg, MS). Norbornenylethyltrichlorosilane (TCS) was purchased from Gelest (Morrisville, PA). Chemical structures of the two types of silane are shown in Figure 3-2. Tetrahydrofuran (THF) was purchased from Fisher Scientific

(Pittsburgh, PA). THF was dried and distilled by refluxing with benzophenone and sodium. Second generation Grubbs' catalyst was recrystallized by freeze-drying from benzene [23] to allow better dissolution in the resin. Other chemicals were used as received, without further purification. Two types of glass fiber materials were used, unidirectional glass fiber and plain weave glass fabric (3.2 oz/sq yd), both of which were provided by Pella Company.

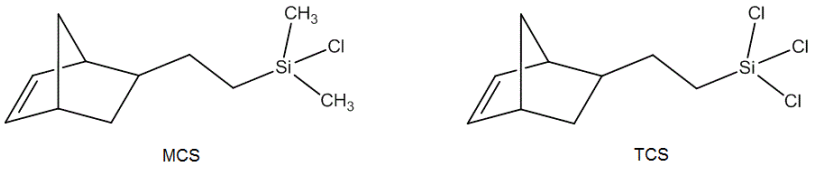

Figure 3-2 Chemical structures of MCS and TCS

The surface of the commercial glass fiber is covered by a thin layer of sizing to protect the single glass filaments from abrasion with neighboring fibers. Prior to surface modification with norbornene silane, the glass fiber was heat-cleaned at 450 °C for 3 h to remove pre-existing sizing and other impurities. Silane (MCS or TCS) and pyridine were mixed in dried THF to yield a silane concentration of 2% v/v and then heat-cleaned glass fibers were added. Surface modification reaction was carried out under reflux conditions at 90 °C for 48 h. After that, glass fabric was rinsed thoroughly with THF and then dried in an oven at 110 °C for 10 h. Four different types of fibers were evaluated: as received fibers with the original sizing (*untreated*), fibers in which the original sizing was removed using the heat-cleaning procedure described above (*heat-cleaned*), fibers in which the heat-cleaned fibers are further reacted with the MCS (*MCS-treated*) or with the TCS (*TCS-treated*). Unidirectional fiber was used to prepare microbond samples and

plain weave fabric was used to prepare all other samples (include XPS samples and composite laminates).

3.3.2 Fabrication of Glass Fiber Reinforced Bio-resin Composites

Based on previous results regarding ring-opening metathesis polymerization of Dilulin and DCPD [13], a composition of 30 wt.% Dilulin and 70 wt.% DCPD was selected because of its relatively high mechanical properties (strength and stiffness) compared to other compositions. Resin was prepared on an 80 g scale. After Dilulin and DCPD were mixed well, 100 mg (0.125 wt.%) recrystallized 2^{nd} generation Grubbs' catalyst was added and stirred evenly. The composites were made by hand-layup method. Twenty plies glass fabric were placed in a mold one by one and resin was added after each fabric to wet it out. Then the mold was pre-cured on a hot press at 65 °C and 689 kPa for 1 h followed by post-cure at 150 °C for 3 h in a convection oven. The resulting composites had a nominal weight fraction of glass fiber of 50%.

3.3.3 Characterization

Surface elemental concentrations for different treated glass fibers were obtained using X-ray photoelectron spectroscopy (XPS, PHI55000) with an Al Kα (1486.6 eV) source. Microbond pull-out tests were carried out on a dynamic mechanical analyzer (DMA) (Model Q800, TA Instruments) with tension clamp and iso-strain mode. Figure 3-3 (a) shows a schematic representation of the microbond technique. Small microdrops, diameter range of 300-400 µm, were placed on a single glass fiber (25 µm in diameter) and cured in place. During testing, one end of the fiber was attached to the fixed load

frame of the tension fixture, and the microdrop was gripped by a microvise. When the microvise moved downward at a rate of 1 μm/s, the load and displacement signals were recorded until pull-out occurred. The interfacial shear strength (IFSS) was determined by the following equation:

$$\sigma^{IFSS} = \frac{F_m}{2\pi r l_e} \tag{1}$$

where F_m is the maximum force observed during pull-out test, l_e is the embedded length of the fiber in the microdrop and r is the fiber radius, both of which were measured with an optical microscope. At least 20 samples were tested for each type of fiber. After the pull-out tests, the failure mechanisms were identified using SEM. Dynamic mechanical analysis of composite samples was also performed on the Q800 DMA with 3-point bending mode. Tests were operated with an amplitude of 25 μm, a preload force of 0.01 N, and a force track of 150%. The glass transition temperature (T_g) was determined by the peak of the tan δ curve. Short beam shear tests (SBS) were carried out on an Instron universal testing machine (Mode 5569 with 50 kN load cell and Bluehill software) with a 3-point bending fixture. The SBS specimen has dimensions of 25 mm x 5 mm x 3 mm. A nominal 4:1 span-to-depth ratio was used following standard testing procedure described in ASTM D2344 for glass fiber laminates. Five measurements were conducted for each type of laminate. Interlaminar shear strength (ILSS) was calculated with the following equation:

$$\sigma^{ILSS} = 0.75 \times \frac{P_m}{b \times h} \tag{2}$$

where P_m is the maximum load, b and h are specimen width and thickness, respectively. An optical microscope was used to observe the side surface of the specimen after SBS testing. Scanning electron microscopy (SEM) analysis was carried out on a field-emission scanning electron microscope (FE-SEM, FEI Quanta 250) operating at 20 kV in high vacuum to examine the morphology of the fracture surfaces of the composites (sputtered with gold).

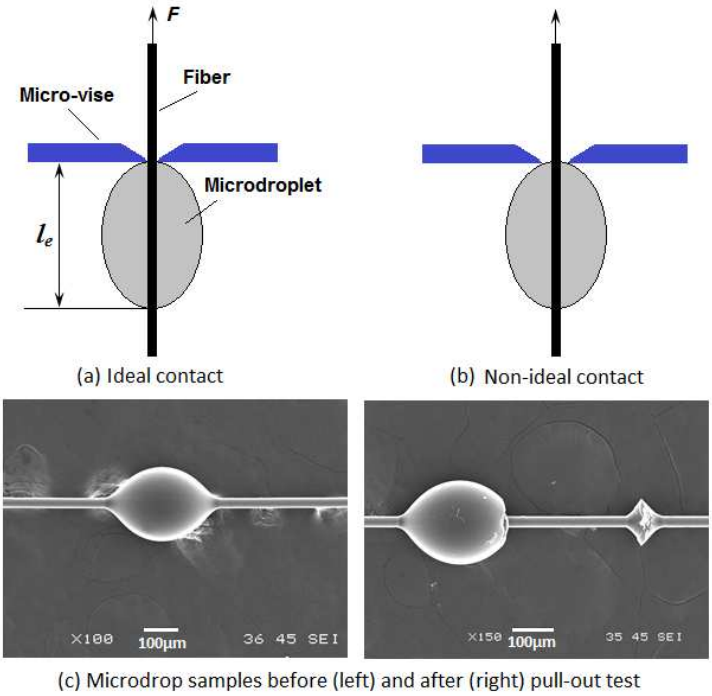

Figure 3-3 Schematic diagram for microbond pull-out test and microdrop samples before and after pull-out test

3.4 Result and Discussion

3.4.1 X-ray Photoelectron Spectroscopy

Elemental concentrations of C, O, and Si for differently treated fibers are listed in Table 3-1 Summary of XPS, DMA and interfacial strength data. For untreated fibers, the carbon concentration on the surface is as high as 79.7%, which mainly originates from

organic parts in the original sizing, such as film former, silane, and surfactant. After heat-cleaning, the carbon concentration significantly decreases from 79.7% to 12.8%, because most organics were oxidized and volatilized as CO_2 or water. Surface modification with silane coupling agents resulted in increased carbon concentrations compared to heat-cleaned fibers, indicating that the silane coupling agents were successfully grafted onto the fiber surface. MCS-treated fibers exhibited the highest carbon concentration, with 39.1%, and TCS-treated fibers exhibited a carbon concentration of 30.4%. Considering the stoichiometry of MCS ($C_{11}SiCl$) and TCS (C_9SiCl_3), numbers of grafted molecules for MCS and TCS can be calculated as 2.39% ((39.12-12.83)/11) and 1.95% ((30.37-12.83)/9), respectively.

Table 3-1 Summary of XPS, DMA and interfacial strength data

	Elemental concentration (%)			Thermal-mechanical properties		Interfacial strength (MPa)	
	C	Si	O	T_g (°C)	E' at 25°C (MPa)	σ^{IFSS}	σ^{ILSS}
Untreated	79.72	19.74	0.53	80.4	11432	2.3±0.5	14.9±0.3
Heat-cleaned	12.83	66.72	20.45	74.5	9675	1.2±0.3	19.2±0.3
MCS-treated	39.12	43.66	17.22	84.8	12241	6.2±1.0	25.2±0.7
TCS-treated	30.37	52.48	17.14	76.8	11280	3.3±0.8	19.3±0.7

Although there are several possible mechanisms for the promotion of adhesion using silane coupling agents, the chemical bond theory, where silane coupling agents form covalent bonds with both polymer matrix and inorganic fillers, was strongly supported by the work of Plueddemann [24]. Silane coupling agents are usually applied in solution, where silanes hydrolyze in the presence of water, forming silanols and then

those silanols undergo condensation with hydroxyl groups on the glass surface to form strong siloxane bonds. Figure 3-4 (a) and (b) show the two step reactions between MCS and glass fiber. Since MCS has only one hydrolyzable group in the molecule (Si-Cl), only one type of covalent attachment to the surface is possible. TCS has three hydrolyzable groups and is expected to be more reactive and more complicated than MCS. In the first step, TCS are hydrolyzed to form trisilanols. During the condensation step, trisilanols can react either with surface hydroxyl groups (surface condensation) or with hydroxyl groups on neighboring silanols (self-condensation). Which reaction is dominant depends on the kinetics for both reactions. It has been proposed that in solution, self-condensation is favored over surface condensation [25]. Oligomers of trichlorosilane are formed in solution and then adsorbed onto the glass surface, followed by surface condensation. Usually, the condensation of the first hydroxyl group of a trisilanol occurs readily; however, the condensation of the second and third hydroxyl groups attached to the same silicon atom become increasingly more difficult due to steric hindrance effects. To gain more surface bonding attachments, post-cure is necessary to complete the condensation reaction. Figure 3-4(c) shows the condensation reaction between trisilanol and surface hydroxyl groups on a glass substrate. Modified surfaces with varied structures (horizontal polymerization and vertical polymerization) were formed as the result of competition between self-condensation and surface condensation.

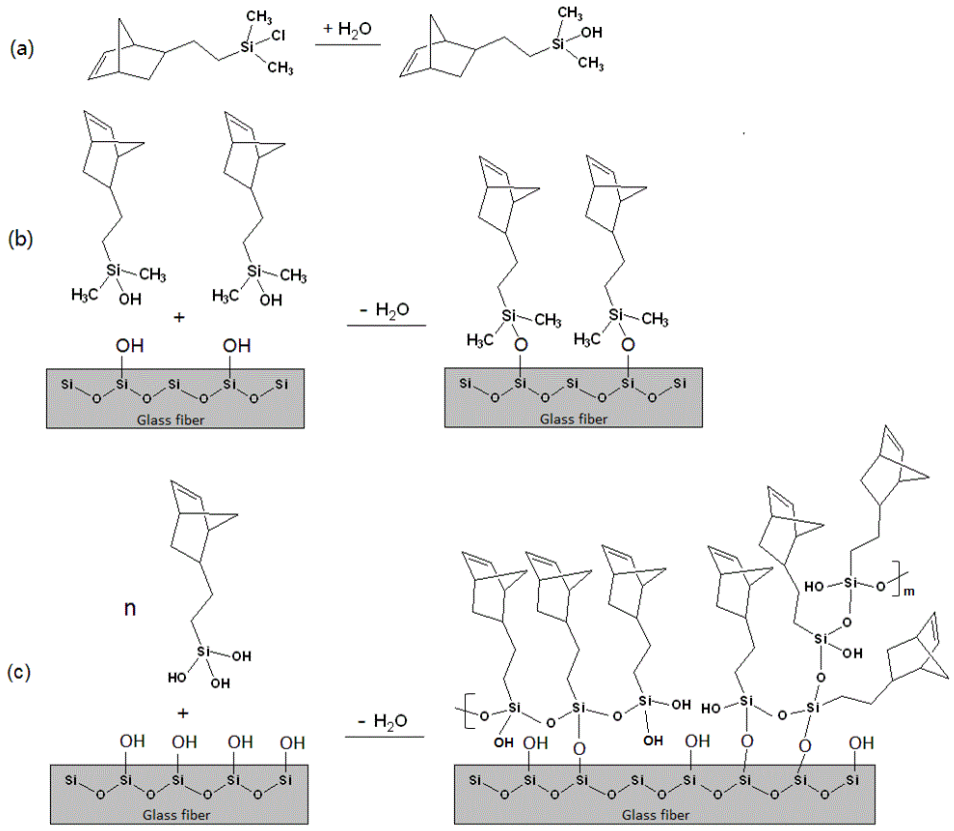

Figure 3-4 Silane reactions: (a) hydrolysis of MCS; (b) surface condensation reaction of monosilanol; (c) surface condensation reaction of trisilanol

Tripp's research [26] on the reactivity of trichloro-, dichloro-, and monochloromethylsilanes with silica surfaces shows that disilanol and monosilanol can fully condense with surface hydroxyl groups, but only limited covalent bonds to the surface were observed for trisilanols. The reactivity of mono-, di-, and tri-chloromethylsilanes on silica surfaces were shown to occur in the following order: $(CH_3)_3SiOH > (CH_3)_2Si(OH)_2 > CH_3Si(OH)_3$. Although the silanes used in this research had different non-hydrolyzable groups, and glass fibers were modified rather than silica, we may still expect a similar trend, where the condensation reaction of MCS with surface hydroxyl groups is more reactive than TCS. It is possible that MCS results in

higher covalent bond density on glass fiber surfaces than TCS. As we mentioned earlier, the increased carbon concentrations after surface modification are attributed to successfully grafted silane molecules. For MCS-modified glass fibers, the increased carbon concentration is proportional to the amount of silane molecules and the number of surface covalent bonds due to its reaction mechanism. But for TCS-modified glass fiber, every silane molecule may not be chemically bonded directly to the glass surface, as can be seen in Figure 3-4(c).

3.4.2 Microbond Pullout Testing

Figure 3-3(c) shows SEM images of microdrop samples before and after pull-out testing. In the ideal cases, a perfectly spherical droplet is expected to form on the single fiber. However, axisymmetrical elliptical droplets were observed as shown in Figure 3-3(c). Wu and Claypool [27] have demonstrated that this change in shape does not significantly affect the stress distribution along the embedded length of the fiber. In Figure 3-3(c), a cone-shaped piece of resin is left behind after the pull-out test. This is caused by the imperfect contact position of the micro-vise blade edges with the microdrop surface, see Figure 3-3(b). Resin failure was initiated at the contact point where stress concentrated during testing. In the ideal case, the opening of the micro-vise is just large enough to allow fiber sliding in order to prevent resin rupture, as shown in Figure 3-3(a), but in practice, it is difficult to eliminate the resin rupture completely. Therefore, in this research, a fixed opening of the micro-vise was used to reduce the contact position impact.

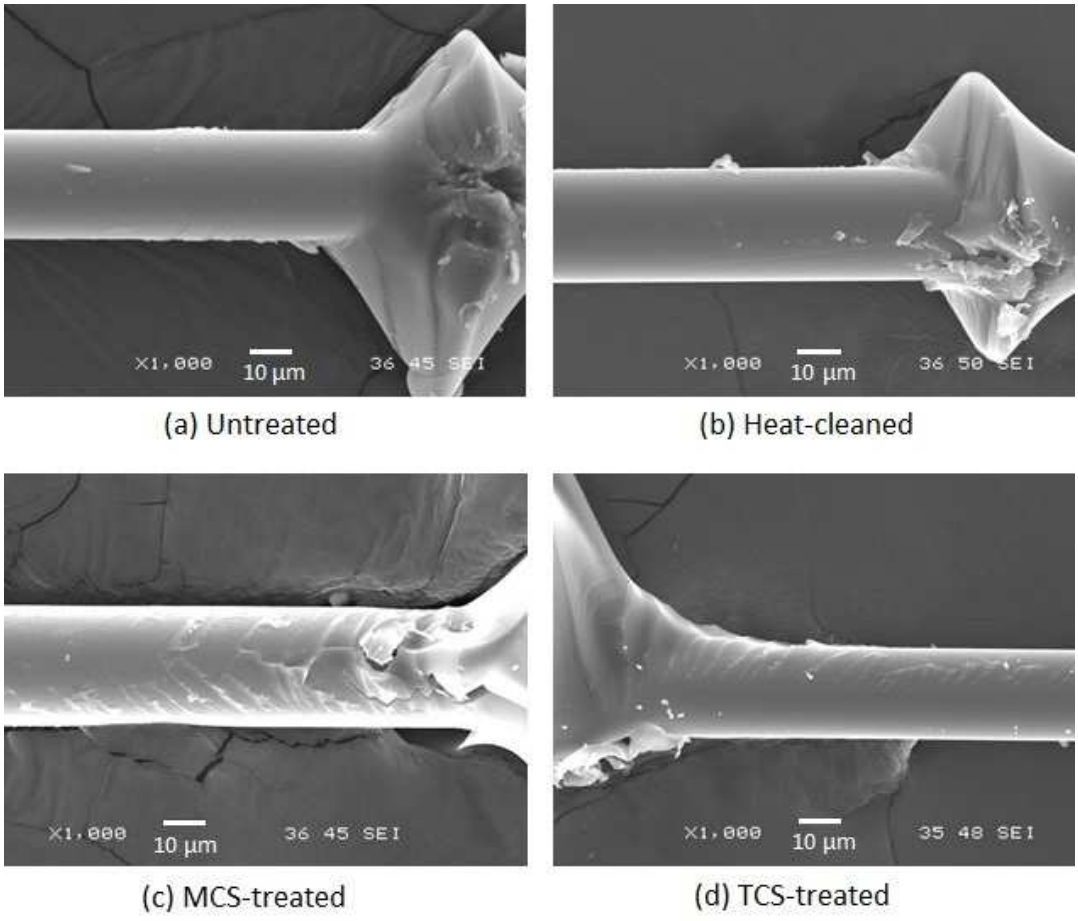

Figure 3-5 SEM images of interfacial surfaces of microbond samples after pull-out test

Interfacial shear strengths (IFSS) for the four different fiber types (untreated, heat-cleaned, MCS, and TCS) are summarized in Table 3-1 Summary of XPS, DMA and interfacial strength data. Postmortem SEM images of microbond samples are shown in Figure 3-5. IFSS values for heat-cleaned glass fibers are lower than those for untreated fibers. The only difference between these two samples is that the sizing layer was removed by heat cleaning. There is no evidence that suggests that the original sizing on the untreated fibers can form chemical bonds with the bio-based polymer, but some matrix monomer may diffuse into the sizing layer and form an interpenetrating cross-linked network after cure, which could improve the interaction between fiber and matrix

to some degree. Because the sizing layer was removed, a decrease in IFSS value is not surprising for heat-cleaned samples. This result is consistent with what is shown in the SEM images (Figure 3-5). Small amounts of residual polymer are present on the failure surface of untreated fiber, whereas a clean and smooth failure surface was observed for heat-cleaned fiber. After surface modification with silane coupling agents, interfacial adhesion is improved to varying degrees. It is apparent that MCS treated fibers exhibit the highest value of interfacial shear strength, which is attributed to the chemically grafted MCS silane on the fiber surface that can also form covalent bonds with the polymer matrix under ROMP polymerization. In Figure 3-5(c), it can be seen that a large amount of polymer adhered to the interfacial surface of MCS-treated fiber, indicating that IFSS for MCS-treated fiber/bio-polymer is higher or at least comparable to the strength of polymer matrix after the fiber surface modification. Compared to heat-cleaned fibers, TCS treated fibers also display improved IFSS values, but they are not as high as those for MCS-fibers. Like the MCS treated fibers, SEM images of the TCS treated fiber shows a mixture of adhesive failure and cohesive failure, but less polymer matrix is present on the glass fiber surface than for the MCS-fiber. As explained in the XPS test, MCS can form more covalent bonds directly with the surface hydroxyl groups than TCS. The interfacial shear strength results show substantial variability—coefficient of variation (CV) is observed in the range of 15%-25%—which is consistent with results reported by others who also work with this technique [19, 28].

3.4.3 Dynamic Mechanical Analysis

The temperature dependence of storage modulus (E') for glass fiber/bio-based polymer composites with varied surface treatments is shown in Figure 3-6(a). It is clear that samples exhibit similar behaviors in the storage modulus versus temperature curves

which stay constant at low temperatures and then drops sharply in the temperature range between 50-100 °C, followed by a plateau at higher temperatures. Storage modulus around room temperature was enlarged in the inset of Figure 3-6(a) to view detailed information. It is noticeable that a decrease of approx. 15% in modulus is observed for composites made with heat-cleaned fibers compared to untreated fiber composites. This is probably due to the same reason as discussed in the microbond test, that heat-cleaning damages the diffusion-induced interaction resulting in a weak interface limiting effective stress transfer from matrix to fiber, and a resulting lower storage modulus. A significant improvement in interfacial adhesion has been achieved with MCS-treated fibers which is consistent with microbond testing results, indicating that covalent bonding between fiber and matrix can enhance the load transfer at the interphase and increase stiffness. Composites made with TCS-treated glass fiber also show improved storage modulus values, but are not as high as for MCS samples.

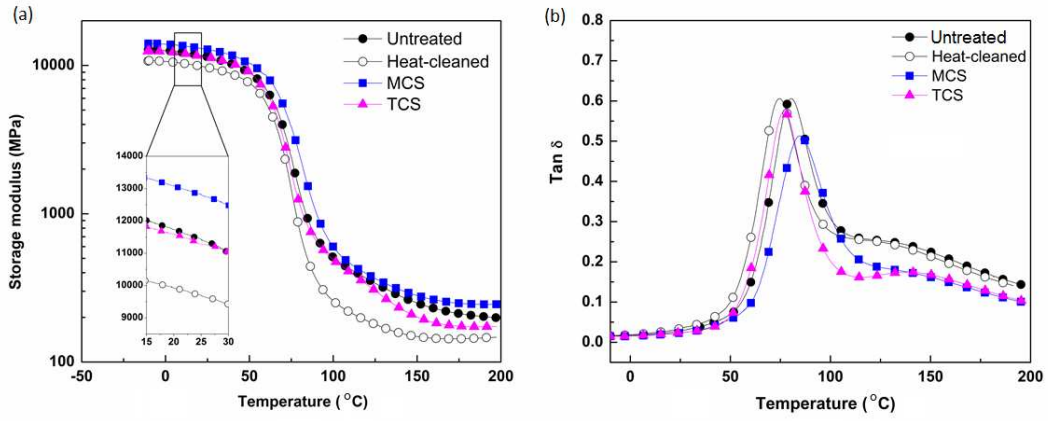

Figure 3-6 Storage modulus curves and Tan δ curves for composites made with different type of fibers

The loss factor, tan δ, is plotted in Figure 3-6(b) as a function of temperature. Glass transition temperature (T_g) is taken from the peak of the tan δ curves, indicating

the start of large-scale motions of the polymer chains in the material. All samples here show glass transitions in the range of 70-85 °C. The decrease of T_g for the heat-cleaned samples is likely the result of the same influences as the reduced storage modulus. Poor interfacial interaction in heat-cleaned fiber composites weakens the restraint on large-scale motion of polymer chains. In comparison to the heat-cleaned samples, a significant increase in T_g, from 75 °C to 85 °C has been seen with MCS sample which is believed to be the result of improved interfacial adhesion. Once covalent bonds are formed between glass fibers and polymer matrix, the polymer chains that are bonded to a fiber are restrained from movement. In this case, higher temperature is required to activate large-scale chain motion and an increased T_g is seen on the tan δ curve. A lower magnitude in the tan δ peak for MCS samples than for other samples is additional evidence for improved interfacial bonding according to Keusch [29]. In addition, tan δ curves have a small shoulder peak at higher temperatures which is possibly due to phase separation in the bio-based polymer as discussed in our previous work [13].

3.4.4 Short Beam Shear Test (SBS)

Figure 3-7(a) shows flexure load versus cross-head displacement curves obtained from short beam shear tests for composites made with differently treated fibers. It is clearly seen that untreated, MCS, and TCS treated samples behaved like tough materials. Load values increase linearly at the beginning, and then remain almost constant until reaching the preset strain of 20%. However, the heat-cleaned sample showed a more brittle behavior, where the load values drop suddenly after the maximum peak load was reached. In addition, the peak value for untreated fiber composites is much lower than

composites from the other fiber types. To better understand these phenomena, side surfaces of samples after SBS tests were examined by optical microscopy and images are shown in Figure 3-7(b). Apparently, composites made with untreated glass fibers show typical interlaminar failure, where a high number of delamination cracks parallel to the laminate direction were observed as well as two whitening zones caused by stress concentration. The white coloration for both delamination cracks and whitening zones is caused by craze formation between fiber and matrix due to the poor interface. In addition, the whitening zone is also where delamination cracks originate. A large crack was generated on the bottom tensile surface of the heat-cleaned sample and propagated perpendicularly through the thickness of the sample. This tension failure mechanism in short beam shear tests is presumably a consequence of negative effects of heat-cleaning treatment on mechanical strength of the glass fibers. Without the protection offered by sizing, heat-cleaned glass fiber reinforced composites become brittle. In other words, heat-cleaning may sacrifice some mechanical properties attributed to the glass fibers. Images of failed MCS and TCS samples show that no transverse cracks and less delaminations were generated, demonstrating that improved interfaces were obtained after surface modification with silane coupling agents.

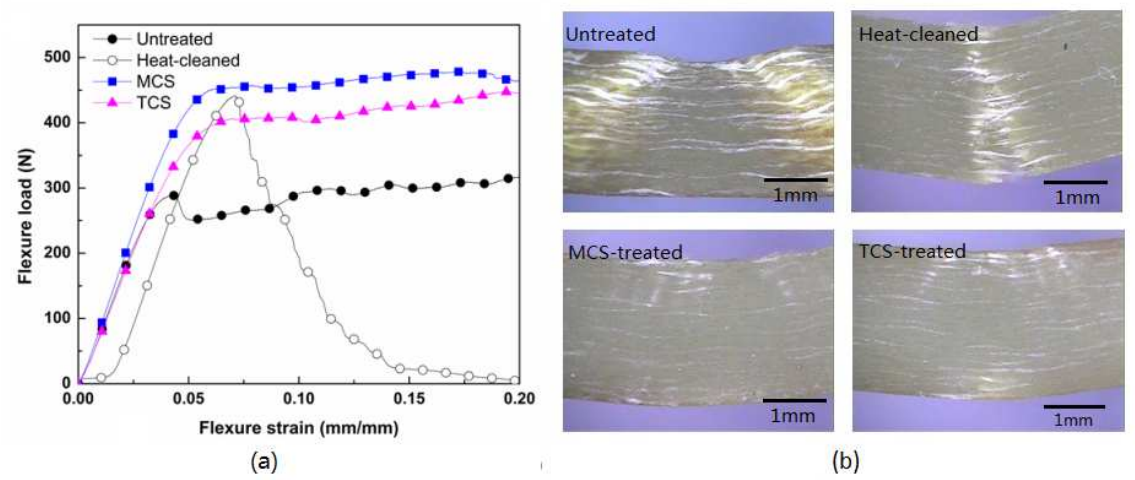

Figure 3-7 (a) Load-strain curves for short beam shear test; (b) OM images for laminates after short beam shear test

The interlaminar shear strength (ILSS) for the four sample types is summarized in Table 3-1. Based on results from microbond testing and DMA, it is not surprising to see that ILSS values for MCS samples far exceeded all others. It further confirms the conclusion that MCS treatment is indeed well suited for improving the interfacial adhesion in glass fiber reinforced bio-based polymer composites. Although TCS treatment can also form chemical bonds between the glass fiber and the polymer matrix, it is less effective at improving the interfacial properties than MCS treatment. It is unexpected to see that heat-cleaned samples show even higher ILSS values than untreated fiber samples. This trend is different from what we have seen in other tests. It does not mean that heat-cleaned samples have better interface than untreated fiber composites. As mentioned earlier, the heat-cleaned samples ruptured with tension failure and the ILSS value is the result of mixed effects of interfacial strength and tension strength; however, all other samples failed by interlaminar fracture. The different failure mode prevents direct comparisons with the heat-cleaned samples.

3.4.5 Scanning Electron Microscopy

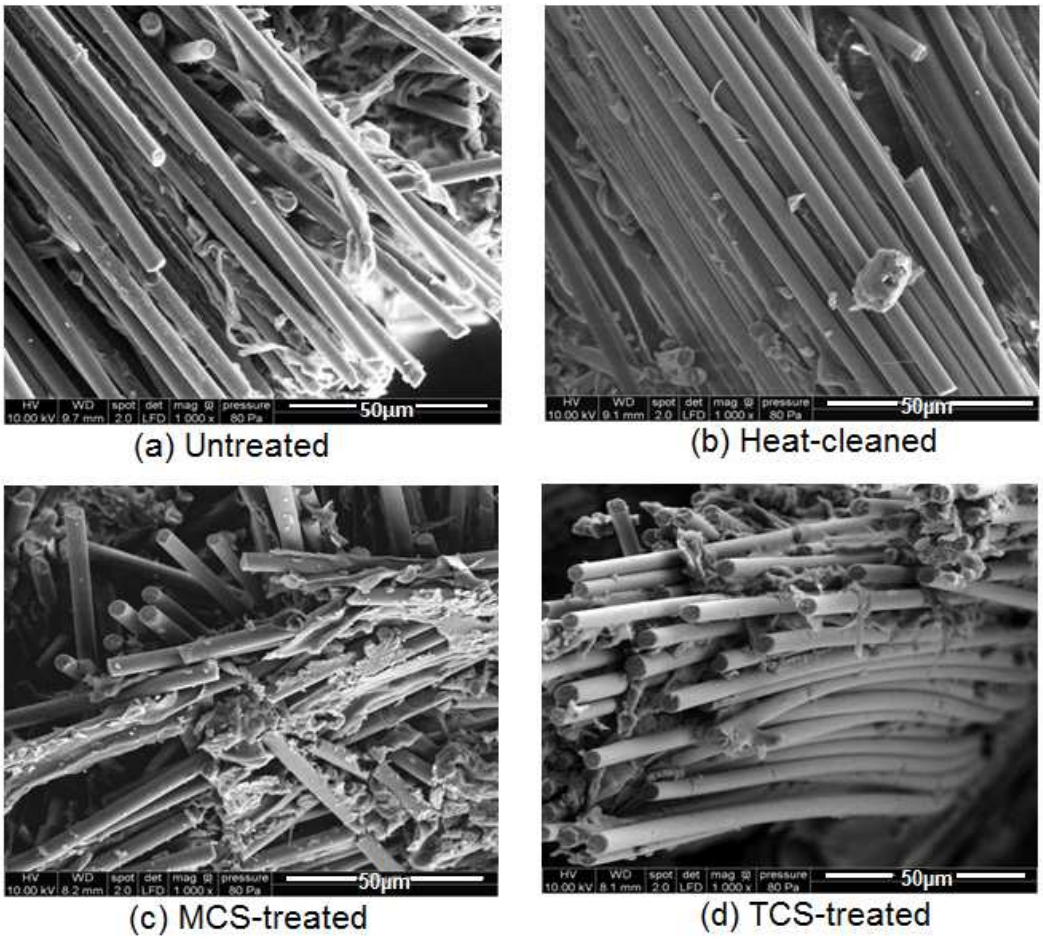

Figure 3-8 SEM images of fracture surfaces for composites made with different type of fibers

In order to examine the microstructure and adhesion between fibers and matrix, fracture surface morphology was investigated by scanning electron microscopy (SEM). SEM images are shown in Figure 3-8. In the case of composites made with MCS-treated fibers, a high number of short fiber fragments and significant amount of adhered resin on the fiber surfaces were observed, both of which are signs of good adhesion between fibers and matrix. However, in all other cases, clean and smooth surfaces of pulled out fiber can be seen in the SEM images.

3.5 Conclusions

The effect of different silane coupling agents on interfacial adhesion between glass fibers and ROMP-based bio-renewable polymers has been studied experimentally. Two types of silane coupling agents, MCS and TCS, were employed to modify glass fiber surfaces. Untreated glass fibers and heat-cleaned glass fibers were also studied as control groups. Successful grafting of silane onto glass fiber surfaces was confirmed by a substantial increase in carbon concentration after surface modification in XPS analysis. The difference in reaction mechanisms between two silanes indicates MCS may have a higher covalent bond density than TCS when same amount of silanes are used in the surface modification procedure. The effect of surface modification on thermomechanical properties was studied by DMA. With the use of silane, especially MCS, composites become stiffer compared to the control groups, which is presumed to correspond to the successful establishment of covalent bonds in the interfacial region. In addition, the sizing on untreated fibers also has positive influences on interfacial adhesion which is hypothesized to be the result of a diffusion-induced interpenetrating network. Interfacial shear strength and interlaminar shear strength were evaluated by microbond technique and short beam shear testing respectively. Both appear to be sensitive to interface quality and similar results are found. Both techniques demonstrate that MCS has a more profound effect than TCS on improving interfacial adhesion between glass fibers and the bio-based polymer matrix. This conclusion is further confirmed by SEM characterization of composite fracture surfaces.

3.6 References

[1] W Jeong, TC Mauldin, RC Larock, MR Kessler (2009) Macromol Mater Eng 294: 756.

[2] RC Larock, PH Henna (2007) Macromol Mater Eng 292: 1201.

[3] RC Larock, YS Lu (2006) Biomacromolecules 7: 2692.

[4] FK Li, RC Larock (2003) Biomacromolecules 4: 1018.

[5] K Haman, P Badrinarayanan, MR Kessler (2009) Polym Int 58: 738. Doi:Doi 10.1002/Pi.2585

[6] YS Lu, RC Larock (2009) Chemsuschem 2: 136.

[7] TC Mauldin, K Haman, X Sheng, P Henna, RC Larock, MR Kessler (2008) J Polym Sci Pol Chem 46: 6851. Doi:Doi 10.1002/Pola.22995

[8] Y Xia, RC Larock (2010) Green Chem 12: 1893.

[9] LT Drzal, AK Mohanty, M Misra (2001) Compos Interface 8: 313.

[10] SH Lee, SQ Wang (2006) Compos Part a-Appl S 37: 80.

[11] S Thomas, MJ John (2008) Carbohyd Polym 71: 343.

[12] RH Grubbs, S Chang (1998) Tetrahedron 54: 4413.

[13] PH Henna, MR Kessler, RC Larock (2008) Macromol Mater Eng 293: 979.

[14] LT Drzal, M Madhukar (1993) J Mater Sci 28: 569.

[15] EK Drown, H Almoussawi, LT Drzal (1991) J Adhes Sci Technol 5: 865.

[16] GR Baran, S Debnath, SL Wunder, JI McCool (2003) Dent Mater 19: 441.

[17] JL Thomason, LJ Adzima (2001) Compos Part a-Appl S 32: 313.

[18] EP Plueddemann (1991) Silane coupling agents. Plenum Press, New York

[19] U Gaur, B Miller (1989) Compos Sci Technol 34: 35.

[20] PJ Herrerafranco, LT Drzal (1992) Composites 23: 2.

[21] PJ Herrerafranco, V Rao, LT Drzal, MYM Chiang (1992) Compos Eng 2: 31.

[22] B Miller, U Gaur, DE Hirt (1991) Compos Sci Technol 42: 207.

[23] AS Jones, JD Rule, JS Moore, SR White, NR Sottos (2006) Chem Mater 18: 1312.

[24] Plueddem.Ep (1970) J Adhesion 2: 184.

[25] CP Tripp, ML Hair (1993) J Phys Chem-Us 97: 5693.

[26] CP Tripp, ML Hair (1995) Langmuir 11: 149.

[27] HF Wu, CM Claypool (1991) J Mater Sci Lett 10: 260.

[28] B Miller, P Muri, L Rebenfeld (1987) Compos Sci Technol 28: 17.

[29] S Keusch, R Haessler (1999) Compos Part a-Appl S 30: 997.

CHAPTER 4: PULTRUSION WITH BIO-BASED POLYMER AND INTERFACE TAILORING WITH SILANE COUPLING AGENT

A paper to be submitted to *Composites Part A*

Hongyu Cui[1], Michael R. Kessler[2,3]

4.1 Abstract

Economical glass fiber reinforced polymer composites were developed from biorenewable resins utilizing a highly automated pultrusion process. The composites were successfully pultruded with a self-built table-top pultrusion machine. The interfacial interaction of the composites was significantly improved after surface modification with a silane coupling agent. The optimum silane concentration was determined by testing the mechanical properties of the pultruded fiber reinforced composites. Composites reinforced with fibers that were treated with a 3% silane solution exhibited the best properties in DMA and flexural tests.

Keywords: Pultrusion, FRP, bio-based polymer, silane coupling agent

4.2 Introduction

The applications of fiber reinforced polymer (FRP) composites have grown significantly since 1960s because of their excellent overall properties that are either comparable to or better than many traditional metallic materials. FRPs possess superior

[1] Dept. of Materials Science and Engineering, Iowa State University, Ames, IA

[2] School of Mechanical and Materials Engineering, Washington State University, Pullman, WA

[3] Author for correspondence

properties in terms of light weight, high specific strength and stiffness, excellent environmental resistance, high electrical insulation, and low thermal expansion [1]. Over the years, FRP composites have found increasingly wide applications in a variety of fields, such as in the aerospace, transportation, construction, chemical engineering and electrical industries. However, the uses of composites are still limited because of their high material and manufacturing costs. With the growing opportunities for composite materials in civil structural application, the development of inexpensive composites is of great interests.

Pultrusion is a cost-effective, automatic process for the production of continuous composite parts with constant cross-sectional profiles [1, 2]. Figure 1-3 provides a schematic representation of the pultrusion process. During pultrusion, fibers are impregnated with resin by being pulled through a resin bath or a resin injection chamber. The wet fibers then pass through a hot die, where the resin undergoes polymerization. Multiple heating zones are used along the die, depending on the type of resin used. Pultrusion has a number of advantages over other composite manufacturing methods:

- Increased strength because the fibers are aligned in the tension state.
- Highly automatic process with little manual interface, so that it is possible to efficiently produce high fiber volume composites with consistent quality.

- Low cost, typically 80 – 90% of the cost for pultruded profiles are the raw material costs.

Based on these advantages, pultrusion is the technique of choice for the production of glass fiber reinforced composites when low cost and good mechanical properties are required.

Growing concerns regarding the limited petroleum resources, the volatile price of oil, and the environmental impact of fossil feedstocks have led to an increasing demand for the development of polymeric materials from sustainable resources. Vegetable oils are ideal raw materials for the polymer industry because of their ready availability, structural variety, chemical versatility and relatively low cost. The major components in vegetable oils are triglycerides which contain several reactive sites and functionalities that can be utilized in a variety of synthetic transformations. Over the past ten years, a series of bio-based polymers has been synthesized and developed from vegetable oils using various polymerization methods [3, 4]. Among them is a copolymer that was prepared from modified linseed oil (Dilulin) and dicyclopentadiene (DCPD) by ring opening metathesis (ROMP) polymerization and that shows promising mechanical properties [5, 6]. In addition, the low viscosity of the copolymer and its fast cure kinetics make it a good resin candidate for the pultrusion process. Pultrusion is the most cost-effective manufacturing method, and combined with low-cost biorenewable resins allows for the production of inexpensive composites for structural applications.

Here, we pultruded Dilulin/DCPD copolymers to produce low-cost, bio-based composites with good mechanical properties. The resin formulation and process pultrusion parameters were optimized based on performances. Surface modification of glass fibers by a silane coupling agent was used to improve the interfacial adhesion of the composites.

4.3 **Experimental**

4.3.1 Materials

The materials used in this study are listed in Table 4-1; they include two monomers, a catalyst, lubricant, fillers, and glass fibers. Dilulin and DCPD monomers were mixed at a ratio of 3:7. Then 0.125 wt.% catalyst was added prior to processing. The Grubbs' catalyst was recrystallized by freeze-drying from benzene to allow better dissolution in the resin [7]. Dilulin which is commercially available from Cargill is synthesized from linseed oil and cyclopentadiene using a high temperature, high pressure Diels-Alder reaction. The chemical structure of Dilulin has been studied thoroughly by NMR and FTIR, indicating an average of one norbornene ring pendant group per triglyceride [5, 7].

Table 4-1 Materials used in this study

Material	Parts by weight	Specification	Supplier
Dilulin	30	Dilulin monomer, modified linseed oil	Cargill, MN
DCPD	70	Dicyclopentadiene monomer	Sigma-Aldrich, WI
Catalyst	0.125	2nd Generation Grubbs' Catalyst	Sigma-Aldrich, WI
Lubricant	5	Tech Lube SR-150-W2	TECHNICK, NJ
Filler	10	ASP-400p, Kaolin clay	BASF, GA
Glass fiber	NA	Continuous E-glass, 56 yield	Pella, IA
MCS	NA	Norbornenylethyldimethylchlorosilane, Silane coupling agent	Gelest, PA

4.3.2 Pultrusion Processing

A table-top pultrusion machine was designed and built in order to manufacture the composite on a lab-scale. The machine consisted of resin injection block, a pultrusion die with dimensions of 60 mm × 2.5 mm × 1 mm (length × width × thickness), one heating zone, and a puller. The surface of the die was coated with high temperature ultra-slippery PTFE tapes. Although only one heating zone was used in the pultrusion machine, a water circulation system was designed on each end of the die to keep the entrance and the exit of the die cool. The optimized processing temperatures along the die are shown in Figure 4-1 Temperature distribution along length of the die. Fiber reinforced polymer composites were made with 5 rovings of unidirectional glass fiber with a total fiber content of 50 % by volume. The pulling rate was 0.075 m/min and varied slightly throughout the process. The pultruded fiber glass reinforced biopolymer composites are shown in Figure 4-2.

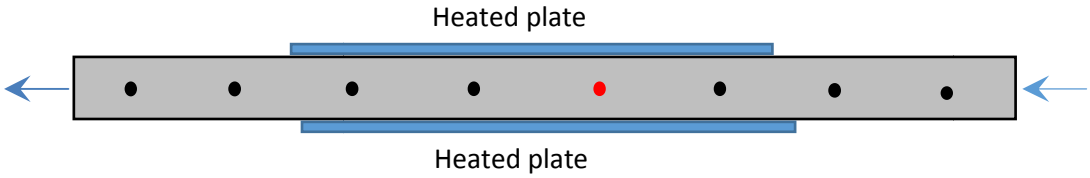

1	2	3	4	5	6	7	8
43.5°C	68.5°C	145.4°C	194°C	200°C	166°C	92°C	39.5°C

Figure 4-1 Temperature distribution along length of the die

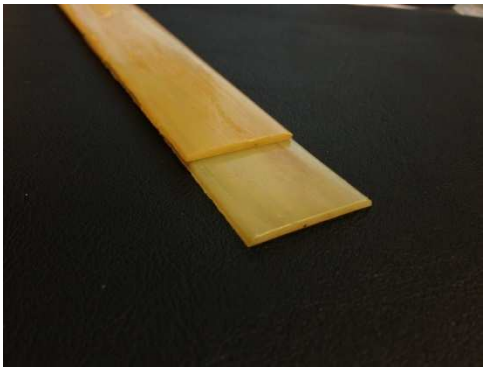

Figure 4-2 Pultruded composites from bio-based polymer

4.3.3 Glass Fiber Surface Modification

To improve the interfacial adhesion between the glass fibers and the resin in FRP composites, the glass fibers were modified with a silane coupling agent priot to pultrusion. According to a previous study [8], norbornenylethyldimethylchlorosilane (Monochlorosilane, MCS) offered better coupling effects compared to norbornenylethtyltrichlorosilane (Trichlorosilane, TCS) because of the reproducible grafting result. Five rovings of glass fibers were cut long enough for one pultrusion running. The fibers were heat-cleaned in a convection oven at 450 °C for 3 h to remove the existing sizing. Silane/alcohol solutions with varied concentrations of MCS were prepared by mixing silane with anhydrous isopropanol alcohol. The solution was warmed to 40 °C for 30 min to promote a reaction between the silane and the alcohol. The heat-cleaned glass fibers were dipped in the silane solution for 3 min and then rinsed with excess isopropanol alcohol. The treated fibers were cured at 120 °C for 10 h to improve silanol condensation reactions on the fiber surfaces.

4.3.4 Characterizations

Surface elemental concentrations of glass fibers treated with varied silane solutions were measured by utilizing X-ray photoelectron spectroscopy (XPS, PHI55000) with an Al Kα (1486.6 eV) source. Dynamic mechanical tests of the copolymers were carried out by using a TA Q800 dynamic mechanical analyzer (DMA) in a tension mode. Tests were operated with an oscillation amplitude of 10 μm, a preload force of 0.01 N, and a force track of 125%. Samples were cooled down to -20 °C and held isothermally for 2 min, followed by heating up to 250 °C at a rate of 3 °C/min. The glass transition temperature (T_g) was determined by the peak of the tan δ curve. Flexural tests were carried out on an Instron 5569 universal testing machine (50 kN load cell and Bluehill software) with a 3-point bending fixture at a crosshead speed of 2 mm/min. Two types of samples were prepared: along fiber direction and transverse to the fiber directions. Flexural strength and modulus were calculated based on at least five samples. The fracture surfaces of the specimens were investigated by a field-emission scanning electron microscope (FE-SEM, FEI Quanta 250) operating at 8 kV in high vacuum to correlate the microstructure and the fracture behavior. The samples were sputtered with 5 nm Iridium film.

4.4 **Results and Discussion**

4.4.1 XPS

Elemental concentrations for fibers treated with different silane coupling agents are summarized in Table 4-2. Pristine glass fiber had the highest carbon concentration because of the existing sizing on the surface that was applied during fiber

manufacturing. Sizing consists of multiple components, including film former, silane, lubricant, and an antistatic agent, which are mostly organic compounds with a large number of carbon atoms in their structure. This high carbon concentration was greatly reduced after heat-cleaning. The small amount of residual carbon may have been caused by contamination. It can be seen in Table 4-2 that as the concentration of silane solution increased, the concentration of carbon atoms initially increases and then remained at a constant value.

The chemical reaction during surface modification is described as follows. MCS reacts with the alcohol, producing an alkoxysilane and HCl. Mild warming of the solution facilitates the removal of HCl and the completion of the reaction. Then some HCl react with alcohol to produce a small amount of water and alkyl halide. The water causes hydrolysis of alkoxysilane to form silanols. Finally, silanols condense with hydroxyl groups on fiber surface, forming covalent bonds between silane and glass fiber. The coupling effect of monofunctional silane is promising and reproducible, because only one type of grafting is possible [9]. The maximum bonding density is limited by the size of the dimethylsilyl group [10]. However, the reactions of monofunctional silanes at the solution-solid interface are very slow in the later stages of the reaction, and long reaction times (several days) are necessary to achieve maximum bonding density [11, 12]. In our case, the glass fibers were immersed in the silane solution for only 3 min. It can be seen in later section that the interfacial adhesion has been improved greatly with such short time treatment. The XPS measurement revealed that under the treatment conditions used in our investigation, the highest concentration of carbon atoms was

20%. Compared to the results of refluxing reactions used in a previous study [8], we obtained a lower bonding density; however, our approach was time-saving and allowed for the treatment of fibers in large quantities. In a later section we will show that the mechanical properties improved significantly, even with the lowered bonding density.

Table 4-2 Elemental concentrations on glass fiber surface

	C (%)	O (%)	Si (%)
Pristine fiber	79.72	19.74	0.53
Heat-cleaned fiber	11.4	69.1	19.5
MCS-0.5%	15.8	65.1	19.2
MCS-1%	17.6	63.9	18.5
MCS-2%	19.5	62.0	18.5
MCS-3%	20.6	61.1	18.3
MCS-4%	19.4	61.5	19.1

4.4.2 DMA

DMA specimens were cut and tested transverse to the fiber direction. The temperature dependent storage modulus and tan δ are presented in Figure 4-3Figure 4-3 Temperature dependent storage modulus (a) and tan δ (b). The storage modulus for all samples showed the typical three-stage behavior: it staid constant in the glassy state and then dropped suddenly in the temperature range between 50 and 100 ºC, finally reaching the rubbery plateau. In Figure 4-3, the curves between 0-50 ºC were enlarged to provide more details. The storage moduli at 25 ºC and 175 ºC are summarized in Table 4-3. It can be seen that compared to regular fiber composites, the storage modulus of composites made with silane-treated fibers was improved significantly, even when a dilute silane solution was used. The storage modulus at room temperature tripled after silane treatment, indicating that the interfacial interaction between glass fibers and

polymer matrix was significantly enhanced. As the concentration of the silane solution increased, the storage modulus increased as well; however, the increase levelled off for concentration above 2 wt.%. It is interesting to note that the storage modulus in the rubbery state (175 ºC) did not show the large differences as in the glassy state. The rubbery modulus is related to the cross-link density of polymeric materials. The surface modification with silane coupling agents affected only the interfacial bonding and had little effect on the cross-link density of the bulk polymer.

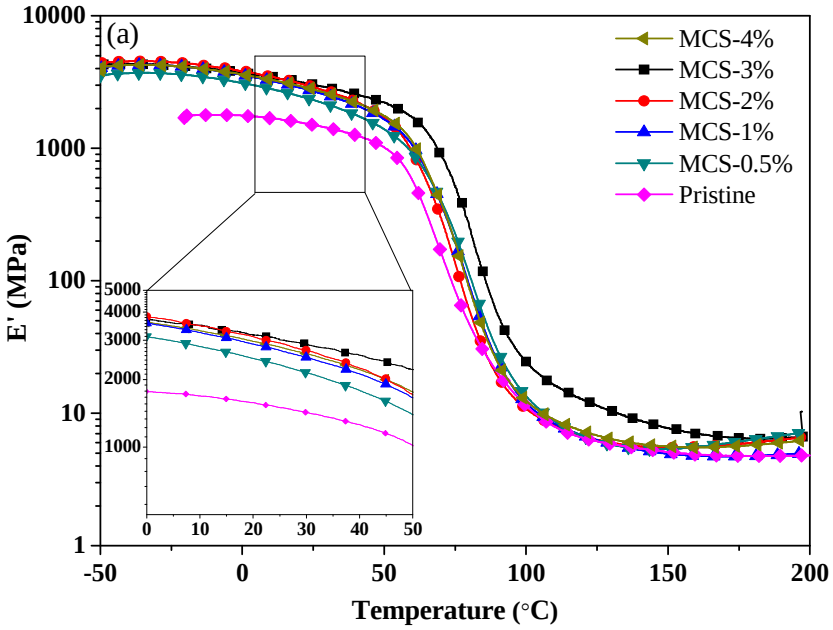

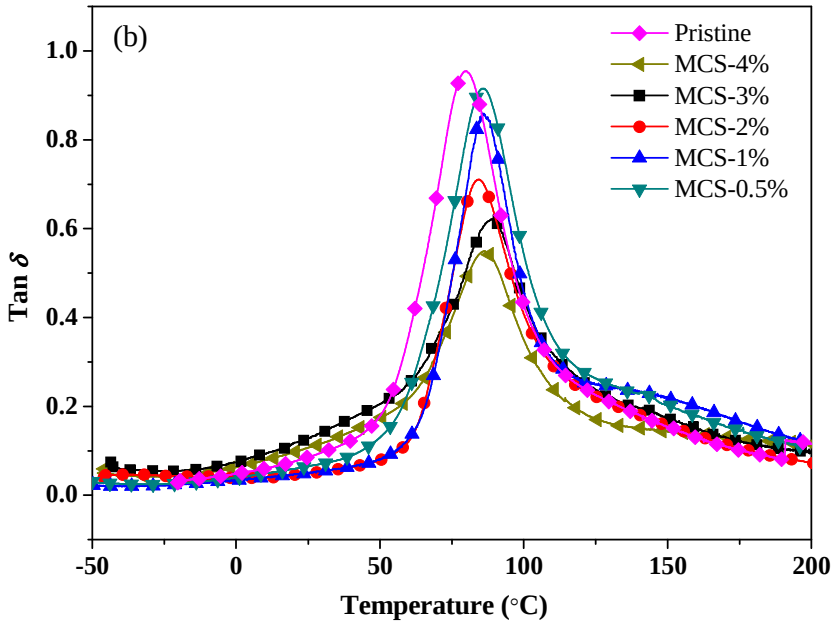

Figure 4-3 Temperature dependent storage modulus (a) and tan δ (b)

The glass transition temperatures obtained from the tan δ curves are also listed in Table 4-3. It can be seen that all samples exhibited a glass transition temperature of approx. 85 °C. The tan δ curves provided not only the glass transition temperatures but also information regarding damping properties which are measured as the magnitude of the tan δ peak. Damping is a sensitive indicator of molecular motions [13]. Under deformation, the fibers usually carry a major part of the stress and allow only small portion of it to strain the interface because of the rigid bonding at the fiber/matrix interface. Therefore, a strong interfacial bond will restrict large-scale movement of more polymer chains, leading to a reduced damping value. Many researchers [14-16] confirmed that the magnitude of tan δ is inversely proportional to interfacial adhesion. In Figure 4-3b, a gradual decrease in the tan δ value was observed as the silane

concentration increased. As discussed earlier, this suggests that improved interfacial bonding was obtained after surface modification with silane.

Table 4-3 DMA data summary

	Tg (°C)	E'(MPa) at 25°C	E' (MPa) at 175°C
Pristine	79.5	1491	4.77
MCS-0.5%	85.0	2325	5.37
MCS-1%	86.3	2700	4.94
MCS-2%	84.5	2902	5.49
MCS-3%	88.6	3002	7.77
MCS-4%	86.8	2790	5.6

4.4.3 Flexural Tests

Flexural tests were carried out with samples cut both in fiber direction and transverse to fiber direction. Flexural strength and the stress-strain curves of samples cut in fiber direction are displayed in Figure 4-4. Both flexural strength and flexural modulus increased significantly after surface modification with silane. Composites made with pristine fibers exhibited a flexural strength of only 110 MPa and a flexural modulus of 6 GPa. The flexural strength doubled and the flexural modulus near doubled for treated glass fibers, even when the glass fibers were treated with 1% silane solution for 3 min. Effective interfacial interactions were obtained through covalent bonding, making the resulting composites stiffer. During deformation, good interfaces transfer stress from matrix to reinforcement effectively and the strain is restrained by the rigid reinforcement. Therefore, composites with good interfacial bonds require higher forces for the same amount of deformation compared to composites with poor interfacial bonds.

Samples made with fibers treated with 3% silane showed the highest flexural properties. Further increases in silane concentration did not further improve the flexural properties. Figure 4-4b shows typical stress-strain curves obtained by flexural tests. Samples made with pristine, 0.5% silane-treated and 1% silane-treated fibers showed ductile behavior, where stresses change slightly after yielding point. Severe delamination was observed in these samples. Other composites were seen to fail in semi-brittle manner with less delamination.

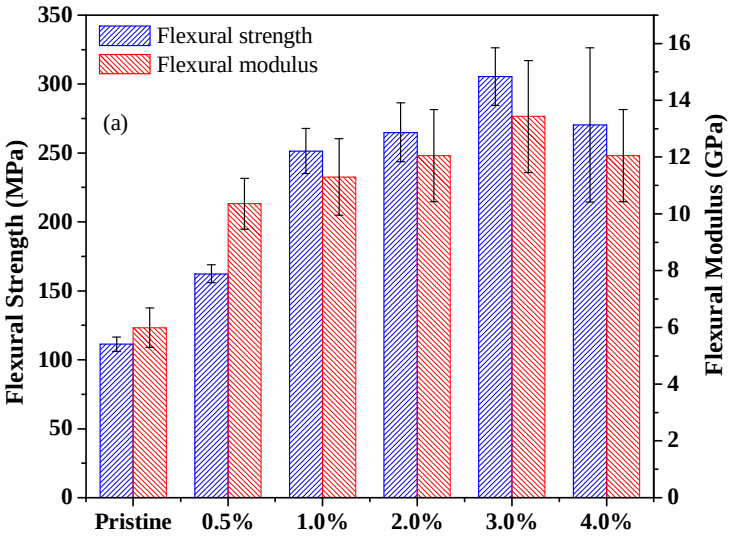

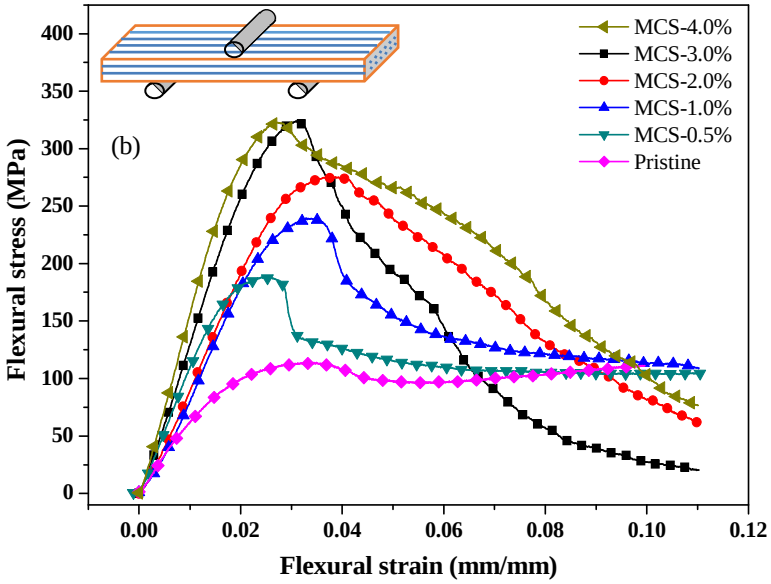

Figure 4-4 Flexure test in fiber direction (a) flexural strength and flexural modulus (b) typical stress-strain curves for different composites.

Flexural strength and stress-strain curves for samples cut transverse to the fiber direction are presented in Figure 4-5. For unidirectional fiber composites, transverse flexural strength and modulus are matrix-sensitive and interface-sensitive. Figure 4-5 shows that transverse flexural strength is much lower than flexural strength in fiber direction; however, both show a similar, increasing trend. Composites made with 2% and 3% silane-treated fibers show similar transverse flexural strength, while composites made with 4% silane-treated fibers showed reduced flexural strength due to the huge error. The transverse flexural strength of the composites is lower than the flexural strength of pure Dil30DCPD70, which is around 50 MPa. Transverse flexural strength of unidirectional fiber reinforced composites is rather sensitive to defects. Any defects, both inside or outside, in sample cause stress concentrations, initiating cracks that will propagate, finally causing failure of the sample. The interface between fibers and matrix

in composites is the weakest point, even the interfaces are strengthened by a silane coupling agent, because no perfect modification can be obtained.

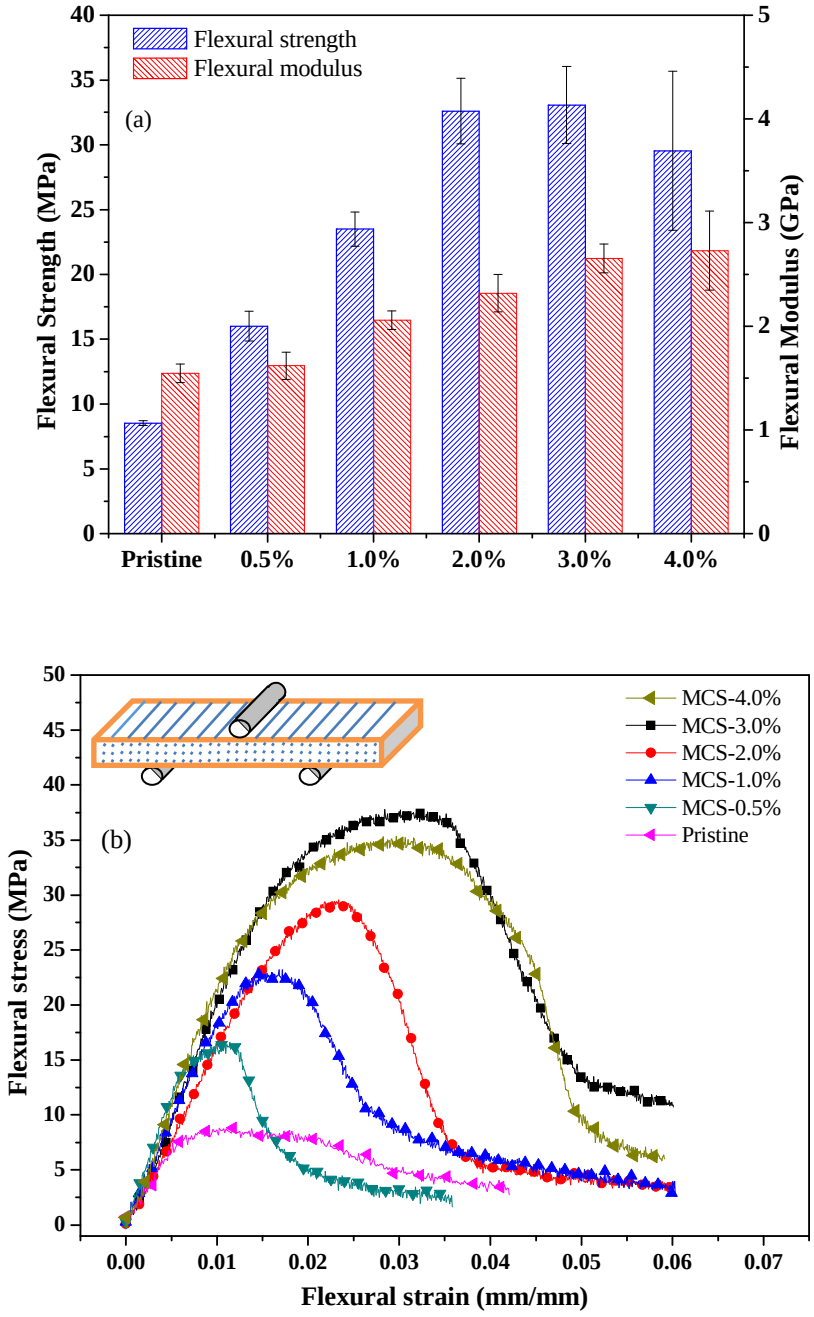

Figure 4-5 Flexure test in transverse direction (a) flexural strength and flexural modulus (b) typical stress-strain curves for different composites.

4.4.4 SEM

Figure 4-6 shows SEM micrographs of the fracture surfaces of fiber reinforced composites. It can be seen that long glass fibers were pulled out from the polymer matrix (Figure 4-6 a and b). The fiber surfaces looks clean and smooth, indicating poor interfacial bonding in these composites. For composites made with 1% silane-treated fibers (Figure 4-6 c), some resin sticks on fiber surfaces after fracture, confirming that interfacial interaction was improved with silane treatment. Figure 4-6 d-f shows similar fracture morphologies, where fibers were pulled from the polymer matrix but still bonded tightly to the matrix resin after fracture.

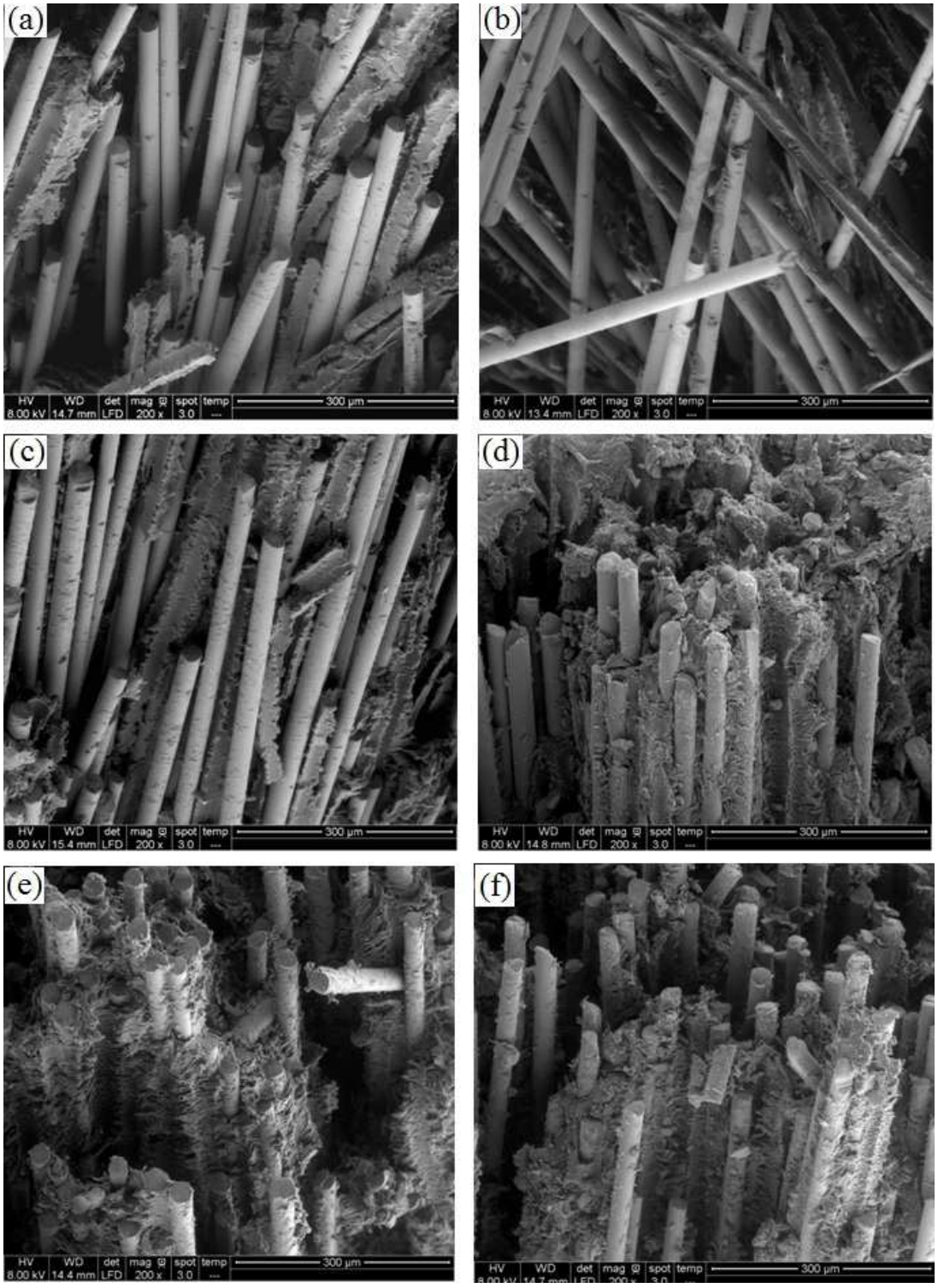

Figure 4-6 SEM images of fracture surfaces of different composites (a) Pristine fiber ; (b) 0.5%-silane-treated fiber; (c) 1% silane-treated fiber; (d) 2% silane-treated fiber; (e) 3% silane-treated fiber; (f) 4% silane-treated fiber.

4.5 Conclusions

To improve the interfacial adhesion of pultruded glass fiber/bioresin composites, the glass fibers were treated with silane/alcohol solution in various concentrations. Although the fibers were immersed in silane solution for only 3 min, the interfacial adhesion was enhanced significantly. XPS measurements demonstrated that as the silane concentration increased, the elemental concentration of carbon atom initially increased and reached a maximum level of about 20% with a silane concentration of 2%. DMA tests revealed that the storage modulus was significantly improved after surface modification. The reduced magnitude of the tan δ peak also confirmed that improved interfacial adhesion was obtained. Flexural strength and modulus both in fiber and transverse to fiber direction showed consistent results. DMA and flexure test both indicated that increasing the silane concentration from 3% to 4% did not increase interfacial bonding too much. Therefore, 3 wt.% of silane in isopropanol was determined as the optimum concentration for surface modification with a simple dipping method. The morphology of the fracture surfaces of the composites also confirmed our conclusions.

4.6 References

[1] PK Mallick (2008) Fiber-reinforced composites : materials, manufacturing, and design. CRC Press, Boca Raton, FL

[2] TF Starr (2000) Pultrusion for engineers. CRC Press, Boca Raton, FL

[3] YS Lu, RC Larock (2009) Chemsuschem 2: 136.

[4] Y Xia, RC Larock (2010) Green Chem 12: 1893.

[5] P Henna, RC Larock (2009) J Appl Polym Sci 112: 1788.

[6] PH Henna, MR Kessler, RC Larock (2008) Macromol Mater Eng 293: 979.

[7] TC Mauldin, K Haman, X Sheng, P Henna, RC Larock, MR Kessler (2008) J Polym Sci Pol Chem 46: 6851. Doi:Doi 10.1002/Pola.22995

[8] HY Cui, MR Kessler (2012) Compos Sci Technol 72: 1264. Doi:DOI 10.1016/j.compscitech.2012.04.013

[9] AY Fadeev, TJ McCarthy (2000) Langmuir 16: 7268. Doi:Doi 10.1021/La000471z

[10] P Claudy, JM Letoffe, C Gaget, D Morel, J Serpinet (1985) J Chromatogr 329: 331. Doi:Doi 10.1016/S0021-9673(01)81940-3

[11] AY Fadeev, TJ McCarthy (1999) Langmuir 15: 3759. Doi:Doi 10.1021/La981486o

[12] AY Fadeev, TJ McCarthy (1999) Langmuir 15: 7238. Doi:Doi 10.1021/La9903806

[13] S Dong, R Gauvin (1993) Polym Composite 14: 414. Doi:Doi 10.1002/Pc.750140508

[14] S Keusch, R Haessler (1999) Compos Part a-Appl S 30: 997.

[15] S Mohanty, SK Verma, SK Nayak (2006) Compos Sci Technol 66: 538. Doi:DOI 10.1016/j.compscitech.2005.06.014

[16] MS Huda, LT Drzal, AK Mohanty, M Misra (2007) Compos Part B-Eng 38: 367. Doi:DOI 10.1016/j.compositesb.2006.06.010

CHAPTER 5: DEGRADATION OF ROMP-BASED BIO-RENEWABLE POLYMERS BY UV RADIATION

A paper published in polymer degradation and stability

Hongyu Cui[1], Riley Hanus[1], Michael R. Kessler[2,3]

5.1 Abstract

The degradation of a bio-renewable polymer under UV exposure was studied using various methods. Degradation of the bio-renewable polymer increased with increasing exposure time. Enhanced cross-link density in the early stage of degradation was confirmed by Soxhlet extraction. Tensile testing showed a transition from ductile failure to brittle fracture. Surface cracks and embrittlement were primary reasons for most reductions in mechanical properties, such as tensile strength and breaking strain. The effects of degradation were confined to the surface of thick bio-based polymer specimens, confirmed by both SEM and PAS-FTIR. Depth profile studies of degraded samples showed that the concentration of oxidation products, such as hydroxyl and carbonyl groups, varied with depth depending on the diffusion of oxygen.

Keywords: UV degradation; photo-degradation; bio-renewable; auto-oxidation

5.2 Introduction

Aging is the primary effect limiting the lifetime of plastics. It usually leads to irreversible changes in material properties. Materials exposed to environmental

[1] Dept. of Materials Science and Engineering, Iowa State University, Ames, IA
[2] School of Mechanical and Materials Engineering, Washington State University, Pullman, WA
[3] Author for correspondence

influences, such as light, temperature, and humidity may lose ductility, color, or transparency. In outdoor applications of plastic materials, UV radiation is responsible for most aging damages, because the quantum energy of UV radiation is high enough to cause chain cleavage in the molecules, and this, in turn, resulting in one or more of the following chemical changes: depolymerization, crosslinking, formation of double bonds in the polymer chain and other low-molecular compounds [1]. These effects are usually classified as photo-degradation. Photo-degradation generally leads to an embrittlement of polymer materials and often causes a transition from ductile failure to brittle fracture. A reduction in yield stress, tensile stress, and elongation at break was observed in many photo-degraded materials [2-5]. Conductivity and dielectricity are also affected by photo-degradation [6, 7]. Because degradation will eventually cause material failure, examining and understanding the degradation effects on material properties provides key indicators when predicting the service life of a material.

The basic mechanism of photo-degradation is auto-oxidation, consisting of several steps:

Initiation	$RH \longrightarrow R\cdot + H\cdot$		(1)
Propagation	$R\cdot + {}^3O_2 \longrightarrow ROO\cdot$		(2)
	$ROO\cdot + RH \longrightarrow ROOH + R\cdot$		(3)
Termination	$ROO\cdot + R\cdot \longrightarrow ROOR$		(4)
	$R\cdot + R\cdot \longrightarrow RR$		(5)

The absorption of UV light provides sufficient energy to break chemical bonds in the polymer to generate free radicals, leading to the initiation of photo-degradation. Catalyst

residues and impurities in the polymer are other sources for radical initiation [8]. During the propagation step, hydrocarbon free radicals react with triplet oxygen (the ground state for oxygen) to form peroxy radicals where oxygen is largely consumed. Then peroxy radicals subtract hydrogen from polymer chain, producing a hydroperoxides and other hydrocarbon radicals in reaction (3). Reactions (1), (2), and (3) form a self-accelerated auto-oxidation cycle [9]. The decomposition of hydroperoxide can lead to backbone cleavage of O-O bonds followed by β-scission mechanisms [10]. Photo-degradation is terminated when two free radicals combine, as shown in reactions (4) and (5). This typically results in cross-linking, branching, or formation of short segments of the polymer.

Henna and Larock [11] developed a bio-renewable polymer using ring-opening metathesis polymerization (ROMP) that showed promising thermal-mechanical properties, and a viable industrial processing method for these new thermosets is currently being developed. The bio-renewable polymer was prepared by copolymerizing a mixture of Dilulin and DCPD with 2nd generation Grubbs' catalyst. The ring opening metathesis polymerization (ROMP) mechanism of two monomers is shown in Figure 3-1. Dilulin is synthesized from linseed oil and cyclopentadiene through a high temperature, high pressure Diels-Alder reaction. Chemical structure of Dilulin has been studied thoroughly with NMR and FTIR, indicating an average of one norbornene ring pendant group per triglyceride [11, 12]. In the polymerization of the copolymer, the unsaturated norbornene ring in Dilulin can undergo ROMP with DCPD to form a cross-linked structure. However, even after complete cure, the copolymer still contains a

number of unreacted double bonds, such as unsaturated bonds in fatty acid chains in Dilulin and double bonds in cyclopentene rings in DCPD (discussed later). These unsaturated bonds are likely to be attacked by UV radiation to form free radicals during photo-degradation. Catalyst residue and other impurities in the polymer also absorb UV radiation, producing free radicals. Understanding the degradation behavior of this bio-renewable polymer is essential for exploring possible practical applications.

In this paper, the effect of UV radiation on physical and chemical properties of thick, bio-renewable polymer samples was studied utilizing various methods. In general, photo-degradation in thick specimen is governed by diffusion of oxygen into the polymer over time [13]. The distribution of oxygen through the specimen thickness results in varying concentrations of oxidation products with changing depth [14-16]. Profile analysis of photo-degraded samples was used as an effective way to study the time dependent degradation process. Photo-acoustic FTIR (PAS-FTIR) was used to examine chemicals on the surface layer of degraded materials. Together with an MTEC microlap system, it allowed to generate depth profiles of degraded materials with good resolutions.

5.3 **Experimental**

5.3.1 Sample Preparation

All samples were prepared from bio-renewable polymers consisting of 30 wt.% Dilulin and 70 wt.% dicyclopentadiene (DCPD, Sigma-Aldrich). Dilulin was used as a commercially available, modified linseed oil from Cargill (MN). The mixture of Dilulin and DCPD was cured with 0.125 wt.% recrystallized 2nd generation Grubbs' catalyst

[12] following a cure schedule of 1 h at 65 °C and subsequent 3 h at 150 °C. The resin was used to manufacture 100 mm × 60 mm × 0.8 mm sheets via a modified injection molding process. The mold consisted of a rubber gasket sandwiched between two glass plates. Resin was injected slowly from the top of the mold with a syringe. Dogbone samples for tensile tests were punched from the sheet material using an ASTM D 638 type-V punch. Six dogbone samples were produced from one piece of sheet. The remaining sheet was cut into rectangular specimens (30 mm × 40 mm) for further characterization analysis. The samples were attached to aluminum plates (75 mm × 125 mm) to fit the sample holder in the environmental chamber.

5.3.2 Exposure Procedure

The specimen were exposed to UV radiation according to ASTM G 154-06 (cycle 1 in ANNEX 2) in a QUV accelerated weathering chamber with a UVA-340 lamp. UV-340 lamps typically have little or no UV output below 300 nm wavelength (cut-off wavelength), which closely matches terrestrial solar radiation in the ultra-violet range. Samples were exposed on a 12 h cycle: 8 h UV at 60 °C black panel temperature followed by 4 h condensation at 50 °C black panel temperature, for total exposure times of 250 h, 500 h, 750 h, 1000 h, and 2000 h, respectively. A group of control samples was stored in a desiccator in dark cabinet to avoid exposure to light before further characterization.

5.3.3 Characterization

Tensile tests were carried out on an Instron 5569 universal testing machine (50 kN load cell and Bluehill software) with a constant crosshead speed of 1 mm/min. The longitudinal strain was measured by a non-contacting video extensometer (AVE). Young's modulus (E), ultimate strength (σ_m), breaking strain (ε_b), and tensile toughness were calculated and analyzed.

Soxhlet extraction was carried out to estimate the crosslink density. Samples weighing between 0.8 and 1.0 g were cut from unexposed and exposed polymer sheet and refluxed in 750 ml methylene chloride at a temperature of 60 °C for 24 h. After extraction, the solution was concentrated in a rotary evaporator and subsequently vacuum dried. ^{1}H NMR spectra of the soluble portion were taken with a Virian spectrometer (Palo Alto, CA) at 300 MHz using $CDCl_3$ as the solvent. The insoluble portion was dried in a vacuum oven overnight at 60 °C and then weighed.

The chemical changes that occurred on the sample surface after varied amounts of UV radiation were analyzed by Fourier transform infrared photo-acoustic spectroscopy (PAS-FTIR). PAS-FTIR is a non-destructive, near-surface analysis technique widely used for analysis of layered [17, 18] and degraded materials [19, 20]. During testing, samples were put in a sealed chamber filled with helium gas. The temperature fluctuation on the sample surface caused by absorbed infrared radiation initiated a pressure change in the surrounding gas, thus generating acoustic waves in the sample chamber. These acoustic signals were detected by a sensitive microphone and then underwent Fourier transformation. A Digilab FTS 7000 FTIR spectrometer

equipped with an AMTEC Photoacoustic (PAC300) detector was used to acquire PAS spectra. These spectra were collected at a modulation frequency of 5 kHz and a spectral resolution of 8 cm^{-1}.

An MTEC Microlap system coupled with PAS was used to measure IR spectra of degraded materials as a function of depth. The Microlap system contained a micro-abrasive machine and a micro-gage, allowing control of the thickness of the removed layer within several micrometers. PAS spectra were collected on each new surface after abrasive removal of about 10 µm of the top layer until the spectra did not show any additional change. Then, typical spectra were selected to show a clear surface depth profile of the degraded layer. In this test, PAS spectra were collected at a spectral resolution of 8 cm^{-1} and a modulation frequency of 20 kHz.

The morphology of the exposed and the transverse surfaces, cut with a razor blade, were studied using scanning electron microscopy (SEM, JSM-6060LV) operating at 20 kV in high vacuum. Polymer samples were sputtered with carbon prior to examination.

5.4 **Results and Discussion**

5.4.1 Appearance of the Degraded Surfaces

A discoloration from yellow and transparent to dark brown was observed with increasing UV exposure time. Discoloration is a common sign of plastic aging and usually caused by the formation of chromophores during photo-oxidation reactions. Figure 5-1 shows the SEM images of degraded surfaces after varied exposure times. Surface cracks formed spontaneously during UV exposure and the degree of degradation

increased with increasing exposure time. It can be seen that even after only 250 h of UV exposure, many cracks formed randomly on the sample surface. Surface cracking is usually caused by the gradient stress in degraded samples. Post-crosslinking of the surface material initiated by UV radiation, which usually results in tension stress on the surface, is a major reason why gradient stress builds up in materials from the surface to the inner layers [21]. With increasing exposure time, cracks propagated and intersected with each other, forming a network structure, as can be seen in Figure 5-1(b) and (c).

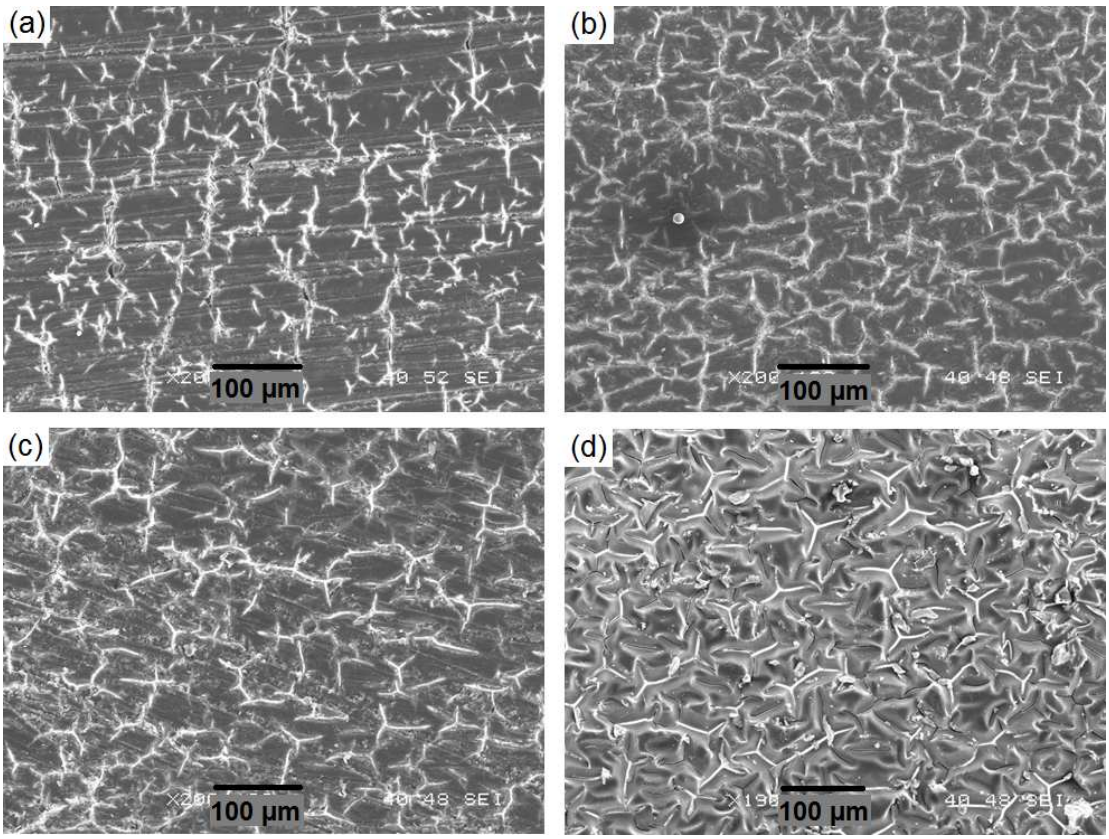

Figure 5-1 SEM images of degraded surfaces after varied UV exposure times. (a) 250 h; (b) 500 h; (c) 1000 h; (d) 2000 h

In the accelerated weathering test, the cycling changes in moisture and temperature were additional important factors that caused the formation of surface cracks. Bulk samples

expanded and contracted with cyclic temperature conditions, while sample surfaces swelled and shrank under cyclic condensation conditions as a result of absorbing and desorbing moisture. These alternating changes caused a gradient stress from the surface to the inner layers of the sample, initiating crack formation. Figure 5-1(d) shows the "wrinkled" surface of a sample exposed to UV radiation for 2000 h. This surface effect is presumably a consequence of the increasing mismatch of thermal-induced expansion and contraction between surface and interior of the sample.

5.4.2 Soxhlet Extraction Analysis

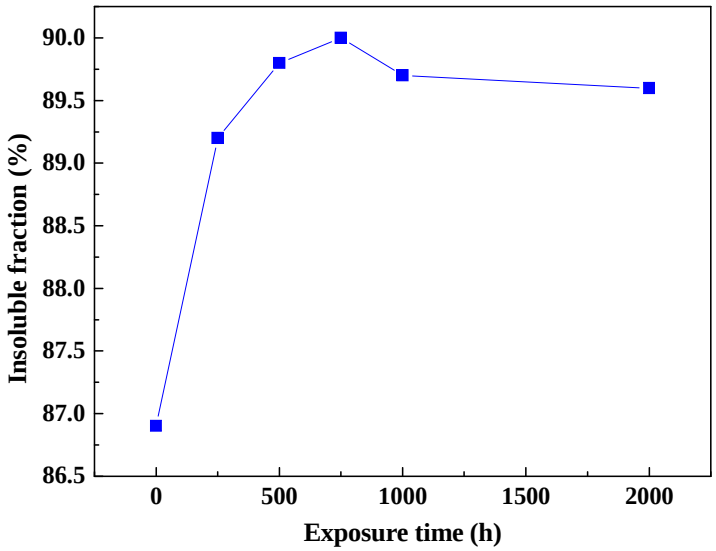

Figure 5-2 Insoluble fraction of degraded samples with varied UV exposure times

The insoluble fraction is plotted as function of exposure time in Figure 5-2. The insoluble fraction increased from 86.9% for unexposed specimens to 90% for specimens exposed for 750 h, which is mainly attributed to UV induced post-crosslinking. With exposure time increasing beyond 750 h, the insoluble fraction slightly decreased. It is

possible that after 750 h of exposure, UV-induced chain scission became the dominant degradation process. As exposure time further increased, more bulk material was decomposed and the cross-linked structure was broken into small segments. These decomposed segments were extracted by methylene chloride in the Soxhlet extraction process, resulting in a decrease in insoluble fraction.

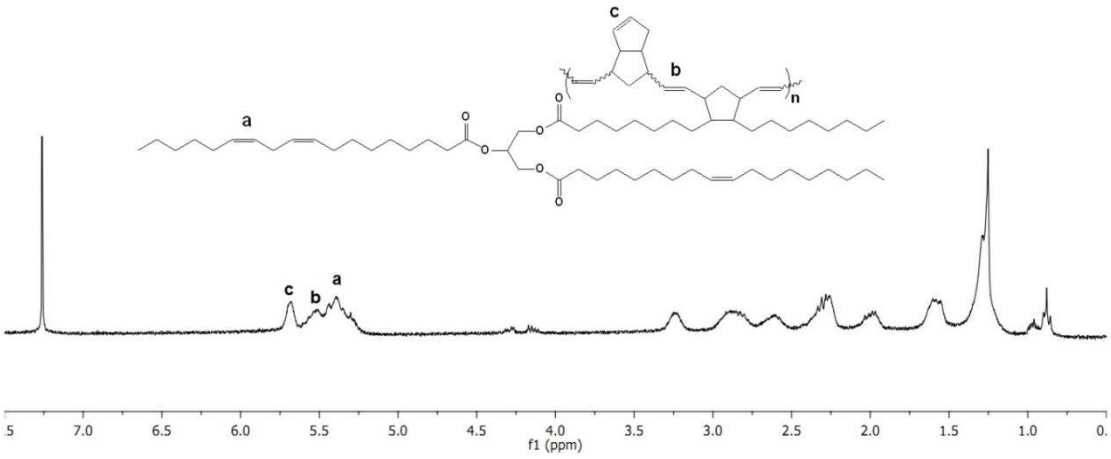

Figure 5-3 Structure representative of copolymer and 1H NMR spectra of soluble extracts from sample aged for 250 h

^{1}H NMR spectral analysis of soluble extracts revealed the presence of unreacted monomers and oligomers after copolymerization. The representative structure of the copolymer and ^{1}H NMR spectra of soluble extracts from 250 h-treated sample are shown in Figure 5-3 (other ^{1}H NMR spectra can be found in supporting materials). The characteristic peaks at δ = 4.1 and 4.3 correspond to the hydrogen atoms of the glycerol unit in the Dilulin. The presence of carbon-carbon double bonds in the fatty acid chains (labeled *a*) in Dilulin is confirmed by the appearance of a peak at δ = 5.38. The peak at δ = 5.45 can be attributed to the metathesized double bonds of the polymeric backbone (labeled *b*). The small peak at δ = 5.68 corresponds to double bonds in the cyclopentene

portion of DCPD (labeled *c*). DCPD is a diene with a rigid bicyclic structure containing two double bonds of unequal reactivity: one norbornene double bond that undergoes rapid olefin metathesis and one less reactive cyclopentene double bond. The absence of peaks between δ = 5.9 and δ = 6.1 confirm that all C=C bonds in the norbornene rings in DCPD have reacted.

Table 5-1 Soxhlet extraction data

	Insoluble %	Soluble %	Area under peak c	Area under peak a and b
Untreated	86.9	13.1	1.73	4.78
250h	89.2	10.8	1.54	4.58
500h	89.8	10.2	1.36	4.15
750h	90.0	10.0	1.1	3.93
1000h	89.7	10.3	1.51	4.27
2000h	89.6	10.4	2.22	9.69

The peak areas of unsaturated bonds (*a*, *b*, and *c*) were compared between aged samples by setting the integrated area under the peaks at 4.1 and 4.3 to 1. Due to the difficulties in integrating peaks area at 5.38 and 5.45 separately, the overall area between 5.3 and 5.5 is measured. As listed in Table 5-1, a decreasing trend was found for all unsaturated bonds within 750 h exposure, which is primarily due to the post-crosslinking in samples subject to UV irradiation. The decrease of the peak area indicates that the number of C=C was reduced greatly in the early stage of degradation. This is the net effect of double bond consumption and generation. In other words, the consumption rate of double bonds is higher than the rate of generation. There are several ways to convert C=C bonds in UV degradation. C=C bonds are chromophoric groups which absorb UV light and form hydrocarbon radicals quickly. If this happens at the sample surface where

sufficient oxygen is available, hydrocarbon radicals will be oxidized immediately to form hydroperoxides, as shown in equation (2) and (3). If the hydrocarbon radicals were formed at the inner part of the sample, it could combine with other hydrocarbon radicals to form cross-linked structure. In our case, from the polymer property aspect, the cross-link density of the copolymer increased after a short-term UV irradiation. Then beyond 750 h exposure, peak areas start to increase instead, indicating a growth in the number of unsaturated bonds in the soluble extracts. The increased double bonds are likely from a Norrish II reaction (Figure 5-4 Norrish reactions of carbonyl groups) duringphoto-degradation. As we know, a large number of carbonyl groups are formed in polymer materials upon UV irradiation. Those carbonyl groups absorb UV light readily and decompose through two types of Norrish reactions, see Figure 5-4. The Norrish II reaction, which usually breaks the polymer backbone into enol and alkene, is more probable since its activation energy (0.85 kcal/mol) at room temperature is lower than that of Norrish I reaction (4.8 kcal/mol)[10]. Oligomers containing enols and alkenes from Norrish reactions could be extracted by methylene chloride, leading to the decrease of insoluble fraction and the increase of unsaturated bonds.

To sum up, in UV degradation of unsaturated polymers, the evidence suggests that UV-induced post-crosslinking and chain-scission occur simultaneously and compete with each other. The insoluble fraction curve and NMR analysis of soluble extracts both demonstrate that post-crosslinking dominates at the early stage of exposure (<= 750 h) and then decomposition and chain-scission dominate the later stage.

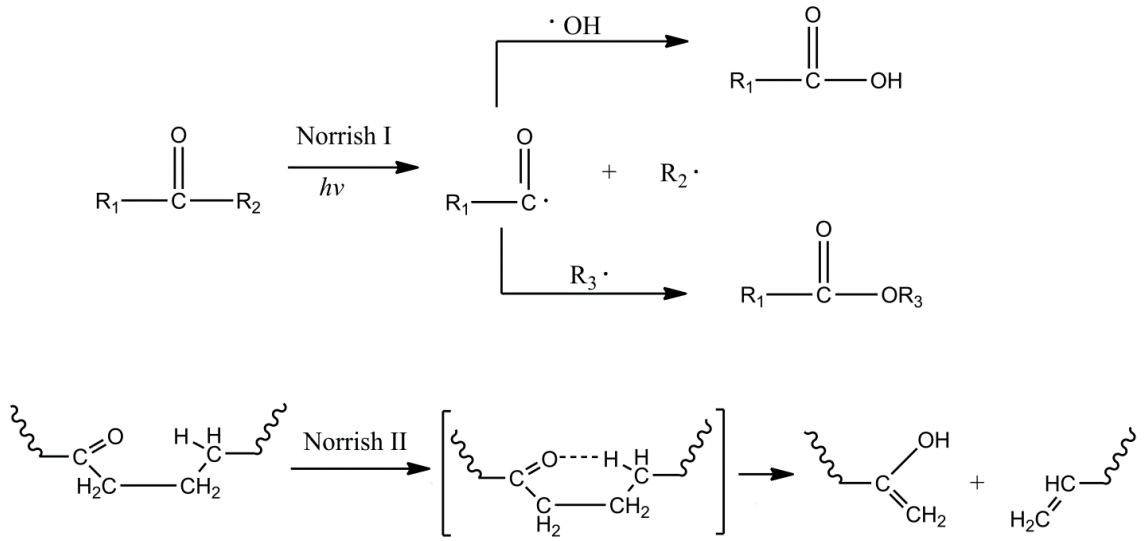

Figure 5-4 Norrish reactions of carbonyl groups

5.4.3 Tensile Test

The effect of UV exposure on mechanical properties was evaluated by tensile testing. Strain-stress curves for specimens after various times of UV exposure are shown in Figure 5-5. Tensile strength, average breaking strain, Young's modulus, and tensile toughness are summarized in Table 5-2. The control specimens (no exposure to UV radiation) showed ductile behavior with a clear yielding point and a low degree of plastic deformation. As exposure time increased, a ductile–brittle transition was observed in the strain-stress curves. After UV exposure for 750 h, the specimen exhibited brittle failure. Both breaking strain and tensile toughness dropped dramatically. The average breaking strain decreased from 17.8% for the control specimens to 2.9% after 750 h and 2% after 2000 h of UV exposure. The tensile toughness dropped from 4.7 MPa for the control specimens to 0.4 MPa for specimens exposed to UV radiation for 2000 h. The significant decrease in breaking strain and tensile toughness was mainly attributed to the formation of surface cracks during photo-degradation. It is interesting to note that the Young's

modulus E_Y exhibited an increase beyond the value of the control specimen after 500 h of UV exposure, which is presumably a consequence of UV-induced post cross-linking.

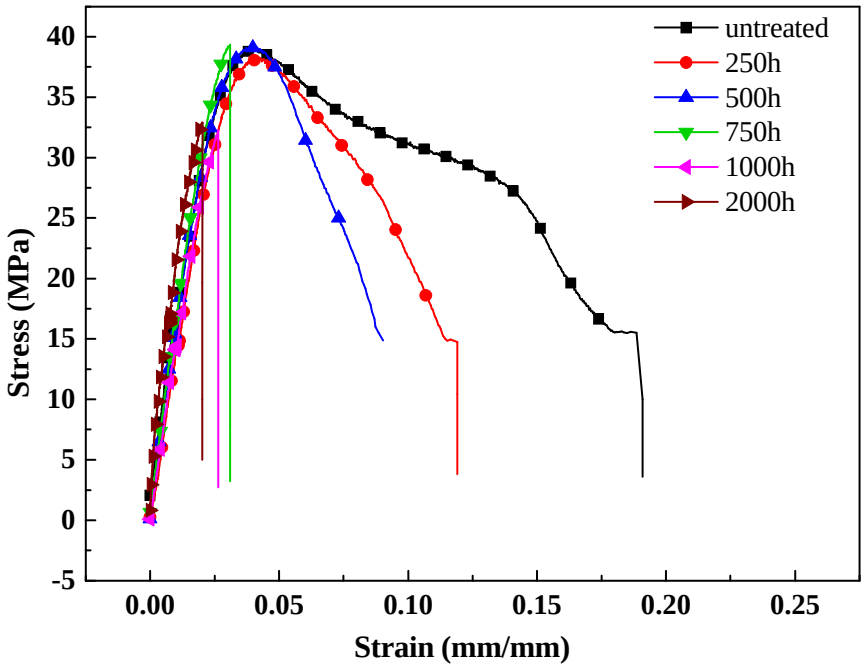

Figure 5-5 Stress-strain curves for samples after varied UV exposure times

Table 5-2 Tensile test data

	σ_{max} (MPa)	ε_b (%)	E_Y (GPa)	Toughness (MPa)
Untreated	38.6 ± 1.4	17.8 ± 3	1.74 ± 0.11	4.65 ± 1
250h	40.2 ± 2.6	13 ± 3	1.46 ± 0.06	2.55 ± 0.97
500h	38.5 ± 1.5	11 ± 2	1.82 ± 0.23	2.74 ± 0.43
750h	39.2 ± 0.6	2.9 ± 0.4	1.86 ± 0.23	0.67 ± 0.09
1000h	33.3 ± 4.7	2.5 ± 0.4	1.8 ± 0.21	0.49 ± 0.16
2000h	31.6 ± 2.9	2 ± 0.08	1.6 ± 0.04	0.38 ± 0.05

At the same time, tensile strength for samples exposed to UV radiation for less than 750 h showed only minimal changes. A similar trend was observed by J.R. White in a study of photo-degradation in polypropylene [22], which reported a ductile band between the

degraded surface and the interior in specimens that were exposed to UV radiation for a short time. During tensile testing, cracks initiated at the surface started to grow and propagated into the sample interior. The propagation was arrested by the ductile layer, so that the undamaged interior showed ductile deformation. These samples still showed slightly ductile behavior and left serrated fracture surfaces, formed at about 45° to the tensile stress direction. As the exposure time further increased, the strength of the degraded layer became too low to transfer stress at the crack tip into the interior and crack growth terminated. At sufficiently long exposure times, the degraded layer became partially detached from the inner material layers and flaked off. Embrittlement is another factor that affects tensile properties. During polymer degradation, embrittlement is caused by oxidation reaction, chain-scission, and decomposition of materials. Embrittlement develops gradually over time, from the surface into the interior of the sample. Samples exposed to UV radiation for more than 750 h showed typical brittle fracture behavior, as shown in Figure 5-5. This behavior was likely the result of the combined effects of surface cracks and embrittlement.

5.4.4 Fourier Transform Infrared Photoacoustic Spectroscopy (PAS-FTIR)

In PAS experiment, the effective sample depth at which signals can be collected is determined by the thermal diffusion length (μ) of the sample. The thermal diffusion length not only depends on the thermal diffusivity (α) of the sample, but also on the modulation frequency (f) of the incident radiation. Here, $f = 2v\upsilon$, where v is the velocity of the mirror (cm/s) and υ is the excitation frequency (wavenumber, cm^{-1}).

$$\mu = \left[\frac{\alpha}{\pi f}\right]^{1/2} = \left[\frac{\alpha}{\pi \nu \upsilon}\right]^{1/2}$$

As a result, signals penetrate deeper at low excitation frequencies and shallower at high excitation frequencies. For the materials studied here, spectra at a frequency of 4000 cm^{-1} originated from a depth of 5.6 µm and spectra at a frequency of 400 cm^{-1} originated from a depth of 17.7 µm. The thermal diffusivity value used here was 1.25 × 10^{-7} m^2/s, which is a mid-value for common polymers.

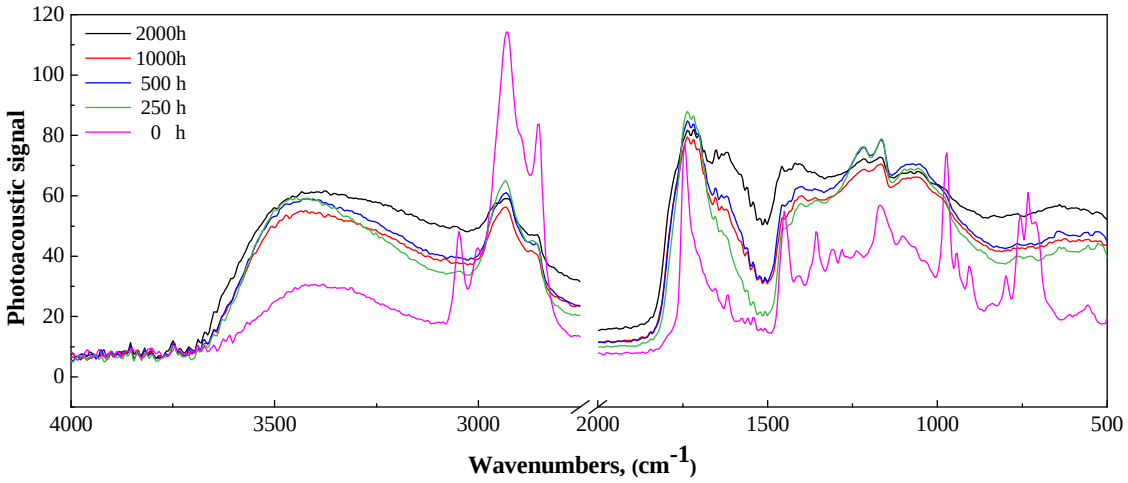

Figure 5-6 PAS-FTIR spectra of degraded samples after varied UV exposure times

The PAS spectra of degraded bio-polymer specimens after different UV exposure times are shown in Figure 5-6. The wide absorption peak at 3400 cm^{-1} was assigned to the hydroxyl group associated with oxidation products, such as hydroperoxide, carboxylic acid, and alcohols. The absorption between 2850 and 2950 cm^{-1} was attributed to stretched C-H bonds. The peak at 1740 cm^{-1} was associated with stretch vibration of the carbonyl group in ketones, acids, esters, and aldehydes. In the fingerprint region, multi-peaks at 1000–1300 cm^{-1} were generally associated with C-O stretch

vibrations that are largely formed during photo-degradation. The decreases in intensity of C-H bond absorption after UV exposure indicated that a large number of C-H bonds were consumed during the photooxidation reaction. UV radiation either converted them into free radicals by removing the hydrogen atom during the initiation step; or they reacted with a peroxy radical to form hydroperoxide and another free radical during the propagation step. Simultaneously, the intensities of the hydroxyl and the carbonyl peak increased, because both hydroperoxides and carbonyls are the main products of photo-degradation. It is interesting to note that as the exposure time increases, IR peaks tended to broaden and overlap with each other, while detailed features for absorption peaks were lost in the spectrum. This effect was probably caused by oxidation products that contain a very large number of individual molecules, so that the examined bond, e.g., the hydroxyl group, showed IR absorption at slightly different frequencies for each of these bonds. Thus, as a result, the IR peak is the average of all these slightly different absorptions and appears broadened. The PAS spectra in Figure 5-7, recorded at a modulation frequency of 20 kHz, represent chemical changes with various surface depth of specimen aged for 1000 h. Spectrum collected on the surface after a removal of 43 µm is labeled 43 µm.

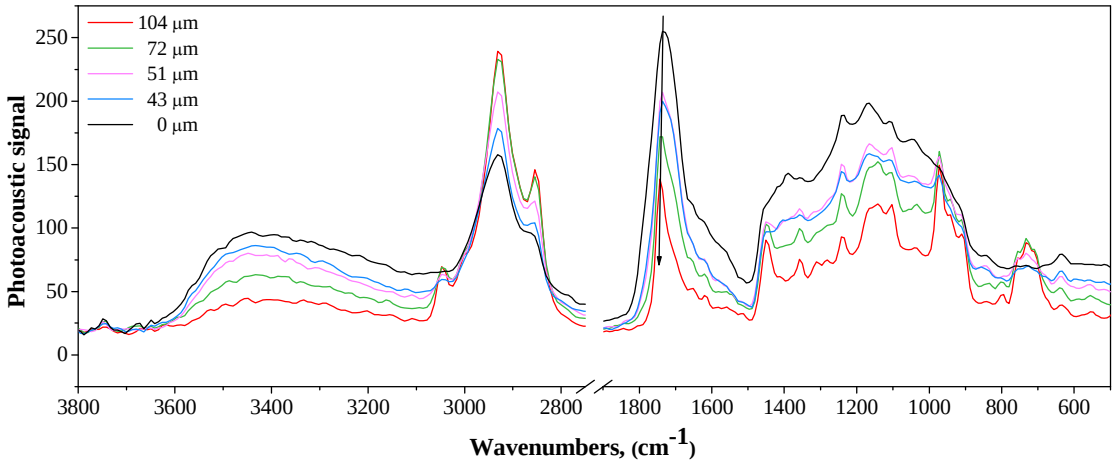

Figure 5-7 Depth-profiling using PAS-FTIR for sample after 1000 h exposure time

Figure 5-7 shows that while going from 0 to 104 µm, an increase of the band intensity of C-H absorption was observed, indicating that the consumption of C-H bonds decreased with penetration depth. At the top surface of the sample a large number of C-H bonds are consumed by UV-induced cleavage and free radical reactions. As the penetration depth increases, both reactions decreased as a result of insufficient oxygen and UV radiations availability. Finally, when the undamaged region was reached, the spectra did not change any further and the intensity of C-H absorption was the highest. It is also important to note that all peaks related to oxidation products (hydroxyl, carbonyl, and C-O) decreased rapidly with increasing penetration depth. This is caused by two photo-degradation reactions: the formation and the decomposition of hydroperoxide. The process of conversion of the formed hydrocarbon radicals to peroxy radicals is the main oxygen-consuming reaction. This reaction occurs readily just after hydrocarbon radicals are formed, and the reaction rate depends on the concentration of oxygen “inside” the polymer [23]. Next the peroxy radical abstracts one hydrogen atom from the polymer

chain to form a hydroperoxide and another hydrocarbon radical. At sample surface, there is sufficient oxygen available to produce abundant hydroperoxides. As going further away from the surface, less hydroperoxide is formed because the oxygen concentration decreases dramatically in polymer. The formation of most oxidation products (alcohols, ketones, aldehydes) is related to the radiation-induced decomposition of hydroperoxide. UV radiation is sufficient to causes cleavage of O-O, R-O, and O-H bonds in hydroperoxide whose dissociation energy values are 42, 70 and 90 kcal/mol respectively; O-O cleavage is predominant in polymer photo-oxidation due to its low bond dissociation energy[10]. After cleavage, the alkoxy radical undergoes a variety of reactions to form different oxidation products, as shown in Figure 5-8: abstracting hydrogen from other hydrocarbons to form alcohols, reacting with hydroxyl to form ketones, undergoing chain scission and atom rearrangement to form aldehydes. The carbonyl group formed during photooxidation also plays an important role, because it absorbs UV light readily after formation and then decomposes through a Norrish reaction. Acids, esters, enols and alkenes are general products of Norrish reaction, as shown in Figure 5-4.

Figure 5-7 also showed that carbonyl absorption shifted to higher frequencies at greater depths. In shallower material layers, carbonyl groups mainly originated from oxidation products, such as ketones (1705–1725 cm^{-1}), acids (1700–1725 cm^{-1}) and aldehydes (1720–1740 cm^{-1}). At greater depth, the oxidized material decreased and undamaged material increased. Carbonyl groups in undamaged materials mainly originated from ester groups that exhibit an excitation frequency of 1730–1750 cm^{-1},

slightly higher than other oxidation products. The shifting of the carbonyl peak is evidence of the fact that the amount of oxidation products decreased with penetration depth.

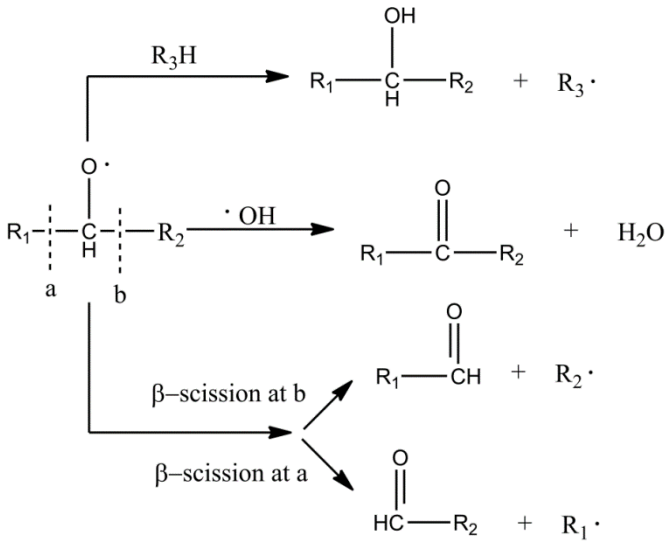

Figure 5-8 Second oxidation reactions for alkoxy radical

The formation of oxidation products depends strongly on oxygen content and decreases exponentially with increasing distance from the surface. In our case, PAS spectra vary a lot with depth shallower than 104 µm and stay unchanged beyond 104 µm, indicating that oxidation mainly occurs in the top layer (~104 µm) of the material.

5.4.5 SEM of Transverse Surface

To obtain a measure of the depth of surface cracks, transverse sections of aged samples were examined using scanning electron microscopy, as shown in Figure 5-9. The transverse sections were prepared by cutting samples with a razor blade. All images were collected on the exposed edge.

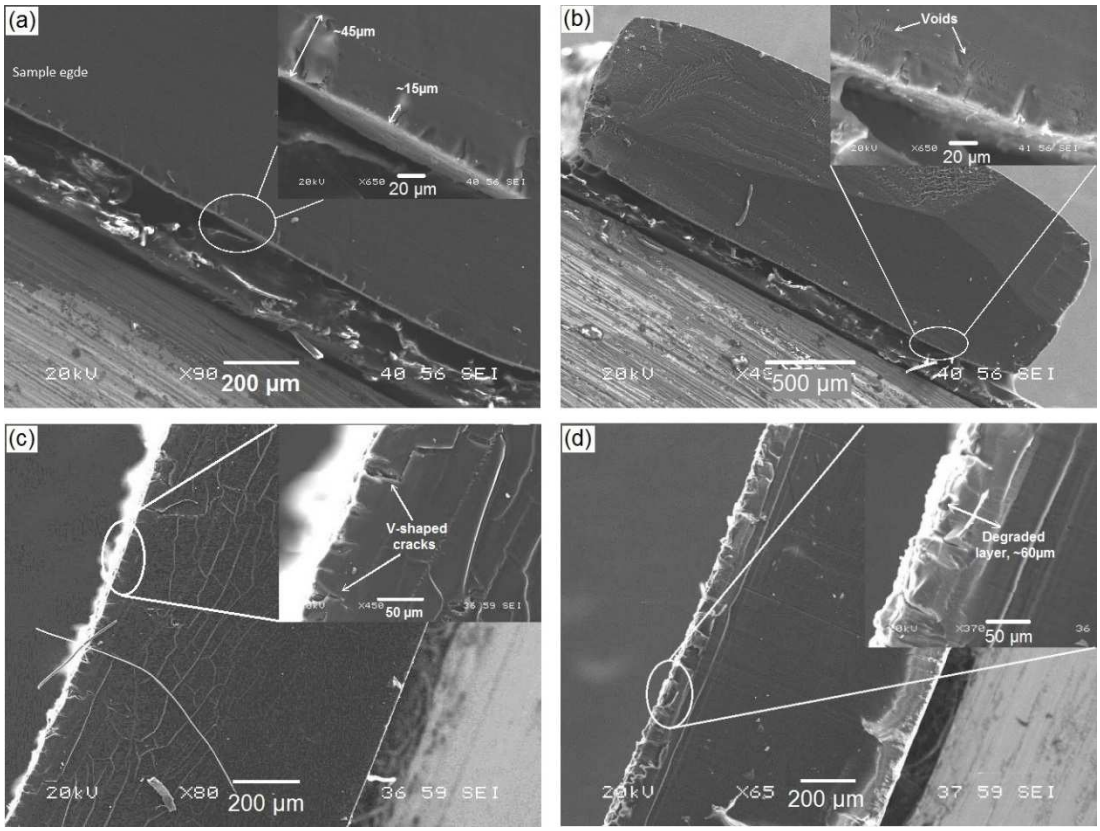

Figure 5-9 SEM images of cross-sections of UV-degraded samples after exposure times of (a) 250 h; (b) 500 h; (c) 1000 h; (d) 2000 h

Figure 5-9 (a) shows the cross-section of a sample exposed to UV radiation for 250 h. The cracks penetrated into the sample to depths varying from ~15 μm to ~40 μm. The material between cracks looked undamaged, similar to interior layers. Figure 5-9(b) shows that for samples exposed to UV radiation for 500 h the crack penetration depth did not increase. However, numerous voids were generated in the material around the cracks. The created cracks also increased the area exposed to UV radiation and oxygen. Thus, oxygen diffused into the material not only from the exposed surface but also from the crack surfaces. As the exposure time further increased, cracks became wider and also penetrated deeper into the material, shown in V-shaped profiles in Figure 5-9 (c). The

tensile stress on the sample surface initiated cracks that grew inwards from the surface. After UV exposure times of 1000 h, the crack depth reached 50 µm. In Figure 5-9 (d), a severely degraded layer is shown at the edge. The degraded layer (shown in lighter color in the image) is about 60 µm thick. This value is much smaller than the degraded depth from PAS depth profile test, indicating that invisible degradation had occurred below the visible damaged layer.

5.5 **Conclusions**

Photo-degradation by UV radiation of thick, bio-renewable polymer sheets was studied and SEM and photoacoustic FTIR showed that photo-degradation increased with increasing exposure time. The formation of surface cracks was attributed to the gradient stress in degraded material layers caused by UV-induced post-crosslinking and cycled weathering conditions. Soxhlet extraction test indicated that UV-induced post-crosslinking dominated during the beginning stage (less than 750 h of exposure) of photo-degradation, before chain scission and decomposition determined the effects of long time UV exposure. Mechanical properties were significantly reduced after UV exposure. Surface cracks and embrittlement were the major contributors to the failure mechanisms encountered in tensile testing. The sudden reduction in breaking strain was attributed to surface cracks. However, tensile strength and Young's modulus were not sensitive to surface cracks after short time exposure. Depth profiles and SEM results both indicated that degradation occurred only in a thin surface layer because of limited oxygen diffusion into the interior layers. Hydroperoxides and various carbonyl groups were formed as the main degradation products, as observed in PAS-FTIR. In a next step,

the effects of adding anti-oxidants and photo-stabilizers will be studied to enhance the photo-stability of biopolymers created by ROMP.

5.6 References

[1] G Scott (1990) Mechanisms of polymer degradation and stabilisation. Elsevier Applied Science ; Sole distributor in the USA, Elsevier Science Pub. Co., London ; New York New York, NY, USA

[2] D Briassoulis, A Aristopoulou, M Bonora, I Verlodt (2004) Biosyst Eng 88: 131. Doi:DOI 10.1016/j.biosystemseng.2004.02.010

[3] B Fayolle, L Audouin, J Verdu (2000) Polym Degrad Stabil 70: 333. Doi:Doi 10.1016/S0141-3910(00)00108-7

[4] M Ito, K Nagai (2007) Polym Degrad Stabil 92: 260. Doi:DOI 10.1016/j.polymdegradstab.2006.11.003

[5] TJ Turton, JR White (2001) Plast Rubber Compos 30: 175.

[6] CW Reed, SW Cichanowski (1994) Ieee T Dielect El In 1: 904. Doi:Doi 10.1109/94.326658

[7] S Sakkopoulos, E Vitoratos, E Dalas (1998) Synthetic Met 92: 63. Doi:Doi 10.1016/S0379-6779(98)80024-6

[8] E Choe, DB Min (2006) Compr Rev Food Sci F 5: 169. Doi:DOI 10.1111/j.1541-4337.2006.00009.x

[9] Y I, DW Lai, M Guigon (2004) Polym Degrad Stabil 86: 59. Doi:DOI 10.1016/j.polymdegradstab.2004.01.013

[10] T Kelen (1983) Polymer degradation. Van Nostrand Reinhold Co., New York

[11] P Henna, RC Larock (2009) J Appl Polym Sci 112: 1788.

[12] TC Mauldin, K Haman, X Sheng, P Henna, RC Larock, MR Kessler (2008) J Polym Sci Pol Chem 46: 6851. Doi:Doi 10.1002/Pola.22995

[13] L Audouin, V Langlois, J Verdu, JCM Debruijn (1994) J Mater Sci 29: 569. Doi:Doi 10.1007/Bf00445968

[14] H Kim, MW Urban (2000) Langmuir 16: 5382. Doi:Doi 10.1021/La990619i

[15] GE Schoolenberg, P Vink (1991) Polymer 32: 432. Doi:Doi 10.1016/0032-3861(91)90446-P

[16] B Yeom, YJ Yu, HA McKellop, R Salovey (1998) J Polym Sci Pol Chem 36: 329. Doi:Doi 10.1002/(Sici)1099-0518(19980130)36:2<329::Aid-Pola16>3.0.Co;2-Q

[17] RM Dittmar, JL Chao, RA Palmer (1991) Appl Spectrosc 45: 1104. Doi:Doi 10.1366/0003702914336138

[18] PA Dolby, R Mcintyre (1991) Polymer 32: 586. Doi:Doi 10.1016/0032-3861(91)90468-X

[19] L Gonon, OJ Vasseur, JL Gardette (1999) Appl Spectrosc 53: 157.

[20] MW Urban (1987) J Coating Technol 59: 29.

[21] PJ Sereda, GG Litvan, ASTM Committee E-6 on Performance of Building Constructions. (1980) Durability of building materials and components : proceedings of the first international conference : a symposium presented at Ottawa, Canada, 21-23 Aug. 1978. ASTM, Philadelphia

[22] MS Rabello, JR White (1997) Polym Degrad Stabil 56: 55. Doi:Doi 10.1016/S0141-3910(96)00202-9

[23] J Velasco, ML Andersen, LH Skibsted (2004) Food Chem 85: 623. Doi:DOI 10.1016/j.foodchem.2003.07.020

CHAPTER 6: GENERAL CONCLUSIONS

6.1 General Discussions

In the study of fracture toughness of Dilulin/DCPD system, DMA measurement reveals that glass transition temperature was reduced with the Dilulin content due to the decrease of cross-link density. Two α-transition peaks on tan δ curves indicate that reaction-induced phase separation occurred in the copolymer. A composition-dependent morphology is examined and confirmed by SEM. Dilulin/DCPD copolymers show huge variations in mechanical properties from very brittle to very ductile within a small change in composition. The EWF concept is reasonable for evaluating the fracture toughness of copolymers with ductile properties. Our investigation indicates that the mechanical and fracture mechanical properties of Dilulin/DCPD copolymers are largely controlled by both composition and morphological structure. Fracture surface analysis by SEM revealed a clear transition in the fracture mechanism from brittle failure to ductile failure as the incorporation of Dilulin increased. The enhancement in resistance to crack propagation of Dil40DCPD60 as indicated by the maximum in the non-essential work of fracture is attributed to the formation of rigid DCPD-phase which toughened the copolymer through crack pinning mechanism. The highest essential work of fracture as measurement of resistance to crack initiation was observed with Dil30DCPD70 which is probably due to the less heterogeneous structure and high cross-link density.

The effect of different silane coupling agents on interfacial adhesion between glass fibers and ROMP-based bio-renewable polymers has been studied experimentally. Two types of silane coupling agents, MCS and TCS, were employed to modify glass fiber surfaces. Untreated glass fibers and heat-cleaned glass fibers were also studied as control groups. Successful grafting of silane onto glass fiber surfaces was confirmed by a substantial increase in carbon concentration after surface modification in XPS analysis. The difference in reaction mechanisms between two silanes indicates MCS may have a higher covalent bond density than TCS when same amount of silanes are used in the surface modification procedure. The effect of surface modification on thermomechanical properties was studied by DMA. With the use of silane, especially MCS, composites become stiffer compared to the control groups, which is presumed to correspond to the successful establishment of covalent bonds in the interfacial region. In addition, the sizing on untreated fibers also has positive influences on interfacial adhesion which is hypothesized to be the result of a diffusion-induced interpenetrating network. Interfacial shear strength and interlaminar shear strength were evaluated by microbond technique and short beam shear testing respectively. Both appear to be sensitive to interface quality and similar results are found. Both techniques demonstrate that MCS has a more profound effect than TCS on improving interfacial adhesion between glass fibers and the bio-based polymer matrix. This conclusion is further confirmed by SEM characterization of composite fracture surfaces.

To improve the interfacial adhesion of the pultruded glass fiber/bioresin composites, glass fiber was treated with MCS silane/alcohol solution with varied

concentration. Although fiber was only immerged in silane solution for 3 min, the interfacial adhesion was enhanced significantly. XPS measurements demonstrate that as the silane concentration increases, elemental concentration of carbon atom is found to increase accordingly at first and then reach a maximum level of about 20% with a silane concentration of 2%. DMA tests reveal that storage modulus was improved greatly after surface modification. Reduced magnitude of tan δ peak also confirms that improved interfacial adhesion was obtained. Flexural strength and modulus in both fiber and transverse directions show consistent results as DMA. DMA and flexure test both indicate that further increasing the silane concentration from 3% to 4% didn't bring the interfacial interaction to higher level. Therefore, 3 wt% of silane in isopropanol is selected as the optimized concentration for surface modification with simply dipping method. Morphology of fracture surfaces of composites double confirmed the conclusions.

Photo-degradation by UV radiation of thick, bio-renewable polymer sheets was studied and SEM and photoacoustic FTIR showed that photo-degradation increased with increasing exposure time. The formation of surface cracks was attributed to the gradient stress in degraded material layers caused by UV-induced post-crosslinking and cycled weathering conditions. Soxhlet extraction test indicated that UV-induced post-crosslinking dominated during the beginning stage (less than 750 h of exposure) of photo-degradation, before chain scission and decomposition determined the effects of long time UV exposure. Mechanical properties were significantly reduced after UV exposure. Surface cracks and embrittlement were the major contributors to the failure

mechanisms encountered in tensile testing. The sudden reduction in breaking strain was attributed to surface cracks. However, tensile strength and Young's modulus were not sensitive to surface cracks after short time exposure. Depth profiles and SEM results both indicated that degradation occurred only in a thin surface layer because of limited oxygen diffusion into the interior layers. Hydroperoxides and various carbonyl groups were formed as the main degradation products, as observed in PAS-FTIR. In the next step, the effects of adding anti-oxidants and photo-stabilizers will be studied to enhance the photo-stability of biopolymers created by ROMP.

6.2 Recommendations for Future Research

Natural fiber reinforced composites have shown a growth of interest due to the economic and environmental advantages and the attractive specific properties. Therefore, applying natural fibers in pultrusion is of great interests since it provides a possible way to make composites at very low cost. Although natural fibers normally present lower strength than traditional fibers used in current composites, the natural fibers are strong enough as reinforcements for making composites used in packaging, construction, and electrical engineering where high performance is not required. As I summarized in section 1.3.3, natural fibers such as flax, hemp, and jute or natural/glass hybrid fibers have already been applied in pultrusion process [1-4]. However, the polymer matrixes in these studies are PP, epoxy and polyester which are all petroleum-based resins. It is very interesting to applied natural fiber and biopolymer in pultrusion simultaneously to make even greener bio-composites.

In this study, we just reviewed biopolyemers that have been developed at ISU. There are a wide range of biopolymers that maybe available for pultrusion process [5, 6]. Commercially available acrylated epoxidized soybean oil (AESO), synthesized from the reaction of acrylic acid with epoxidized soybean oil, has been extensively studied in polymers and composites [7]. AESO can be blended with reactive diluents, such as ST, to improve its processability and the mechanical property of resulting AESO-ST thermosets can be optimized through adjusting the mixing ratio. The AESO-ST system is also a potential candidate for pultrusion applications.

6.3 References

[1] N Nosbi, HM Akil, ZAM Ishak, A Abu Bakar (2010) Mater Design 31: 4960. Doi:DOI 10.1016/j.matdes.2010.04.037

[2] MH Zamri, HM Akil, A Abu Bakar, ZAM Ishak, LW Cheng (2012) J Compos Mater 46: 51. Doi:Doi 10.1177/0021998311410488

[3] HM Akil, IM De Rosa, C Santulli, F Sarasini (2010) Mat Sci Eng a-Struct 527: 2942. Doi:DOI 10.1016/j.msea.2010.01.028

[4] X Peng, MZ Fan, J Hartley, M Al-Zubaidy (2012) J Compos Mater 46: 237. Doi:Doi 10.1177/0021998311410474

[5] YS Lu, RC Larock (2009) Chemsuschem 2: 136.

[6] Y Xia, RC Larock (2010) Green Chem 12: 1893.

[7] J Lu, S Khot, RP Wool (2005) Polymer 46: 71. Doi:DOI 10.1016/j.polymer.2004.10.060